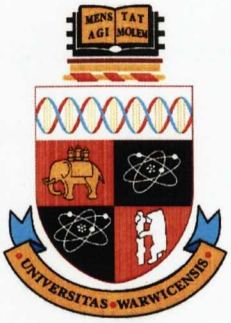

The Korringa-Kohn-Rostoker Nonlocal Coherent-Potential Approximation: a new method for calculating the electronic structure of disordered metallic systems

by

Derwyn Andrew Rowlands

Thesis

Submitted to the University of Warwick

for the degree of

Doctor of Philosophy

Department of Physics

February 2004

THE UNIVERSITY OF WARWICK

Contents

List of Tables

List of Figures

Acknowledgments

I would especially like to thank Professor Julie Staunton for her excellent supervision during the last three years. Thanks also to Professor Balazs Györffy for useful discussions and to EPSRC for the funding. Above all I would like to thank my parents, for without their encouragement and support throughout my education none of this would have been possible.

Declarations

This thesis is submitted to the University of Warwick as my application towards the degree of Doctor of Philosophy, and presents details of research carried out in the Theoretical Group of the Department of Physics at the University of Warwick between October 2000 and October 2003. The content of this thesis is my own work, unless stated otherwise, carried out under the supervision of Professor Julie B. Staunton, and has not been submitted for a research degree at any other institution.

Parts of this work have been published in the following paper:

D.A. Rowlands, J.B. Staunton, and B.L. Györffy, "Korringa-Kohn-Rostoker nonlocal coherent-potential approximation", Phys. Rev. B **67**, 115109, (March 2003)

Abstract

The limitations of the current 'first-principles' effective medium approach to calculating the electronic structure of disordered systems are described. These limitations can be addressed by a cluster theory, and only very recently the first satisfactory cluster theory, the nonlocal coherent potential approximation, has been developed within a tight-binding framework. However an approach based on KKR multiple scattering is needed in order to treat the problem from first principles for ab-initio calculations. In this thesis, these ideas are reformulated in terms of multiple scattering theory and the Korringa-Kohn-Rostoker non-local coherent potential approximation (KKR-NLCPA) is introduced for describing the electronic structure of disordered systems. The KKR-NLCPA systematically provides a hierarchy of improvements upon the widely used local mean-field KKR-CPA approach and includes nonlocal correlations in the disorder configurations by means of a self-consistently embedded cluster. The KKR-NLCPA method satisfies all of the requirements for a successful cluster generalisation of the KKR-CPA; it determines a site-to-site translationally-invariant effective medium, it is herglotz analytic, becomes exact in the limit of large cluster sizes, reduces to the KKR-CPA for a single-site cluster, is straightforward to implement numerically, and enables the effects of short-range order upon the electronic structure to be investigated. In particular, it is suitable for combination with electronic density functional theory to give an ab-initio description of disordered systems. Future applications to charge correlation and lattice displacement effects in alloys and spin fluctuations in magnets amongst others are very promising. The method is illustrated by application to a simple one-dimensional model.

Abbreviations

CPA Coherent Potential Approximation

DCA Dynamical Cluster Approximation

DLM Disordered Local Moment

DFT Density Functional Theory

ECM Embedded Cluster Method

KKR Korringa-Kohn-Rostoker

LDA Local Density Approximation

MCPA Molecular Coherent Potential Approximation

NLCPA Nonlocal Coherent Potential Approximation

SCF Self Consistent Field

SRO Short Range Order

Chapter 1

Introduction

At high temperatures, metallic liquid mixtures of more than one type of atom often crystallize into a 'solid solution' alloy in which there remains an underlying regular lattice, but the atoms occupy these lattice sites in an almost random fashion. This is known as random substitutional disorder and a simple example is shown in Fig. 1.1(a). In such systems there is however always some short-range order (SRO) present i.e. a tendency for atoms to surround themselves with atoms of the same kind (clustering) e.g. $CuNi$, or alternatively to surround themselves with atoms of a different kind (ordering) e.g. $CuAu$. Upon cooling the solid solution, this SRO becomes increasingly more significant. At some critical temperature T_c, the alloy will undergo a phase transition into either an ordered phase or alternatively will phase separate, illustrated in Fig. 1.1(b) and Fig. 1.1(c) respectively. The properties of an alloy also depend on its preparation route, for example the disordered phase may be preserved at room temperature by rapidly quenching from above T_c.

There is growing interest in the understanding of these ordering processes due to the ever increasing technological importance of metallic alloys, for example in the emerging communications and computer industries. This has led to a need for much more realistic theoretical models of disorder which can help to interpret the experimental data and give guidance in developing new alloy systems with properties

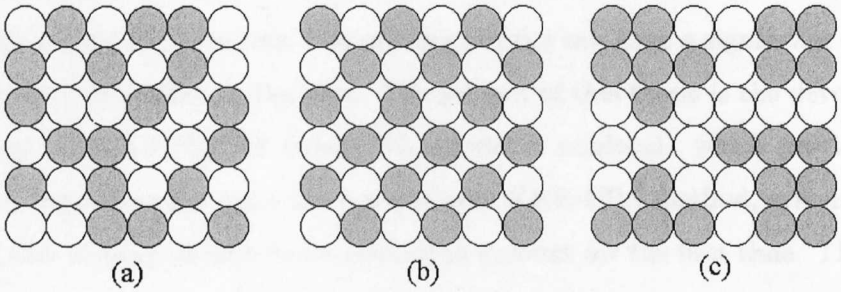

Figure 1.1: Phases of a binary alloy: (a) Disorder (b) Order (c) Segregation

tailored to meet specific requirements [1].

A knowledge of the electronic structure of an alloy is required to calculate observable properties such as photoemission spectra, charge density, magnetic moments, transport properties etc. Although phenomenological 'pair potential' models [2] are commonly used to give an account of phase stability, it is also the electronic structure which ultimately determines the state of compositional order. So to understand the underlying mechanisms governing the properties and controlling the formation of alloys, a fully microscopic electronic theory is needed. A major advantage of such a 'first-principles' electronic approach is that it can be combined with density functional theory for ab-initio calculations which are material and geometry specific without the need for adjustable parameters chosen to give the desired behaviour or fitted from experiment.

Therefore, fundamental to a 'first-principles' theory of the properties and phase stability of alloys is an accurate description of the electronic structure of the disordered phase. Currently, one of the most successful theories has proved to be the Korringa-Kohn-Rostoker coherent-potential approximation (KKR-CPA) [3, 4, 5]. However, as a local mean-field theory of disorder, the KKR-CPA is not a fully-satisfactory theory. In particular it is unable to take into account the effects of short-range order (SRO) and other short-range effects such as lattice relaxation on the electronic structure. In other words the KKR-CPA assumes a completely ran-

dom substitutionally-disordered alloy when calculating the electronic structure and observable properties. However, this missing physics can have a significant effect on many physical properties of the alloy. The subject of this thesis is the development of a theory, the KKR-NLCPA (where NL stands for nonlocal), which provides a hierarchy of improvements upon the conventional KKR-CPA method, systematically enabling this missing physics to be taken into account for the first time. The development of such a theory has been the subject of numerous attempts over the years, but until now these attempts have not been satisfactory [6].

This thesis begins with a brief introduction to first-principles methods. Central to this is electronic density functional theory (DFT), which maps the many-electron Hamiltonian for a metallic system to that of an effective Hamiltonian describing a single-electron. For ab-initio (parameter-free) calculations, the resulting Kohn-Sham equations then need to be solved self-consistently, yielding the electronic structure. A brief review is given of the Korringa-Kohn-Rostoker (KKR) method for solving the Kohn-Sham equations, which is based on a multiple-scattering description of a single electron propagating through the array of effective potentials formed by the nuclei and self-consistently determined electronic density. Although there are many available methods for solving the Kohn-Sham equations, the KKR multiple-scattering approach is the only way of dealing with such a realistic Hamiltonian when we consider disordered systems.

The treatment of disordered systems from first principles is the subject of Chapter 3. The KKR-CPA method is described and then its limitations are discussed in detail. Considerable effort has been spent in trying to improve upon the CPA by formulating a 'cluster' generalisation (Chapter 4). This has turned out to be a very difficult problem [6], and a viable solution has been proposed only recently. The new method has emerged from the Dynamical Cluster Approximation (DCA) [7, 8, 9] which was originally directed at describing dynamical spin and charge fluctuations in simple Hubbard models of strongly-correlated electron systems. Recently, its static limit has been adapted for a simple tight-binding model of electrons moving

in a disordered potential [10, 11, 12].

However, an approach based on multiple scattering theory is needed in order to treat the problem from first principles for ab-initio calculations. Most of the original work in this thesis is contained in Chapters 5-7, which involves reformulating these ideas in terms of multiple scattering theory, and combining them with the KKR-CPA. The resulting KKR-NLCPA (where NL stands for nonlocal) satisfies all the requirements for a satisfactory cluster theory. The difficulty in reformulating the problem has been due to the very different nature of the language of multiple scattering theory to the context in which the DCA is normally applied. The DCA is formulated in reciprocal space where the main object of interest is the self-energy and the diagrammatic language of perturbation theory is used. This is not the case in the real-space formalism of multiple scattering theory, but by introducing a new reference medium I show that the quantities in multiple scattering theory which play the role of the self-energy are the effective site scattering amplitudes (t-matrices) and effective propagator or structure constants.

Chapter 5 contains the formalism for the KKR-NLCPA, explains the algorithm, shows how to include short-range order, and finally explains how to calculate observable quantities such as the configurationally-averaged density of states in preparation for DFT calculations. Chapter 6 illustrates the KKR-NLCPA by application to a simple one-dimensional model which has the same formal basis as a realistic model but is computationally much simpler. The purpose of this model is simply to highlight some of the possible improvements that could be obtained in a realistic calculation. Chapter 7 goes on to show that the KKR-NLCPA is fully applicable to realistic systems by describing in detail how to carry out the necessary 'coarse-graining' procedure with reference to simple cubic, body-centered cubic and face-centered cubic lattices.

Finally, Chapter 8 summarises the main achievements of this thesis and discusses some future work which arises as a result.

Chapter 2

First-Principles Methods

2.1 Density Functional Theory

Equilibrium quantities of a material can be considered as functionals of the electron density $n(\mathbf{r})$, for example the total energy $E[n(\mathbf{r})]$. The electron density is determined by $\Psi(\mathbf{r}_1, ...\mathbf{r}_N)$, the total equilibrium wavefunction for all the electrons in the solid. However, solving the Schrödinger equation for all the electrons in a solid is an impossible task due to the many interactions involved. The main difficulty is that the potential felt by each electron depends on the position of all the other electrons as well as the positions of the atomic nuclei. In order to solve this many body problem, a way forward is to adopt a single electron approach. This means that the electrons are treated as independent of each other, each moving in a local effective potential which, in addition to describing the effect of the ions, must also somehow attempt to take into account the interactions with all the other electrons. In this way it would be possible to solve a Schrödinger equation for each electron separately using the methods of band theory [13]. This transformation of the many-electron problem into many one-electron problems may be achieved using Density Functional Theory (DFT). For a thorough review see Refs. [14, 15]. Although this transformation is exact, in practice an approximation such as the local density ap-

proximation (LDA) [16, 17] still needs to be made. This generally works very well for metals and many other systems except for strongly-correlated electron systems.

2.1.1 The Kohn-Sham Equations

The Born-Oppenheimer approximation treats the electrons as moving in an external potential generated by the static nuclei. The N-electron wavefunction $\Psi(\mathbf{r}_1, \mathbf{r}_2, \ldots, \mathbf{r}_N)$ may then be described by the Hamiltonian

$$H = \sum_{i=1}^{N} -\frac{\hbar^2}{2m}\nabla_i^2 - \frac{1}{4\pi\epsilon_o}\sum_{i=1}^{N}\sum_{n}\frac{Z_n e^2}{|\mathbf{r}_i - \mathbf{R}_n|} + \frac{1}{2}\frac{1}{4\pi\epsilon_o}\sum_{i,j=1, i\neq j}^{N}\frac{e^2}{|\mathbf{r}_i - \mathbf{r}_j|} \tag{2.1}$$

The first term represents the kinetic energy of the electrons, the second term the interaction of the electrons with the external potential due to the ions, and the final term the electron-electron interactions.

Adopting a single-electron approach, Hartree accounted for the final term in Eq. (2.1) by considering a time averaged smooth electron distribution of density $n(\mathbf{r})$, and treating the potential felt by an electron at $\mathbf{r}$ as being generated by the average charge distribution of all the other electrons i.e.

$$V(\mathbf{r}) = e^2 \int d\mathbf{r}' \frac{n(\mathbf{r}')}{|\mathbf{r} - \mathbf{r}'|} \tag{2.2}$$

This enables the many body wavefunction to be written in terms of single-electron wavefunctions. However this many body wavefunction is very complex and requires a large amount of computational effort for large condensed matter systems. The Hartree and Hartree-Fock theories also ignore nonlocal correlation effects between the electrons.

Thomas [18] and Fermi [19] approached the many body problem from a different point of view, focusing on the electron density for the many body system rather than the wavefunction. Their ideas were extended by Hohenberg and Kohn [20] into an exact theory (DFT) based on two theorems;

1. The electron density $n(\mathbf{r})$ is uniquely determined by the external potential $V_{ext}(\mathbf{r})$. It can be shown that it is not possible for two different external potentials to lead to the same electron density, and this implies that the reverse is also true, that the external potential is a unique functional of the electron density. Since the ground state N-electron wavefunction is determined by $V_{ext}(\mathbf{r})$, it is also a unique functional of the electron density. This is also true for the total energy functional which can be written in the form

$$E[n(\mathbf{r})] = \langle\psi|H|\psi\rangle = T[n(\mathbf{r})] + \int d\mathbf{r} V^{ext}(\mathbf{r}) n(\mathbf{r}) + \frac{e^2}{2}\int d\mathbf{r}d\mathbf{r}' \frac{n(\mathbf{r})n(\mathbf{r}')}{|\mathbf{r}-\mathbf{r}'|} + E_{xc}[n(\mathbf{r})] \tag{2.3}$$

2. The energy functional above assumes its minimum value, the ground state energy, for the correct ground state electron density.

In Eq. (2.3), the first term represents the kinetic energy functional, the second term describes the interaction of the electron gas with the external potential, and the third term is the Hartree energy due to the Hartree potential. The final term, known as the exchange-correlation energy, is an unknown functional which contains all the many body contributions which are not taken into account by the first three terms.

Since Eq. (2.3) needs to be minimised and E_{xc} is not known, it may appear that we are no closer to solving the problem. However, Kohn and Sham [16] made use of the second theorem, and found that minimising Eq. (2.3) with respect to the electron density, with the condition that the number of particles is kept constant, leads to an Euler-Lagrange equation

$$\frac{\delta T[n(\mathbf{r})]}{\delta n(\mathbf{r})} + V^{eff}[n(\mathbf{r})] - \mu n(\mathbf{r}) = 0 \tag{2.4}$$

where

$$V^{eff}[n(\mathbf{r})] = V^{ext}[n(\mathbf{r})] + e^2 \int \frac{n(\mathbf{r}')d\mathbf{r}'}{|\mathbf{r}-\mathbf{r}'|} + V_{xc} \tag{2.5}$$

and V_{xc} is the exchange-correlation potential

$$V_{xc} = \frac{\delta E_{xc}[n(\mathbf{r})]}{\delta n(\mathbf{r})} \tag{2.6}$$

Kohn and Sham showed that Eq. (2.4) could be written as a Schrödinger equation for non-interacting electrons moving in the external potential given by V^{eff}, with $T[n]$ the kinetic energy functional of the non-interacting electron gas which has the same electron density as the real interacting system i.e. a set of single-electron Schrödinger type equations known as the Kohn-Sham equations may be defined by

$$\left[-\frac{\hbar^2}{2m}\nabla^2 + V^{eff}(\mathbf{r})\right]\phi_n(\mathbf{r}) = \varepsilon_n\phi_n(\mathbf{r}) \tag{2.7}$$

The electron density can now be defined in terms of single electron states ϕ_n by

$$n(\mathbf{r}) = \sum_{n=1}^{N} |\phi_n(\mathbf{r})|^2 \tag{2.8}$$

Note that the $\{\phi_n(\mathbf{r})\}$ and $\{\varepsilon_n\}$ are auxiliary quantities used to construct the electron density and other observables and are not the wavefunctions and energies of the real electrons.

The DFT formalism up to now is exact. However in deriving the Kohn-Sham equations, all the unknown quantities, namely electron-electron correlations due to Coulomb repulsion and exchange interactions due to the Pauli Exclusion Principle, are put into the exchange-correlation energy functional. Since these quantities are nonlocal and would require the use of many body theory, in practice approximations have to be made. A commonly used approximation is the Local Density Approximation (LDA) [16, 17] where E_{xc} is assumed to take the form

$$E_{xc}[n(\mathbf{r})] = \int \epsilon_{xc}[n(\mathbf{r})]n(\mathbf{r})d\mathbf{r} \tag{2.9}$$

Here $\epsilon_{xc}[n(\mathbf{r})]$ is the exchange-correlation energy per electron in a homogeneous electron gas of density $n_0 = n(\mathbf{r})$. The corresponding exchange-correlation potential obtained from Eq. (2.6) at a point $\mathbf{r}$ thus depends only on the electron density $n(\mathbf{r})$ at $\mathbf{r}$ rather than the functional $[n(\mathbf{r})]$.

Using the LDA exchange-correlation potential, an estimate is made for $V^{eff}(\mathbf{r})$. Various band structure methods can then be used to solve the Kohn-Sham equations, for example Augmented Plane Wave (APW), Orthogonalised Plane Wave (OPW),

Linear Muffin-Tin Orbitals (LMTO), or Pseudo Potential methods etc. (see for example Ref. [21]). Once the $\{\phi_n(\mathbf{r})\}$ have been calculated, the electron density is obtained from Eq. (2.8). This is used to derive a new effective potential $V^{eff}(\mathbf{r})$ and this cycle is repeated until self-consistency is achieved i.e. the input and output effective potentials are the same to a given tolerance. In this thesis, the Korringa-Kohn-Rostoker (KKR) method based on multiple scattering theory is used to solve the Kohn-Sham equations. Rather than finding the single-electron states $\{\phi_n(\mathbf{r})\}$, this method uses the corresponding single-electron Green's function to calculate the electron density and other observables. An advantage of the KKR method is its ability to treat disordered systems (see Chapter 3).

2.2 KKR Multiple Scattering Theory

The theory for the multiple scattering of electrons in a solid was first derived by Korringa [22] in terms of wavefunctions and later by Kohn and Rostoker [23] in terms of Green's functions. For full details of developments in the KKR method see Refs. [24, 25].

The aim is to solve the Kohn-Sham equation Eq. (2.7)

$$\left[-\frac{\hbar^2}{2m}\nabla^2 + V(\mathbf{r})\right]\phi_n(\mathbf{r}) = \varepsilon_n\phi_n(\mathbf{r}) \tag{2.10}$$

where $V(\mathbf{r})$ is the effective potential. As mentioned above, rather than finding the single-electron states $\{\phi_n(\mathbf{r})\}$, the KKR method calculates the corresponding single-electron multiple-scattering Green's function $G(\mathbf{r}, \mathbf{r}', E)$ defined by

$$\left[E + \frac{\hbar^2}{2m}\nabla^2 - V(\mathbf{r})\right]G(\mathbf{r}, \mathbf{r}', E) = \delta(\mathbf{r} - \mathbf{r}') \tag{2.11}$$

From this, observable quantities may be calculated, for example the electron density

$$n(\mathbf{r}) = -\frac{1}{\pi}Im\int_{-\infty}^{E_F} G(\mathbf{r}, \mathbf{r}, E)dE \tag{2.12}$$

for reconstructing the effective potential $V(\mathbf{r})$ in the DFT self-consistency loop.

In this section, the multiple scattering equations are derived in operator form. In subsequent sections, this formalism is put into a coordinate representation, which is what is required to solve Eq. (2.7) with a potential of the form $V(\mathbf{r})$. Furthermore, for computational purposes it will also be necessary to expand in terms of partial waves (angular momentum representation).

First consider the Kohn-Sham equation in operator form

$$(E - \hat{H})|\phi\rangle = 0 \tag{2.13}$$

where $\hat{H}$ is the Hamiltonian operator $\hat{H} = -\frac{\hbar^2}{2m}\nabla^2 + V(\mathbf{r})$. The retarded Green's function operator corresponding to $\hat{H}$ is defined as

$$\hat{G}(E) = (E - \hat{H})^{-1} \tag{2.14}$$

where the energy E is assumed to have an infinitesimal positive imaginary part. Eq. (2.14) is the operator form of Eq. (2.11).

Similarly, in the absence of any potential, the free-electron Schrödinger equation and corresponding free-electron Green's function operator may be defined as

$$(E - \hat{H}_o)|\psi\rangle = 0 \tag{2.15}$$

and

$$\hat{G}_o(E) = (E - \hat{H}_o)^{-1} \tag{2.16}$$

In the following all quantities are in operator form but the circumflex symbol is dropped for clarity. Expressing the full Hamiltonian operator as $H = H_o + V$ and combining Eq. (2.14) and Eq. (2.16) yields the Dyson equation

$$G = G_o + G_o V G \tag{2.17}$$

Now defining the transition operator T such that

$$TG_o = VG = V(G_o + G_o T G_o) = (V + V G_o T)G_o \tag{2.18}$$

means that Eq. (2.17) becomes

$$G = G_o + G_o T G_o \tag{2.19}$$

The transition operator T describes all possible scattering in the system as it relates the free-particle Green's function to the full scattering Green's function. This may be seen explicitly by rewriting in terms of wavefunctions, yielding the Lippmann-Schwinger equation

$$|\phi\rangle = |\psi\rangle + G_o V|\phi\rangle \tag{2.20}$$

or

$$|\phi\rangle = |\psi\rangle + G_o T|\psi\rangle \tag{2.21}$$

which relates the outgoing scattered wave to the incoming wave.

The idea of multiple scattering theory is to *represent the multiple-scattering problem in terms of the scattering properties of the individual sites.*

The first step is to decompose the potential V into a sum of non-overlapping contributions V_i associated with each site i. This ensures that a scattering event due to a given potential V_i ends before another begins.

In a coordinate representation, $V(\mathbf{r})$ is decomposed into a sum of non-overlapping spherical contributions $V_i(\mathbf{r} - \mathbf{R}_i)$ centred at each site $\mathbf{R}_i$, and is set equal to zero or a constant in the interstitial region outside the muffin-tin spheres i.e.

$$V_i(\mathbf{r} - \mathbf{R}_i) = V_i(\mathbf{r}_i) = \begin{cases} V_i(r_i) & \text{for } |\mathbf{r}_i| < r_i^{MT} \\ 0 & \text{otherwise} \end{cases} \tag{2.22}$$

This is the famous muffin-tin potential illustrated in Fig. 2.1.

Returning to operator form [25, 26], by using Eq. (2.18) the transition operator T can now be written as

$$T = V + VG_oT = \sum_i (V_i + V_iG_oT) = \sum_i T^i \tag{2.23}$$

with

$$T^i = V_i + V_iG_oT = V_i + V_iG_o^{ii}T^i + \sum_{j \neq i} V_iG_o^{ij}T^j \tag{2.24}$$

Eq. (2.24) may be manipulated into the form

$$T^i = [1 - V_iG_o^{ii}]^{-1}V_i(1 + \sum_{j \neq i} G_o^{ij}T^j) \tag{2.25}$$

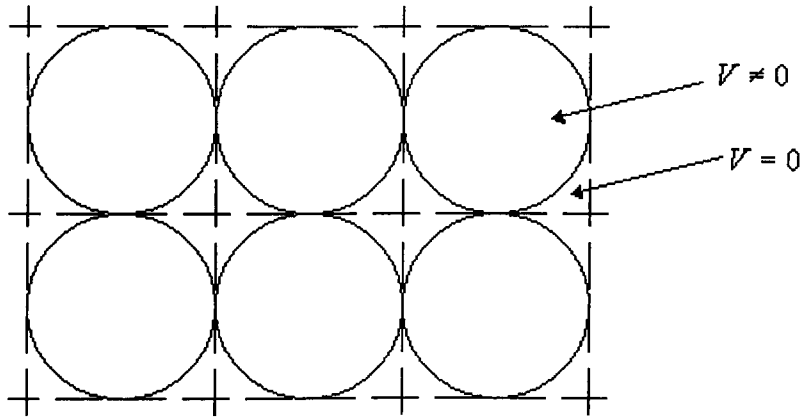

Figure 2.1: Cross-section of a muffin-tin potential

Now consider a single potential associated with a site i. In an analogous fashion to Eq. (2.23), the single-site transition matrix or t-matrix may be defined as

$$t^i = V_i + V_i G_o^{ii} t^i \tag{2.26}$$

or

$$t^i = [1 - V_i G_o^{ii}]^{-1} V_i \tag{2.27}$$

It can be seen that t^i describes all possible scatterings due to the single site i. The single site Green's function may be defined in analogy to Eq. (2.19) by

$$G^i = G_o^{ii}\delta_{ij} + G_o^{ii} t^i G_o^{ii} \tag{2.28}$$

Substituting Eq. (2.27) into Eq. (2.25) yields

$$T^i = t^i + \sum_{j \neq i} t^i G_o^{ij} T^j \tag{2.29}$$

In order to write the solution of the multiple scattering problem in terms of the single-site scattering problem, the next step is to introduce the scattering path operator τ^{ij} of Györffy and Stott [27]

$$\tau^{ij} = t^i \delta_{ij} + \sum_{k \neq i} t^i G_o^{ik} \tau^{kj} \tag{2.30}$$

It can be shown that $T^i = \sum_j \tau^{ij}$ and so the transition operator T may therefore be written in the form

$$T = \sum_i T^i = \sum_{ij} \tau^{ij} \tag{2.31}$$

In order to see explicitly the meaning of the scattering path operator, it is convenient to expand it in a Born series:

$$\tau^{ij} = t^i \delta_{ij} + \sum_{k \neq i} t^i G_o^{ik} t^k \delta_{kj} + \sum_{k \neq i} \sum_{l \neq k} t^i G_o^{ik} t^k G_o^{kl} t^l \delta_{lj} + \cdots \tag{2.32}$$

It is evident that τ^{ij} gives the scattered wave from site j due to a wave incident upon site i, taking into account all possible scatterings in between. For example, the third term in Eq. (2.32) represents a wave incident upon site i which is scattered and propagates to site k via the free-particle Green's function G_o^{ik}, and is scattered again at site k, then propagates to site j where the final scattering occurs. The sum over all intermediate sites k ensures that this term represents all possible scatterings from i to j which involve a single intermediate site. By considering each term in this way, summing the scattering path operator itself over all sites i and j means all waves incident at all scattering sites are being transformed into the outgoing waves from all scattering sites, which is the definition of the transition operator T.

Note that the total multiple-scattering Green's function operator may now be written in terms of the single site Green's function of Eq. (2.28), G^n [28]

$$G = G^n + G^n T^{nn} G^n \tag{2.33}$$

where T^{nn} contains all scatterers except the n^{th} site. In terms of the scattering path operator Eq. (2.33) becomes

$$G = G^n + G^n \sum_{i \neq n} \sum_{j \neq n} \tau^{ij} G^n \tag{2.34}$$

where

$$T^{nn} = \sum_{i \neq n} \sum_{j \neq n} \tau^{ij} \tag{2.35}$$

2.2.1 Single-Site Scattering

For a thorough review of single-site scattering see Refs. [29, 30]. In brief, consider a single muffin-tin potential $V_i(\mathbf{r})$ illustrated in Fig. 2.1. As mentioned earlier, for computational purposes it is necessary to go into an angular momentum representation. Since the muffin-tin potential is spherically-symmetric, the Schrödinger equation involving the single potential $V_i(\mathbf{r})$ may be written in spherical polar coordinates, and the Laplacian operator may be separated into a radial and an angular part. The angular momentum of an electron is conserved in a central potential and so the solutions for a particular value of the orbital angular momentum l and azimuthal angular momentum m can then be written in the form

$$\psi_l^m(\mathbf{r}) = R_l(r)Y_l^m(\hat{r}) \tag{2.36}$$

where $R_l(r)$ satisfies the radial equation

$$\left[-\frac{\hbar^2}{2m}\frac{1}{r^2}\frac{\partial}{\partial r}\left(r^2\frac{\partial}{\partial r}\right) + \frac{\hbar^2}{2mr^2}l(l+1) + V_i(r)\right] R_l(r) = ER_l(r) \tag{2.37}$$

and the $Y_l^m(\hat{r})$ are spherical harmonics. Inside the muffin-tin sphere ($r \leq r^{MT}$) Eq. (2.37) needs to be solved numerically. The solution that is regular at the origin, denoted by $Z_L(\mathbf{r}, E)$, must join smoothly to a linear combination of free-particle solutions (for $r > r^{MT}$) at the muffin-tin boundary. Using the normalisation of Faulkner and Stocks [28], this linear combination is taken to be

$$Z_L(\mathbf{r}, E) = J_L(\mathbf{r}, E)t_l^{-1}(E) - ikH_L(\mathbf{r}, E) \tag{2.38}$$

where $k = \sqrt{2mE/\hbar^2}$. Here a notation has been used such that $J_L(\mathbf{r}, E) = j_l(r, E)Y_l^m(\hat{r})$, and L denotes the angular momentum quantum numbers l, m.

$t_l^{-1}(E)$ is the single-site scattering matrix t in an angular momentum representation, and is related to the phase-shift $\delta_l(E)$ by

$$t_l(E) = -\frac{1}{\sqrt{E}}\sin\delta_l(E)e^{i\delta_l} \tag{2.39}$$

The phase shift and in turn the t-matrix contains all the information about the scattering properties of the single-site potential. For a spherically symmetric potential the t-matrix is diagonal in angular momentum.

The solution that is irregular at the origin, denoted by $\tilde{J}_L(\mathbf{r}, E)$, must join smoothly to the free particle solution $J_L(\mathbf{r}, E)$ at the muffin-tin boundary.

In a coordinate representation the single site Green's function Eq. (2.28) becomes

$$G(\mathbf{r}, \mathbf{r}', E) = G_o(\mathbf{r}, \mathbf{r}', E) + \int\int G_o(\mathbf{r}, \mathbf{r}'', E) t(\mathbf{r}'', \mathbf{r}''', E) G_o(\mathbf{r}''', \mathbf{r}', E) d\mathbf{r}''' d\mathbf{r}'' \quad (2.40)$$

with the free-particle Green's function corresponding to Eq. (2.16) defined as

$$[E - \hat{H}_o(\mathbf{r})] G_o(\mathbf{r}, \mathbf{r}', E) = \delta(\mathbf{r} - \mathbf{r}') \quad (2.41)$$

Eq. (2.41) has plane wave solutions

$$G_o(\mathbf{r}, \mathbf{r}', E) = -\frac{1}{4\pi} \frac{e^{ik|\mathbf{r}-\mathbf{r}'|}}{|\mathbf{r} - \mathbf{r}'|} \quad (2.42)$$

which, using Bauer's identity, may be expanded in terms of spherical functions

$$G_o(\mathbf{r}, \mathbf{r}', E) = -ik \sum_L H_L(\mathbf{r}^>, E) J_L(\mathbf{r}^<, E) \quad (2.43)$$

where $>$ and $<$ denote the larger and smaller value of $\mathbf{r}$ and $\mathbf{r}'$ respectively. Substituting into Eq. (2.40) and using the normalisation of Eq. (2.38) yields the single-site Green's function

$$G^i(\mathbf{r}_i, \mathbf{r'}_i, E) = \sum_L Z_L(\mathbf{r}_i, E) t_l^i(E) Z_L(\mathbf{r'}_i, E) - \sum_L Z_L(\mathbf{r}_i^<, E) \tilde{J}_L(\mathbf{r}_i^>, E) \quad (2.44)$$

with the angular momentum elements of the single-site t-matrix defined as

$$t_l^i(E) = \int\int d\mathbf{r}_i d\mathbf{r'}_i J_L(\mathbf{r}_i, E) t^i(\mathbf{r}_i, \mathbf{r'}_i, E) J_{L'}(\mathbf{r'}_i, E) \quad (2.45)$$

These may be determined by matching solutions at the muffin-tin boundary via Eq. (2.38). Because of the matching, this equation is valid for $\mathbf{r}$ both in the interstitial region and inside the muffin-tin sphere at site i.

2.2.2 Multiple-Site Scattering

In order to derive the multiple scattering Green's function, first consider the scattering path operator Eq. (2.30) in a coordinate representation

$$\begin{aligned} \tau^{ij}(\mathbf{r}_i, \mathbf{r'}_j, E) &= t^i(\mathbf{r}_i, \mathbf{r'}_i, E)\delta_{ij} + \sum_{k \neq i} \int\int \Big\{ t^i(\mathbf{r}_i, \mathbf{r'}_i, E) \\ &\quad G_o(\mathbf{r'}_i + \mathbf{R}_i, \mathbf{r}_k + \mathbf{R}_k, E) \tau^{kj}(\mathbf{r}_k, \mathbf{r'}_j, E) d\mathbf{r}_k d\mathbf{r'}_i \Big\} \end{aligned} \quad (2.46)$$

Here $\mathbf{r}_i$ and $\mathbf{r'}_j$ are local coordinates relative to the centres of the muffin-tin spheres positioned at $\mathbf{R}_i$ and $\mathbf{R}_j$. Using translational invariance the free particle Green's function may be written as

$$\begin{aligned} G_o(\mathbf{r'}_i + \mathbf{R}_i, \mathbf{r}_k + \mathbf{R}_k, E) &= G_o(\mathbf{r'}_i, \mathbf{r}_k + \mathbf{R}_k - \mathbf{R}_i, E) \\ &= G_o(\mathbf{r'}_i, \mathbf{r}_k - \mathbf{R}_{ik}, E) \end{aligned} \tag{2.47}$$

where $\mathbf{R}_{ik} = \mathbf{R}_i - \mathbf{R}_k$. Note that $|\mathbf{r'}_i| < |\mathbf{r}_k - \mathbf{R}_{ik}|$ for $i \neq k$. The free particle Green's function Eq. (2.43) becomes

$$G_o(\mathbf{r'}_i, \mathbf{r}_k - \mathbf{R}_{ik}, E) = -ik \sum_L J_L(\mathbf{r'}_i, E) H_L(\mathbf{r}_k - \mathbf{R}_{ik}, E) \tag{2.48}$$

The spherical Hankel function may be expanded about $\mathbf{R}_{ik}$ in terms of spherical Bessel functions

$$-ikH_L(\mathbf{r}_k - \mathbf{R}_{ik}, E) = \sum_L G^{ik}_{LL'}(\mathbf{R}_{ik}, E) J_L(\mathbf{r}_k, E) \tag{2.49}$$

Substituting Eq. (2.49) into Eq. (2.48) yields

$$G_o(\mathbf{r'}_i, \mathbf{r}_k - \mathbf{R}_{ik}, E) = -ik \sum_{L,L'} J_L(\mathbf{r'}_i, E) G^{ik}_{LL'}(\mathbf{R}_{ik}, E) J_{L'}(\mathbf{r}_k, E) \tag{2.50}$$

The expansion coefficients $G^{ik}_{LL'}(\mathbf{R}_{ik}, E)$ are the matrix elements of the free-particle Green's function in a coordinate and angular momentum representation. They depend only on the relative distance between the centres of the scatterers positioned at sites i and k, being independent of the potentials at these sites, and are therefore referred to as the free-space structure constants. They are given by

$$G^{ik}_{LL'}(\mathbf{R}_{ik}, E) = -4\pi ik \sum_{L''} i^{l-l'+l''} C^{L''}_{LL'} h_{l''}\left(k|\mathbf{R}_i - \mathbf{R}_k|\right) Y_{L''}(\widehat{\mathbf{R}_{ik}}) \tag{2.51}$$

where the $C^{L''}_{LL'}$ are integrals over spherical harmonics

$$C^{L''}_{LL'} = \int Y_{L''}(\Omega) Y_{L'}(\Omega) Y_L(\Omega) d\Omega \tag{2.52}$$

known as the Gaunt coefficients (see for example Ref. [29]).

The matrix elements of the scattering path matrix Eq. (2.46) in an angular momentum representation may be defined as

$$\tau^{ij}_{LL'}(E) = \int\int d\mathbf{r}_i d\mathbf{r'}_j J_L(\mathbf{r}_i, E)\tau^{ij}(\mathbf{r}_i, \mathbf{r'}_j, E)J_{L'}(\mathbf{r'}_j, E) \tag{2.53}$$

Substituting Eq. (2.46) with Eq. (2.50) into Eq. (2.53) leads to

$$\tau^{ij}_{LL'}(E) = t^i_L(E)\delta_{ij}\delta_{LL'} + \sum_{k\neq i}\sum_{L''} t^i_L(E)G^{ik}_{LL''}(\mathbf{R}_{ik}, E)\tau^{kj}_{L''L'}(E) \tag{2.54}$$

Now together with the single-site Green's function Eq. (2.44), using the operator equation Eq. (2.34) leads to the multiple scattering Green's function in the form

$$\begin{aligned} G(\mathbf{r}, \mathbf{r}', E) = &\sum_L Z_L(\mathbf{r}_i, E)\tau^{ij}_{LL'}(E)Z_{L'}(\mathbf{r'}_j, E) \\ &-\delta_{ij}\sum_L Z_L(\mathbf{r}_i^<, E)\tilde{J}_L(\mathbf{r}_i^>, E) \end{aligned} \tag{2.55}$$

where $\mathbf{r} = \mathbf{r}_i + \mathbf{R}_i$ is restricted to lie in the i^{th} bounding sphere and $\mathbf{r}' = \mathbf{r'}_j + \mathbf{R}_j$ to lie in the j^{th} sphere. The expression is also valid for $i = j$.

2.2.3 Calculating the Scattering Path Matrix

In order to calculate the multiple scattering Green's function Eq. (2.55), the remaining quantities to be determined are the scattering path matrix elements $\tau^{ij}_{LL'}$.

Eq. (2.54) may be written as a super-matrix equation

$$\underline{\underline{\tau}} = \left[\underline{\underline{t}}^{-1} - \underline{\underline{G}}\right]^{-1} \tag{2.56}$$

which has site matrix elements

$$\underline{\tau}^{ij}(E) = \underline{t}^i(E)\delta_{ij} + \sum_{k\neq i}\underline{t}^i(E)\underline{G}(\mathbf{R}_{ik}, E)\underline{\tau}^{kj}(E) \tag{2.57}$$

These site matrix elements are themselves matrices in angular momentum space given by Eq. (2.54). Therefore they may be determined by

$$\tau^{ij}_{LL'} = \left[\left(\underline{\underline{t}}^{-1} - \underline{\underline{G}}\right)^{-1}\right]^{ij}_{LL'} \tag{2.58}$$

where the notation implies taking the $\{ij\}^{th}$ and $\{LL'\}^{th}$ element of the super-matrix on the right-hand side. However, for a real system with $N \sim 10^{23}$ scattering centres, this requires the inversion of a huge matrix.

Fortunately, for an ordered system, use may be made of the fact that in the limit $N \to \infty$ the quantities in Eq. (2.57) are *translationally-invariant* i.e. depend only on the difference $i - j$ rather than the absolute positions of sites i and j. Such quantities are diagonal in reciprocal space where they are periodic, and so Eq. (2.54) may instead be solved via a *lattice Fourier transform.* For the path matrix and the structure constants these are defined as

$$\tau_{LL'}(\mathbf{k}, E) = \frac{1}{N} \sum_{ij} \tau^{ij}_{LL'}(E) e^{-i\mathbf{k}(\mathbf{R}_i - \mathbf{R}_j)} \tag{2.59}$$

$$G_{LL'}(\mathbf{k}, E) = \frac{1}{N} \sum_{ij} G^{ij}_{LL'}(\mathbf{R}_i - \mathbf{R}_j, E) e^{-i\mathbf{k}(\mathbf{R}_i - \mathbf{R}_j)} \tag{2.60}$$

where N is the number of lattice sites. The t-matrix is diagonal in the site indices and is therefore independent of $\mathbf{k}$. The path matrix elements $\tau^{ij}_{LL'}$ are now given by the inverse Fourier transform of Eq. (2.59), which as $N \to \infty$ is given by

$$\tau^{ij}_{LL'}(E) = \frac{1}{\Omega_{BZ}} \int d\mathbf{k} \tau_{LL'}(\mathbf{k}, E) e^{i\mathbf{k}(\mathbf{R}_i - \mathbf{R}_j)} \tag{2.61}$$

where Ω_{BZ} is the volume of the first Brillouin zone. The Fourier transform of Eq. (2.57) is

$$\underline{\tau}(\mathbf{k}, E) = \left[\underline{t}^{-1}(E) - \underline{G}(\mathbf{k}, E)\right]^{-1} \tag{2.62}$$

and so finally

$$\tau^{ij}_{LL'}(E) = \frac{1}{\Omega_{BZ}} \int d\mathbf{k} e^{i\mathbf{k}(\mathbf{R}_i - \mathbf{R}_j)} \left[\left(\underline{t}^{-1}(E) - \underline{G}(\mathbf{k}, E)\right)^{-1}\right]_{LL'} \tag{2.63}$$

This Brillouin zone integral is computationally the most demanding task in calculating the single-electron Green's function Eq. (2.55). In practice, it is a reasonable approximation to truncate the angular momentum expansion at $l = 2$ or $l = 3$.

2.2.4 Calculating Observable Quantities

In a spectral decomposed form the total Green's function Eq. (2.14) in a coordinate representation can be written as

$$G(\mathbf{r}, \mathbf{r}', E) = \sum_n \frac{\phi_n(\mathbf{r})\phi_n^\dagger(\mathbf{r}')}{E - E_n} \tag{2.64}$$

The E_n are the energy eigenvalues and $\phi_n(\mathbf{r})$ are the normalised eigenvectors of Eq. (2.10) which form a complete basis set.

It can be seen that the energy eigenvalues occur at the poles of the Green's function, and hence from Eq. (2.55) at the poles of the scattering path matrix. Therefore a way to determine the electronic bandstructure or dispersion relation $E(\mathbf{k})$ is to find the poles of the scattering path matrix. From Eq. (2.62) these occur when

$$\|\underline{t}^{-1}(E) - \underline{G}(\mathbf{k}, E)\| = 0 \tag{2.65}$$

The KKR determinant Eq. (2.65) may be solved as a function of E for a fixed value of $\mathbf{k}$ or vice-versa, referred to as the "E-search" or "k-search" modes respectively. This method of determining the bandstructure is computationally convenient due to the complete separation between the potential and the structural aspects of the scattering problem, which are contained within the t-matrix and the structure constants respectively.

Single-particle observable quantities such as the density of states, charge density, magnetic moments etc. can be calculated from the single-electron Green's function (2.55). For example, it can be shown that the electron density is given by

$$n(\mathbf{r}) = -\frac{1}{\pi} Im \int_{-\infty}^{E_F} G(\mathbf{r}, \mathbf{r}, E) dE \tag{2.66}$$

where the integral is from the lowest eigenvalue up to the Fermi energy E_F. The charge density is then simply given by $\rho(\mathbf{r}) = en(\mathbf{r})$. The density of states per site is given by

$$n(E) = -\frac{1}{\pi} Im \int G(\mathbf{r}, \mathbf{r}, E) dr \tag{2.67}$$

where the integral is over $\mathbf{r}$ within a single site.

This section has explained how to calculate observable quantities for an ordered system. However for a random system where there is no longer any periodicity, Eq. (2.56) cannot be solved using a lattice Fourier transform, and so a different approach is required. The approach to dealing with substitutionally-disordered systems is the subject of the next chapter.

Chapter 3

Disordered Systems

The obvious difficulty in dealing with random substitutionally-disordered systems described in Chapter 1 is the absence of translational invariance (see Fig. 1.1(a)) i.e. Bloch's theorem no longer holds. For comparison with experiment, properties in principle need to be calculated for every possible disorder configuration and then averaged according to the probability of occurrence of each configuration. This is obviously not feasible in practice, and clearly an alternative route must be sought.

One approach is to average over configurations of repeating 'supercells' [31]. This however does not allow disorder effects to be treated beyond the scale of the supercell, and is also a very computationally demanding method. An alternative and widely used approach is to determine an *effective medium* [32, 33] which aims to mimic as closely as possible the properties of the configurationally-averaged alloy. By definition the effective medium is translationally-invariant, and hence Bloch's theorem holds. Techniques such as the lattice Fourier transform used in calculating the properties of pure ordered systems now become valid.

Some simple effective medium approaches, the Virtual Crystal Approximation (VCA) [34], and the Average t-matrix Approximation (ATA) [35] are described below. However, over the past 30 years or so the coherent potential approximation

(CPA) [36, 37] has proved to be the most successful effective medium theory [38, 39]. Within the context of KKR multiple scattering theory, the KKR-CPA [3, 5, 4] determines an effective medium consisting of an ordered array of effective scatterers described by the same t-matrix $\underline{\bar{t}}$. The scattering amplitude describing these effective scatterers is determined using the self-consistency condition that excess scattering off a single-site impurity embedded in such a medium should be zero on the average. However being in essence a single-site mean-field theory [40], the CPA is not a fully-satisfactory theory of disorder and leaves much important physics out of consideration. In this Chapter, the KKR-CPA is described in more detail, some of its successful applications outlined, and then its limitations are explained.

3.1 Effective Medium Theories

When faced with the task of constructing an effective medium, perhaps the most obvious way to proceed would be to attempt to construct some kind of average muffin-tin potential. For example one could simply place the same average potential $\bar{v}^{VCA}(\mathbf{r})$ on each site, obtained by averaging the potentials associated with the constituent atoms of type α i.e.

$$\bar{v}^{VCA}(\mathbf{r}) = \sum_{\alpha} P(\alpha) v_{\alpha}(\mathbf{r}) \tag{3.1}$$

where $P(\alpha)$ is the concentration of sites of type α in the alloy. This is known as the Virtual Crystal Approximation (VCA). The potential $\bar{v}^{VCA}(\mathbf{r})$ is real and its scattering properties are described by the matrix $\underline{\bar{t}}^{VCA}$ which is placed on every site. This translational-invariance means that the scattering path matrix may now be calculated through the Brillouin zone integral

$$\underline{\bar{\tau}}^{ij} = \frac{1}{\Omega_{BZ}} \int_{\Omega_{BZ}} d\mathbf{k} \left((\underline{\bar{t}}^{VCA})^{-1} - \underline{G}(\mathbf{k}) \right)^{-1} e^{i\mathbf{k}(\mathbf{R}_i - \mathbf{R}_j)} \tag{3.2}$$

in analogy to Section 2.2.3. However the VCA is based upon a perturbation theory argument, and can be shown to be mathematically wrong. The energy eigenvalues of an alloy are fundamentally different from those of the pure constituents and therefore

perturbation theory cannot lead from one set of states to another [6]. The VCA can however give reasonable results for a very dilute alloy or when the constituent potentials are similar.

Another way to proceed would be to average the scattering matrices associated with each atomic species α i.e.

$$\underline{\bar{t}}^{ATA}(\mathbf{r}) = \sum_{\alpha} P(\alpha) t_{\alpha}(\mathbf{r}) \tag{3.3}$$

and place this average t-matrix on each site. Translational invariance means that the scattering path matrix may be calculated by

$$\underline{\bar{\tau}}^{ij} = \frac{1}{\Omega_{BZ}} \int_{\Omega_{BZ}} d\mathbf{k} \left((\underline{\bar{t}}^{ATA})^{-1} - \underline{G}(\mathbf{k}) \right)^{-1} e^{i\mathbf{k}(\mathbf{R}_i - \mathbf{R}_j)} \tag{3.4}$$

The ATA is an improvement over the VCA, yielding impurity bands and momentum states with finite lifetimes, but it is incapable of correctly reproducing band edges [6].

3.1.1 Korringa-Kohn-Rostoker Coherent-Potential Approximation (KKR-CPA)

The best and most sophisticated effective medium theory has proved to be the Coherent Potential Approximation (CPA) [36, 37]. The CPA is a vast improvement over the VCA and ATA approaches described in Section 3.1, and is derived within the KKR framework in this section. Many different methods can be used to derive the KKR-CPA equations, but here the 'renormalised interactor' approach [6, 41] is used, as this is the formalism that will be used in Chapter 5 to derive the nonlocal version (KKR-NLCPA).

We begin by considering the usual expression for the scattering path matrix Eq. (2.57)

$$\underline{\tau}^{ij} = \underline{t}^{i}\, \delta_{ij} + \sum_{k \neq i} \underline{t}^{i}\, \underline{G}(\mathbf{R}_{ik}) \underline{\tau}^{kj} \tag{3.5}$$

Now consider the (as of yet undetermined) KKR-CPA effective medium comprising of identical effective scatterers $\underline{\bar{t}}$. The scattering path matrix $\underline{\bar{\tau}}^{ij}$ describing such a

medium is given by

$$\underline{\overline{\tau}}^{ij} = \underline{\overline{t}}^{i}\,\delta_{ij} + \sum_{k\neq i} \underline{\overline{t}}^{i}\,\underline{G}(\mathbf{R}_{ik})\underline{\overline{\tau}}^{kj} \tag{3.6}$$

Now consider a site i. Eq. (3.6) for all paths starting and ending on site i becomes

$$\underline{\overline{\tau}}^{ii} = \underline{\overline{t}}^{i}\,\delta_{ij} + \sum_{k\neq i} \underline{\overline{t}}^{i}\,\underline{G}_0(\mathbf{R}_{ik})\underline{\overline{\tau}}^{ki} \tag{3.7}$$

This may be rewritten as

$$\underline{\overline{\tau}}^{ii} = \underline{\overline{t}}^{i}\,\delta_{ij} + \underline{\overline{t}}^{i}\,\underline{\overline{\Delta}}^{ii}\underline{\overline{\tau}}^{ii} \tag{3.8}$$

or

$$\underline{\overline{\tau}}^{ii} = \left(\underline{\overline{t}}^{i\,-1} - \underline{\overline{\Delta}}^{ii}\right)^{-1} \tag{3.9}$$

where the renormalised interactor $\underline{\overline{\Delta}}^{ii}$ is given by the expansion

$$\underline{\overline{\Delta}}^{ii} = \sum_{k\neq i} \underline{G}_0(\mathbf{R}_{ik})\underline{\overline{t}}^{k}\,\underline{G}_0(\mathbf{R}_{ki}) + \sum_{k\neq i}\sum_{l\neq k,i} \underline{G}_0(\mathbf{R}_{ik})\underline{\overline{t}}^{k}\,\underline{G}_0(\mathbf{R}_{kl})\underline{\overline{t}}^{l}\,\underline{G}_0(\mathbf{R}_{li}) + \cdots \tag{3.10}$$

It can be seen from Eq. (3.10) that the renormalised interactor describes the interaction of site i with the rest of the KKR-CPA medium i.e. describes all paths starting and ending on site i which avoid site i at all intermediate steps. $\underline{\Delta}^{ii}$ is therefore independent of the nature of the potential at site i. This means that if the scatterer at site i is replaced with a real t-matrix of type α (e.g. A or B), then the path matrix for paths starting and ending on this impurity site embedded in the KKR-CPA medium is given by

$$\underline{\tau}_{\alpha}^{ii} = \left(\underline{t}_{\alpha}^{i\,-1} - \underline{\overline{\Delta}}^{ii}\right)^{-1} \tag{3.11}$$

or

$$\underline{\tau}_{\alpha}^{ii} = \left[\underline{\overline{\tau}}^{ii\,-1} + \underline{t}_{\alpha}^{i\,-1} - \underline{\overline{t}}^{i\,-1}\right]^{-1} \tag{3.12}$$

by substituting for $\underline{\Delta}^{ii}$ using Eq. (3.9).

We are now in a position to determine the effective medium. The KKR-CPA requires that excess scattering off this impurity site be zero on the average (i.e. when averaged over the probability of the impurity site being an A or a B site). Formally, the KKR-CPA self-consistency condition requires that

$$\sum_{\alpha} P(\alpha)\underline{\tau}_{\alpha}^{ii} = \underline{\overline{\tau}}^{ii} \tag{3.13}$$

i.e. consider the path matrix for paths starting and ending on the impurity site in the KKR-CPA medium ($\underline{t}_\alpha$ on site i and $\underline{\bar{t}}$ on every other site), and demand that on the average this be equal to the path matrix with no impurity present (i.e. with $\underline{\bar{t}}$ placed on all sites).

Since we require the KKR-CPA effective medium to be translationally-invariant, $\underline{\bar{\tau}}^{ii}$ must also satisfy the Brillouin zone integral

$$\underline{\bar{\tau}}^{ii} = \frac{1}{\Omega_{BZ}} \int_{\Omega_{BZ}} d\mathbf{k} \left(\underline{\bar{t}}^{-1} - G(\mathbf{k}) \right)^{-1} \tag{3.14}$$

which follows by applying a lattice Fourier transform (see Section 2.2.3) to Eq. (3.6) and then considering the ii^{th} matrix element.

Therefore in order to determine the KKR-CPA effective medium, Eq. (3.13) and Eq. (3.14) must both be satisfied simultaneously. There is one unknown matrix parameter $\underline{\bar{t}}$, and so in practice a guess must first be made for $\underline{\bar{t}}$ for example by using the ATA, and then the equations are solved by iteration until self-consistency is achieved (so that the output $\underline{\bar{t}}$ is the same as the input $\underline{\bar{t}}$ to within the desired accuracy).

In order to calculate observable quantities, an expression is needed for the configurationally-averaged multiple-scattering Green's function calculated within the KKR-CPA. The correct way of performing this averaging has been given by Faulkner and Stocks [28]. How to obtain the site-diagonal configurationally-averaged Green's function for a binary alloy is briefly described here.

The expression for the Green's function before averaging is given by Eq. (2.55).

$$\begin{aligned} G(E, \mathbf{r}_i, \mathbf{r}'_j) = & \sum_{LL'} Z^i_L(E, \mathbf{r}_i) \tau^{ij}_{LL'} Z^j_{L'}(E, \mathbf{r}'_j) \\ & - \sum_{L} Z^i_L(E, \mathbf{r}_i) \tilde{J}^i_L(E, \mathbf{r}'_i) \delta_{ij} \end{aligned} \tag{3.15}$$

where $L(= l, m)$ is an angular momentum index and $\mathbf{r}_i(\mathbf{r}'_j)$ lies within the unit cell centered at site $i(j)$. $Z^i_L(E, \mathbf{r}_i)$ and $\tilde{J}^i_L(E, \mathbf{r}_i)$ are the regular and irregular solutions respectively of the single-site problem at site i (see Section 2.2.1).

Now consider a site i so that $\mathbf{r}$ and $\mathbf{r}'$ lie in the neighbourhood of i. The first step is to average Eq. (3.15) over the subset of possible disorder configurations that leave the potential in site i fixed:

$$\langle G(E,\mathbf{r}_i,\mathbf{r}'_i)\rangle = \sum_{LL'} Z^i_L(E,\mathbf{r}_i)\langle\tau^{ii}_{LL'}\rangle_i Z^i_{L'}(E,\mathbf{r}'_i) - \sum_L Z^i_L(E,\mathbf{r}_i)\tilde{J}^i_L(E,\mathbf{r}'_i) \tag{3.16}$$

where $\langle\tau^{ii}_{LL'}\rangle_i$ is the path matrix for paths starting and ending at site i conditionally averaged so that the potential on site i is known (to either be of type A or B). The final step is to average over the possible occupants of site i itself:

$$\begin{aligned}\langle G(E,\mathbf{r}_i,\mathbf{r}'_i)\rangle = \sum_{LL'}\Big[&P(A)Z^A_L(E,\mathbf{r}_i)\langle\tau^{ii}_{LL'}\rangle_A Z^i_{L'}(E,\mathbf{r}'_i) \\ &+P(B)Z^B_L(E,\mathbf{r}_i)\langle\tau^{ii}_{LL'}\rangle_B Z^i_{L'}(E,\mathbf{r}'_i)\Big] \\ -\sum_L\Big[&P(A)Z^A_L(E,\mathbf{r}_i)\tilde{J}^A_L(E,\mathbf{r}'_i) + P(B)Z^B_L(E,\mathbf{r}_i)\tilde{J}^B_L(E,\mathbf{r}'_i)\Big]\end{aligned} \tag{3.17}$$

The above expression is still exact at this stage, but now an approximation has to be made. In the KKR-CPA, $\langle\tau^{ii}_{LL'}\rangle_A$ and $\langle\tau^{ii}_{LL'}\rangle_B$ are constructed using an 'impurity' site of type A or B embedded in the KKR-CPA effective medium. From Eq. (3.12), this is given by

$$\langle\tau^{ii}_{LL'}\rangle_\alpha = \left[\left(\underline{\overline{\tau}}^{ii\,-1} + \underline{t}^{i\,-1}_\alpha - \underline{\overline{t}}^{i\,-1}\right)^{-1}\right]_{LL'} \tag{3.18}$$

where α denotes a site of type A or B. The resulting KKR-CPA approximation to the exact configurationally-averaged Green's function is denoted by $\overline{G}(E,\mathbf{r}_i,\mathbf{r}'_i)$.

Site-diagonal observable quantities can now be calculated from $\overline{G}(E,\mathbf{r}_i,\mathbf{r}'_i)$ in analogy to Section 2.2.4 for pure ordered systems. Furthermore, 'site-restricted-averaged' quantities may also be defined. For example, site-restricted charge densities

$$\rho_\alpha(\mathbf{r}_i) = -\frac{1}{\pi} Im \int_{-\infty}^{E_F} G_\alpha(E,\mathbf{r}_i,\mathbf{r}_i)dE \tag{3.19}$$

and component densities of states

$$n_\alpha(E) = -\frac{1}{\pi} Im \int G_\alpha(E,\mathbf{r}_i,\mathbf{r}_i)dr \tag{3.20}$$

Here $G_\alpha(E, \mathbf{r}_i, \mathbf{r}_i)$ is the site-restricted-averaged Green's function which has an atom of type α residing on site i i.e.

$$\overline{G}_\alpha(E, \mathbf{r}_i, \mathbf{r}'_i) = P(\alpha) \sum_{LL'} Z^i_L(E, \mathbf{r}_i) \langle \tau^{ii}_{LL'} \rangle_i Z^i_{L'}(E, \mathbf{r}'_i) - P(\alpha) \sum_{L} Z^i_L(E, \mathbf{r}_i) \tilde{J}^i_L(E, \mathbf{r}'_i) \tag{3.21}$$

3.1.2 Charge Self-Consistency

The self-consistent field (SCF)-KKR-CPA [42, 43, 44, 45] combines density functional theory (DFT) compatibly with the approximations made in treating the disorder by the KKR-CPA, and has been widely used for calculating the equilibrium properties of disordered phases of alloys. In principle the total energy of an alloy as a functional of the charge density (Eq. (2.3)) should be minimised for each possible disorder configuration individually and then an average taken over all disorder configurations. This is clearly not computationally feasible, and so in the spirit of mean-field theory the SCF-KKR-CPA bypasses these computational difficulties by reversing the order of the minimisation and the configurational averaging.

In brief, the strategy of the SCF-KKR-CPA is to minimise a functional $\Omega[\rho_A(\mathbf{r}), \rho_B(\mathbf{r})]$ with respect to site-restricted-average charge densities $\rho_A(\mathbf{r})$ and $\rho_B(\mathbf{r})$. The functional $\Omega[\rho_A(\mathbf{r}), \rho_B(\mathbf{r})]$ is known as the electronic Grand Potential and is the configurationally-averaged total energy functional with the number of electrons constrained according to the electronic chemical potential μ [46, 2]. For a binary A_cB_{1-c} alloy, $\rho_A(\mathbf{r})$ and $\rho_B(\mathbf{r})$ are the average of the charge densities arising from all disorder configurations that have either an A-type or a B-type atom respectively fixed on one site. This maps the many electron problem to that of a single electron moving through disordered arrangements of single site effective potentials $V^{eff}_A(\mathbf{r} - \mathbf{R}_i)$ and $V^{eff}_B(\mathbf{r} - \mathbf{R}_i)$, which may be solved self-consistently using the KKR-CPA. For a binary alloy, the main steps involved in obtaining charge self-consistency are briefly described below.

1. First assume some input effective single-site potentials $V_A(\mathbf{r}-\mathbf{R}_i)$ and $V_B(\mathbf{r}-\mathbf{R}_i)$. These are taken to depend only on the charge density in the unit cell centred at $\mathbf{R}_i$ and on the average charge density everywhere else i.e. in the spirit of a mean-field theory intersite charge correlations are neglected. From these potentials calculate the single-site t-matrices $\underline{t}_A$ and $\underline{t}_B$.

2. Use the KKR-CPA to determine the effective t-matrix $\bar{\underline{t}}$ and place this on every site. Instead of using $\bar{\underline{\tau}}^{ii}$ to determine the average single-site charge density $\bar{\rho}_i$, do the following:

3. Place a t-matrix $\underline{t}_A$ or $\underline{t}_B$ on an impurity site i (with $\bar{\underline{t}}$ remaining on every other site) and hence determine the impurity path matrix $\underline{\tau}_A^{ii}$ or $\underline{\tau}_B^{ii}$ respectively from Eq. (3.12) for paths starting and ending on the impurity site.

4. Use $\underline{\tau}_A^{ii}$ and $\underline{\tau}_B^{ii}$ to calculate the site-restricted-average charge densities $\bar{\rho}_A(\mathbf{r})$ and $\bar{\rho}_B(\mathbf{r})$ via Eq. (3.19) i.e. approximate site-restricted-average quantities by using a single-site impurity embedded in the KKR-CPA effective medium.

   Note that $P(A)\underline{t}_A + P(B)\underline{t}_B \neq \bar{\underline{t}}$ in general, however $P(A)\underline{\tau}_A^{ii} + P(B)\underline{\tau}_B^{ii} = \bar{\underline{\tau}}^{ii}$ and hence the average single-site charge density is given by $\bar{\rho} = P(A)\bar{\rho}_A + P(B)\bar{\rho}_B$.

5. Place the average single-site charge density $\bar{\rho}$ on every site except at site i place $\bar{\rho}_A$ or $\bar{\rho}_B$. New single site potentials $V_A(\mathbf{r}-\mathbf{R}_i)$ and $V_B(\mathbf{r}-\mathbf{R}_i)$ may now be constructed since they only depend on the charge density at site i and the average charge density everywhere else.

6. Iterate to self-consistency so that the output potentials equal the input potentials to the desired accuracy, thus making them consistent with the site-restricted-average charge densities $\bar{\rho}_A$ and $\bar{\rho}_B$.

7. Once self-consistency is achieved, calculate suitable equilibrium properties such as the total energy, momentum density etc.

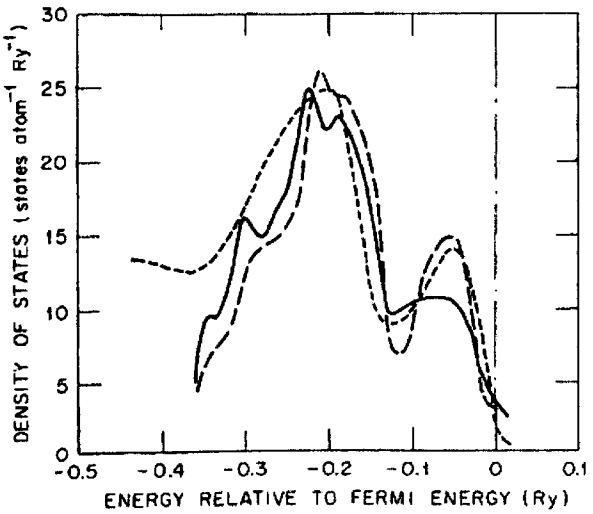

Figure 3.1: Density of states for $Cu_{0.77}Ni_{0.23}$. Full line, KKR-CPA results. Dashed line, model calculations by G. M. Stocks, R. W. Williams, J. S. Faulkner, Phys. Rev. B 4, 4390 (1971). Dotted line, experimental photoemission data by N. J. Shevshik and C. M. Penchina, Phys. Status Solidi (b) 70, 619 (1975). Figure reproduced from G. M. Stocks, W. M. Temmerman, B. L. Gyorffy, Phys. Rev. Lett. 41, 339 (1978)

3.1.3 Successful Applications of the KKR-CPA

There have been numerous successful applications of the KKR-CPA. As a few examples, Fig. 3.1 shows the density of states of $CuNi$, one of the first realistic density of states calculations for an alloy, reproducing a Ni impurity band near the Fermi energy seen in photoemission experiments. Fig. 3.2 shows one of the first SCF-KKR-CPA calculations, giving good agreement with experiment for the calculation of the lattice constant for $CuZn$ alloys. Fig. 3.3 shows the density of states of $NiPt$, predicting the well known low temperature ordered structure in agreement with experiment [47]. More recently the KKR-CPA has given results in good agreement with the first high resolution experimental determination of the Fermi surface of an alloy, $CuPd$, shown in Figs. 3.4 and 3.5.

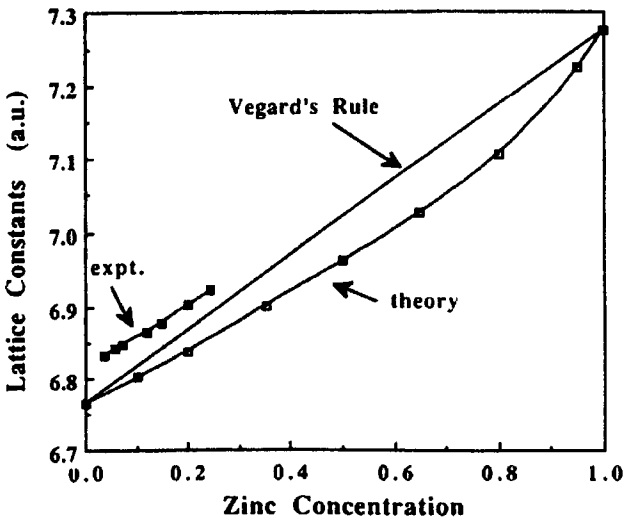

Figure 3.2: Concentration variation of the lattice constant for fcc $CuZn$ alloys. Figure reproduced from D. D. Johnson *et. al.*, Phys. Rev. B 41, 9701 (1990)

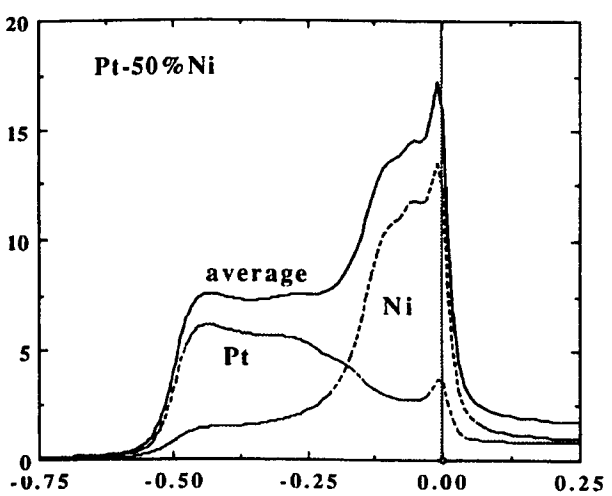

Figure 3.3: The density of states of $Ni_{0.5}Pt_{0.5}$ as a function of energy. The solid line is the average with the dashed lines showing contributions on the Pt and Ni sites. Figure reproduced from F. J. Pinski *et. al.*, Phys. Rev. Lett. 66, 766 (1991)

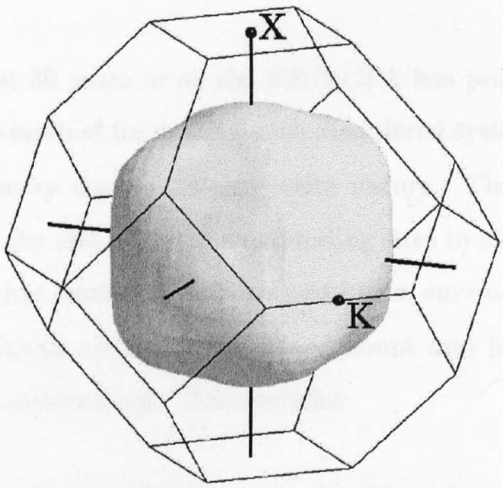

Figure 3.4: The Fermi surface of $Cu_{0.6}Pd_{0.4}$, reconstructed from positron annihilation (2D-ACAR) projections. Figure reproduced from I. Wilkinson *et. al.*, Phys. Rev. Lett. 87, 216401 (2001)

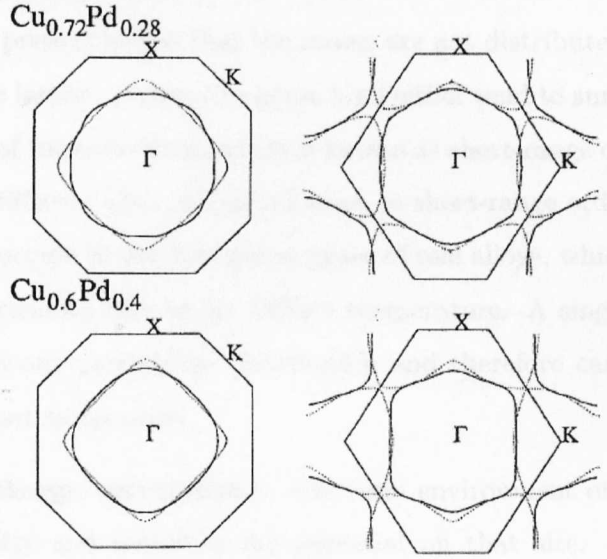

Figure 3.5: (100) (left hand side) and (110) (right hand side) planes through the Fermi surface of $Cu_{0.72}Pd_{0.28}$ (top) and $Cu_{0.6}Pd_{0.4}$ (bottom). The solid lines represent the experimental data and the dashed lines the KKR-CPA calculation; the boundary and selected symmetry points of the first BZ are also shown. Figure reproduced from I. Wilkinson *et. al.*, Phys. Rev. Lett. 87, 216401 (2001)

3.2 Limitations of the KKR-CPA

Although over the past 30 years or so the KKR-CPA has proved to be a generally reliable first principles method for dealing with disordered systems, it is by no means a fully satisfactory theory due to its single-site nature. The KKR-CPA treats a single site exactly but the effects of the surrounding sites in an averaged, mean-field manner. This means that statistical fluctuations in the environment of a site due to the disorder configurations are not taken into account and hence much important physics is left out of consideration. This includes:

1. **Nonlocal scattering correlations** i.e. the effect on the single-electron wavefunction due to multiple scattering off a disordered configuration of a cluster of sites, for example. It is these correlated scatterings which are responsible for band tailing and sharp structure in the density of states [6].

2. **Short-range-order** effects on the electronic structure. An alloy with short-range order present means that the atoms are not distributed completely randomly in the lattice. Atoms of a given kind either tend to surround themselves with atoms of the same kind, which is known as short-range clustering, or with atoms of a different kind, which is known as short-range ordering. This situation always occurs in the disordered phase of real alloys, which are in principle completely random only at an infinite temperature. A single-site theory has only a single-site probability distribution and therefore cannot describe the effects of short-range order.

3. **Nonlocal charge correlations**. The local environment of a site affects the charge density and therefore the potential on that site. Although charge self-consistency for the KKR-CPA is achieved by combination with density functional theory (see SCF-KKR-CPA above), the effects of nonlocal intersite charge-correlations are neglected. Within the SCF-KKR-CPA, charge neutrality requires the average net charge on a single site to vanish. Therefore, the intersite electrostatic energy formed from these single-site charges also

vanishes. This missing 'charge-correlation' or Madelung contribution to the total energy can be substantial [48, 49, 50], and subsequently attempts have been made to find a way of including it approximately within the single-site framework [45, 51].

4. **Lattice displacement effects.** Disordered arrangements of atoms cause the nuclei to be displaced from their perfect lattice positions. This effect is intertwined with charge correlations and is particularly prominent when there is a notable size difference between the constituent atomic species e.g. alloys comprising $3d$ and $5d$ transition metals such as $CuAu$, $NiPt$, CrW etc. Lattice displacements can play a significant role in determining properties, but in all SCF-KKR-CPA calculations to date it has been necessary to assume a rigidly fixed lattice [52].

In addition to the significant impact of the above missing physics upon many calculated physical properties of the material (e.g. formation of magnetic moments, resistivity etc.), an electronic description of the disordered phase is also used as a basis for a first-principles theory [5, 53, 52] of the statistical mechanics of the compositional fluctuations in terms of 'concentration waves' [54]. By considering the linear response of the electronic Grand potential to concentration waves as the temperature is lowered, a measure of the short-range order in the system at a temperature T (above T_c) can be determined and compared with data obtained from X-ray diffuse scattering experiments. Unlike other approaches such as the cluster variational method [55] or Monte Carlo simulations [56], a mean-field theory is able to treat both short and long range interactions. However its accuracy comes into question when fluctuations about such a local mean field are significant. In this case calculations for the transition temperature T_c are often inaccurate and incorrect low temperature behaviour can be predicted. The underlying reason for this is the single-site mean-field nature of the SCF-KKR-CPA description of the electronic structure used to calculate the configurational energies. For example, the concentration-wave theory currently determines a measure of short-range order based upon a descrip-

tion of the electronic structure in which no short-range order can be included at the outset. This is described in more detail in Chapter 8.

In order to improve upon the KKR-CPA, it is clearly necessary to go beyond a single-site local mean-field theory and develop a multi-site or cluster theory. However, this has turned out to be a very difficult problem, and the development of a satisfactory cluster theory is discussed in detail in the next chapter.

Chapter 4

Cluster Theories

The KKR-CPA described in Chapter 3 is universally accepted as the best single-site approximation for calculating the properties of substitutionally-disordered alloys [6]. However, the limitations of the KKR-CPA have been discussed in Section 3.2 and it is evident that these limitations can only be addressed by considering a multi-site or cluster theory.

This chapter briefly reviews some attempts at a satisfactory cluster theory. First a brief description is given of the embedded cluster method (KKR-ECM), [6, 41] which is to my knowledge the only first principles cluster method which has been successfully applied to realistic systems, for example $AgPd$ alloys [57]. However, as a non self-consistent theory, it is not fully satisfactory and the requirements for a satisfactory cluster theory are given. A recent theory within a tight-binding description, the NLCPA (nonlocal coherent potential approximation), is the first to satisfy all these requirements and it is described together with the MCPA (molecular coherent potential approximation), an earlier cluster theory which highlights some problems overcome by the NLCPA.

4.1 Embedded Cluster Method (KKR-ECM)

The KKR-ECM is concerned with the treatment of a cluster of impurity potentials embedded in the predetermined KKR-CPA medium.

The first step is to view the lattice as being made up of a collection of non-overlapping clusters $\{C\}$ and to rewrite the KKR-CPA path matrix equation Eq. (3.6) in the form of a cluster equation

$$\underline{\underline{\tau}}^{CC'} = \underline{\underline{t}}^{C}_{cl}\,\delta_{CC'} + \sum_{C''\neq C} \underline{\underline{t}}^{C}_{cl}\,\underline{\underline{G}}^{CC''}\,\underline{\underline{\tau}}^{C''C'} \tag{4.1}$$

Here the double underscores denote super-matrices in both angular momentum space and cluster-site space. In this way, the site-matrix elements are themselves matrices in angular momentum space i.e.

$$\left[\underline{\underline{\tau}}^{CC'}\right]^{ij} = \underline{\tau}^{ij}, \quad i \in C,\ j \in C' \tag{4.2}$$

$$\left[\underline{\underline{G}}^{CC'}\right]^{ij} = \underline{G}(\mathbf{R}_{ij}), \quad i \in C,\ j \in C',\ C \neq C' \tag{4.3}$$

$$\left\{\left[\underline{\underline{t}}^{C}_{cl}\right]^{-1}\right\}^{ij} = \begin{cases} \{\underline{t}^{-1}\}^{ij}, & i = j,\ i \in C \\ -\underline{G}(\mathbf{R}_{ij}), & i \neq j,\ i \in C,\ j \in C \end{cases} \tag{4.4}$$

The cluster t-matrix $\underline{\underline{t}}^{C}_{cl}$ describes the total scattering from a cluster and $\underline{\underline{G}}^{CC'}$ describes the propagation between clusters. If we consider the cluster-diagonal part of the path matrix $\underline{\underline{\tau}}^{CC}$, then it can be shown [6] that

$$\sum_{C'\neq C} \underline{\underline{G}}^{CC'}\,\underline{\underline{\tau}}^{C'C} = \underline{\underline{\Delta}}^{C}\,\underline{\underline{\tau}}^{CC} \tag{4.5}$$

with the cluster renormalised interactor $\underline{\underline{\Delta}}^{C}$ given by the expansion

$$\left[\underline{\underline{\Delta}}^{C}\right]^{ij} = \sum_{k\notin C} \underline{G}(\mathbf{R}_{ik})\,\underline{t}\,\underline{G}(\mathbf{R}_{kj}) + \sum_{k\notin C, l\notin C} \underline{G}(\mathbf{R}_{ik})\,\underline{t}\,\underline{G}(\mathbf{R}_{kl})\,\underline{t}\,\underline{G}(\mathbf{R}_{lj}) + \cdots \tag{4.6}$$

The cluster-diagonal part of Eq. (4.1) can then be written in the form

$$\underline{\underline{\tau}}^{CC} = \underline{\underline{t}}^{C}_{cl}\,\delta_{CC'} + \underline{\underline{t}}^{C}_{cl}\,\underline{\underline{\Delta}}^{C}\,\underline{\underline{\tau}}^{CC} \tag{4.7}$$

From the expansion in Eq. (4.6), it can be seen that $\underline{\underline{\Delta}}^{C}$ describes all paths from the cluster site i to the cluster site j which only involve intermediate sites outside

of the cluster. It is independent of the contents of the cluster and can be viewed as describing the KKR-CPA effective medium from which the cluster has been removed i.e. replaced by a *cavity*. Therefore this 'renormalisation' of Eq. (4.1) enables us to define an 'impurity cluster' embedded in the effective medium simply by filling up this cavity with a particular configuration of real site potentials.

It follows from Eq. (4.7) that the path matrix for such an impurity cluster is given by

$$\underline{\underline{\tau}}^{CC}_{imp} = \underline{\underline{t}}^{C}_{cl,imp}\,\delta_{CC'} + \underline{\underline{t}}^{C}_{cl,imp}\,\underline{\underline{\Delta}}^{C}\,\underline{\underline{\tau}}^{CC}_{imp} \tag{4.8}$$

Using Eq. (4.7) to eliminate the cluster renormalised interactor yields

$$\underline{\underline{\tau}}^{CC}_{imp} = \left[\left(\underline{\underline{t}}^{C}_{cl,imp}\right)^{-1} - \left(\underline{\underline{\bar{t}}}^{C}_{cl}\right)^{-1} + \left(\underline{\underline{\bar{\tau}}}^{CC}\right)^{-1}\right]^{-1} \tag{4.9}$$

For a particular impurity cluster configuration, the impurity cluster path matrix $\underline{\underline{\tau}}^{CC}_{imp}$ describes all paths starting and ending on the sites of an impurity cluster of real potentials embedded in the KKR-CPA effective medium. The KKR-CPA effective medium cluster path matrix has cluster-site matrix elements given by the usual Brillouin zone integration

$$\left[\underline{\underline{\bar{\tau}}}^{CC}\right]^{ij} = \frac{1}{\Omega_{BZ}}\int_{\Omega_{BZ}} d\mathbf{k}\left(\underline{\underline{\bar{t}}}^{-1} - \underline{\underline{G}}(\mathbf{k})\right)^{-1} e^{i\mathbf{k}(\mathbf{R}_i - \mathbf{R}_j)} \tag{4.10}$$

for sites i,j within the cluster C. The Green's function associated with any sites i,j in the cluster for any particular cluster configuration may now be obtained from Eq. (3.15). Therefore observable quantities such as the density of states for a particular site (usually taken to be the central site) with any given cluster configuration can be obtained. The density of states for the material is then usually approximated by taking the configurational average of this over all the cluster configurations.

The KKR-ECM does give analytic results which take into account local environment effects involving the cluster sites (such as scattering correlations) and is able to take into account the effects of short-range order, albeit non self-consistently [57]. The major limitation of the KKR-ECM is that as a non self-consistent theory, it does not yield a new translationally-invariant effective medium determined self-consistently with respect to the cluster. This is insufficient for describing many

systems since the effects of cluster self-consistency can have a significant effect on the properties. This lack of cluster self-consistency also restricts possible future developments such as combining with density functional theory and obtaining charge self-consistency. However, the development of a satisfactory self-consistent cluster theory has remained a long standing problem.

4.2 A Satisfactory Cluster Theory

The requirements for a successful cluster theory have been described by Gonis [6]. In particular, such a theory should:

- yield herglotz analytic results
- take account of local environment effects in a self-consistent way
- yield an effective medium which possesses the translational-invariance of the original lattice
- become exact in all physical limits
- allow the treatment of the effects of short-range order
- be computationally feasible

Since the CPA was first formulated [36, 37], many attempts were made to develop a successful cluster generalisation. The first attempts (collectively known as CPAn) were based on diagrammatic methods but unfortunately were found to lead to non-analytic results [58]. Most other attempts have mainly been within the framework of a simple tight-binding description of the Hamiltonian. Unfortunately none of these theories satisfy all of the requirements for a successful cluster theory described above. Indeed, while most could be derived within a first-principles framework by formal analogy, only the KKR-ECM described above has found application to realistic systems, mainly due to the physically unsatisfactory or computationally

prohibitive nature of these theories even within a tight-binding description. The Traveling Cluster Approximation (TCA) [59] based on diagrammatic methods and the Cluster CPA (CCPA) [60] based on the Augmented Space Formalism [61] do retain herglotz analytic properties but have proved to be computationally tractable only for pair clusters.

The development of a successful cluster theory has thus remained a long-standing problem, however what appears to be a viable solution within a tight-binding description has been proposed very recently. The new method has emerged from the Dynamical Cluster Approximation [7, 8, 9] (DCA) which was originally invented to describe dynamical short-range correlations within the framework of the Dynamical Mean Field Theory [62] (DMFT) of spin and charge fluctuations in simple Hubbard models of strongly-correlated electron systems. Since DMFT can be regarded as the dynamical generalisation of the CPA for the Hubbard 'alloy analogy' problem [63, 64], it is natural to investigate the static limit of the DCA as a generalisation of the CPA which includes a description of short-range order. Indeed, its static limit has recently been adapted by Jarrell and Krishnamurthy for a simple tight-binding model of electrons moving in a disordered potential [10]. The same problem was investigated by Moradian *et al.* [11, 12] and the theory was named the nonlocal coherent potential approximation (NLCPA). Unlike previous attempts, the NLCPA does satisfy all of the requirements for a satisfactory cluster theory listed above, and is described shortly.

4.2.1 The Tight-Binding Formalism

The tight-binding Hamiltonian operator may be expressed as

$$\hat{H} = \sum_{i,\alpha} \epsilon_{i\alpha}\, c^{+}_{i\alpha} c_{i\alpha} + \sum_{i,j,\alpha,\beta} W_{i\alpha,j\beta}\, c^{+}_{i\alpha} c_{j\beta} \tag{4.11}$$

where $c^{+}_{i\alpha}$ and $c_{i\alpha}$ are the creation and annihilation operators for state vectors associated with 'orbitals' α centred on site i. The $\{\epsilon_i\}$ are the 'site energies' and $\{W_{ij}\}$

the hopping terms. In a basis labelled by the sites of the direct lattice this becomes

$$H_{ij} = \epsilon_i \delta_{ij} + W_{ij}(1 - \delta_{ij}) \tag{4.12}$$

Defining the Green's function operator by $G(E) = (E - H)^{-1}$, with E assumed to have an infinitesimal positive imaginary part, from Eq. (4.12) we obtain the 'locator' equation of motion

$$G_{ij}(E) = g_i \delta_{ij} + g_i \sum_{k \neq i} W_{ik} G_{kj}(E), \tag{4.13}$$

with the bare locator g_i for site i defined as

$$g_i = (E - \epsilon_i)^{-1}. \tag{4.14}$$

Eq. (4.13) can also be put into the form of a Dyson equation or 'propagator' equation of motion

$$G_{ij}(E) = G^0_{ij}(E) + \sum_k G^0_{ik}(E) \epsilon_k G_{kj}(E), \tag{4.15}$$

where the free-particle Green's function $G^0_{ij}(E)$ is the solution of Eq. (4.13) for all site energies $\{\epsilon_i\}$ set to zero. Eq. (4.15) can be iterated to yield the multi-site expansion

$$G_{ij}(E) = G^0_{ij}(E) + \sum_k G^0_{ik}(E) \epsilon_k G^0_{kj}(E) + \sum_{k,l} G^0_{ik}(E) \epsilon_k G^0_{kl}(E) \epsilon_l G^0_{lj}(E) + \cdots \tag{4.16}$$

We are interested in the case of a substitutionally disordered alloy where the site energies $\{\epsilon_i\}$ vary from site to site in a random fashion, and the evaluation of $\langle G \rangle$, the ensemble average of G over all possible disorder configurations. To do this, we define the exact self-energy Σ such that the ensemble averaged Green's function in Eq. (4.16) can be written in the form

$$\langle G_{ij}(E) \rangle = G^0_{ij}(E) + \sum_{k,l} G^0_{ik}(E) \Sigma_{kl}(E) \langle G_{lj}(E) \rangle \tag{4.17}$$

i.e. the translationally-invariant configurationally-averaged medium described by $\langle G \rangle$ is characterised by the translationally-invariant self-energy Σ. Therefore effective medium theories within the tight-binding formalism are concerned with the approximate evaluation of the exact self-energy. For example, the coherent potential approximation (CPA) yields a site-diagonal self-energy $\Sigma_i \delta_{ij}$, the 'coherent

potential', which is analogous to the effective single-site t-matrix in the KKR-CPA (Section 3.1.1). This is a consequence of its failure to take into account local environment effects as described in Section 3.2, a problem which can be addressed by a cluster theory.

4.2.2 Molecular Coherent Potential Approximation (MCPA)

The MCPA [65, 2] is a self-consistent and analytic (though unsatisfactory) cluster theory, and it is described here because it highlights some important problems which are overcome by the NLCPA (Section 4.2.3), in particular the problem of obtaining translational invariance.

The CPA and cluster extensions can be derived in many different ways within the tight-binding framework, for example the 'locator' or 'propagator' methods. Here I rederive the MCPA in terms of the 'cavity Green's function' (or 'cluster excluded propagator') formalism in order for comparison to be made with the NLCPA which has been derived using this approach [10, 11, 12].

In the MCPA, the lattice is viewed as being made up of a collection of identical non-overlapping clusters, a 'superlattice', and the electron wave as being the sum of scattering contributions from these clusters. The main assumption made is that the self-energy is *cluster-diagonal*, and for each cluster C it may be written as a matrix in cluster-site space as $\underline{\Sigma}_C \delta_{CC'}$ with matrix elements

$$[\underline{\Sigma}_C]_{IJ} = \begin{cases} \Sigma_I \delta_{IJ} & \\ \Sigma_{IJ}(1-\delta_{IJ}) & I, J \in C \end{cases} \tag{4.18}$$

It follows from Eq. (4.17) that the Green's function $\overline{G}$ for this MCPA effective medium may also be written in terms of cluster quantities as

$$\underline{\overline{G}}_{CC'} = \underline{G}^0_{CC'} + \sum_{C''} \underline{G}^0_{CC''} \underline{\Sigma}_{C''} \underline{\overline{G}}_{C''C'} \tag{4.19}$$

with matrix elements of the form

$$\left[\underline{\overline{G}}_{CC'}\right]_{ij} = \overline{G}_{ij}, \; i \in C, \; j \in C' \tag{4.20}$$

and

$$\left[\underline{G}^0_{CC'}\right]_{ij} = G^0_{ij},\ i \in C,\ j \in C' \tag{4.21}$$

For clarity, the explicit dependence on energy E has been dropped.

A cluster-diagonal self-energy means that there are no self-energy terms relating sites in different clusters, and hence the medium only has the translational invariance of the super-lattice. This means that the cluster dependence of the above quantities may be removed by defining Fourier transforms of the form

$$\overline{\underline{G}}_{CC}(\mathbf{q}) = \sum_{C'} \overline{\underline{G}}_{CC'} e^{i\mathbf{q}.\mathbf{R}_{CC'}} \tag{4.22}$$

with $\mathbf{R}_{CC'}$ the vector distance between the centres of clusters C and C', and $\mathbf{q}$ a vector in the Brillouin zone of the super-lattice (which will clearly be a smaller Brillouin zone than that of the original lattice). The self-energy is unaffected as it is cluster-diagonal. Eq. (4.19) now becomes

$$\overline{\underline{G}}_{CC}(\mathbf{q}) = \underline{G}^0_{CC}(\mathbf{q}) + \underline{G}^0_{CC}(\mathbf{q})\underline{\Sigma}_C\overline{\underline{G}}_{CC}(\mathbf{q}) \tag{4.23}$$

or

$$\overline{\underline{G}}_{CC}(\mathbf{q}) = \left(\left(\underline{G}^0_{CC}(\mathbf{q})\right)^{-1} - \underline{\Sigma}_C\right)^{-1} \tag{4.24}$$

with free-particle Green's function

$$\underline{G}^0_{CC}(\mathbf{q}) = \left(\underline{E} - \underline{W}_{CC}(\mathbf{q})\right)^{-1} \tag{4.25}$$

It follows that the real-space Green's function for the cluster sites is given by

$$\overline{\underline{G}}_{CC} = \frac{1}{\Omega_{BZ}} \int_{\Omega_{BZ}} d\mathbf{q}\, (\underline{E} - \underline{W}_{CC}(\mathbf{q}) - \underline{\Sigma}_C)^{-1} \tag{4.26}$$

where the integral is over the first Brillouin zone of the super-lattice.

The question now arises as to how this effective medium is determined. This may be done by considering a cluster C, and from Eq. (4.19) the cluster-diagonal part of the Green's function is given by

$$\overline{\underline{G}}_{CC} = \underline{G}^0_{CC} + \sum_{C'} \underline{G}^0_{CC'}\underline{\Sigma}_{C'}\overline{\underline{G}}_{C'C} \tag{4.27}$$

This may be rewritten as

$$\underline{\overline{G}}_{CC} = \underline{\mathcal{G}}_{CC} + \underline{\mathcal{G}}_{CC}\underline{\Sigma}_C\underline{\overline{G}}_{CC} \tag{4.28}$$

where the sum over all clusters has been removed, and these neglected terms have been replaced by introducing the 'cavity Green's function' $\underline{\mathcal{G}}_{CC}$ in place of the free-particle Green's function. The cavity Green's function, in a similar fashion to the cluster renormalised interactor within the KKR framework, describes the effective medium from which the cluster sites have been removed, in other words replaced by a cavity. Since Eq. (4.28) only involves matrices in the space of the sites belonging to the cluster C, it is convenient to label the site matrix elements by capital letters i.e.

$$\overline{G}_{IJ} = \mathcal{G}_{IJ} + \sum_{K,L} \mathcal{G}_{IK}\Sigma_{KL}\overline{G}_{LJ} \tag{4.29}$$

An impurity cluster embedded in the effective medium may now be defined by filling up the cavity with a particular configuration of site energies $\{\epsilon_I\}$ i.e.

$$G^{imp}_{IJ} = \mathcal{G}_{IJ} + \sum_{K} \mathcal{G}_{IK}\epsilon_K G^{imp}_{KJ} \tag{4.30}$$

The MCPA self-consistency condition now follows by demanding that the average of the Green's function over all impurity cluster configurations be equal to that for the effective medium itself i.e.

$$\left\langle G^{imp}_{IJ} \right\rangle = \overline{G}_{IJ} \tag{4.31}$$

The matrix elements $\overline{G}_{IJ}$ must also of course be matrix elements of $\underline{\overline{G}}_{CC}$ defined in Eq. (4.26), and so this process is iterated until Eq. (4.26) and Eq. (4.31) are satisfied simultaneously so that self-consistency is achieved.

As a cluster theory, the MCPA has two major disadvantages. Firstly, it yields an effective medium which does not possess the site-to-site translational invariance of the underlying lattice. Sites in different clusters are not explicitly connected (although interactions between different clusters are treated at a mean-field level) and so there are no self-energy terms relating sites in different clusters. The introduction

of these artificial boundaries can affect the calculation of transport properties etc. This also means that different sites in a cluster give different results when calculating properties. Secondly, the theory is computationally very demanding, mainly due to the integration in Eq. (4.26) which involves matrices in cluster-site space which increase in dimension with increasing cluster size. These drawbacks have prevented the MCPA from being generally applied to realistic systems.

4.2.3 Nonlocal Coherent Potential Approximation (NLCPA)

The NLCPA satisfies all of the requirements for a satisfactory cluster theory described in Section 4.2, and a brief review is given in this section. As the static limit of the DCA, the NLCPA was first derived by Jarrell and Krishnamurthy using the diagrammatic language of perturbation theory [10], however the derivation presented here is consistent with the usual approach of effective medium theories given by Moradian *et. al.* [11, 12].

First note that the exact self-energy defined in Eq. (4.17) is translationally-invariant and may be represented in reciprocal space by the function $\Sigma(\mathbf{k})$. Applying a lattice Fourier transform to Eq. (4.17) gives

$$\langle G(\mathbf{k})\rangle = G^0(\mathbf{k}) + G^0(\mathbf{k})\Sigma(\mathbf{k})\,\langle G(\mathbf{k})\rangle \tag{4.32}$$

The self-energy $\Sigma(\mathbf{k})$ defined in Eq. (4.32) is the static limit of the self-energy central to the Dynamical Cluster Approximation introduced by Hettler *et al.* [7, 8, 9]. In this context, the idea is to sample $\Sigma(\mathbf{k})$ at a finite number of points $\{\mathbf{K}_n\}$ in the first Brillouin zone so that $\Sigma(\mathbf{k}) \to \{\Sigma(\mathbf{K}_n)\}$. This means that the range of nonlocal correlations treated exactly in the self-energy is reduced, but importantly the translational invariance of the medium is retained. This means that the problem can be mapped to that of a self-consistently embedded finite-sized cluster problem.

In more detail, the idea is to divide or 'coarse-grain' the first Brillouin zone into tiles centred at the points $\{\mathbf{K}_n\}$, and to approximate the self-energy $\Sigma(\mathbf{k})$ by the set of coarse-grained values $\Sigma(\mathbf{K}_n)$, each of which are defined to be the average of

$\Sigma(\mathbf{k})$ over the momenta lying within the tile centred at $\mathbf{K}_n$. Consistent with this approximation, the corresponding averaged Green's function $\langle G(\mathbf{k})\rangle$ is approximated by the set of coarse-grained values $\overline{G}(\mathbf{K}_n)$, each of which are defined as

$$\overline{G}(\mathbf{K}_n) = \frac{N_c}{\Omega_{BZ}} \int_{\Omega_{\mathbf{K}_n}} d\mathbf{k} \left(\left(G^0(\mathbf{k}) \right)^{-1} - \Sigma(\mathbf{K}_n) \right)^{-1} \tag{4.33}$$

where $G^0(\mathbf{k}) = (E - W(\mathbf{k}))^{-1}$, and the integral is over the reciprocal space tile surrounding $\mathbf{K}_n$. Here N_c is the number of tiles or $\mathbf{K}_n$ values. Note that these integrals are straightforward since the self-energy is constant within each tile.

As has already been mentioned, approximating the self-energy in reciprocal space in this manner has the effect of reducing the range of the nonlocal correlations treated exactly in real space. In particular, coarse-graining reciprocal space into tiles may be interpreted as coarse-graining real space into tiles i.e. a set of periodically repeating clusters. The set of $\mathbf{K}_n$ values are related to a set of cluster sites $\{I, J\}$ in real space by the Fourier transformation

$$\frac{1}{N_c} \sum_{\mathbf{K}_n} e^{i\mathbf{K}_n(\mathbf{R}_I - \mathbf{R}_J)} = \delta_{IJ}. \tag{4.34}$$

N_c is the number of sites in a cluster, and is the same as the number of $\mathbf{K}_n$ values and tiles in reciprocal space. The shape of the reciprocal space tiles corresponds to the reciprocal space of the shape of the real space tiles or clusters. However a restriction is that the real space tiles and corresponding reciprocal space tiles must preserve the point-group symmetry of the lattice. This is to ensure that equivalent momenta are mapped to the same tile.

In Ref. [10], the self-energy is only considered as a function in coarse-grained reciprocal space, and the problem is Fourier transformed to real space for the impurity problem. Moradian *et al.* [11, 12] used the Fourier transformation Eq. (4.34) to consider the self-energy and Green's function in real space, which is more consistent with the usual approach of effective medium theories and aids physical interpretation of the theory. The self-energy is given by

$$\Sigma_{IJ} = \frac{1}{N_c} \sum_{\mathbf{K}_n} \Sigma(\mathbf{K}_n) e^{i\mathbf{K}_n(\mathbf{R}_I - \mathbf{R}_J)} \tag{4.35}$$

and the Green's function by

$$\overline{G}_{IJ} = \frac{1}{N_c} \sum_{\mathbf{K}_n} G(\mathbf{K}_n) e^{i\mathbf{K}_n(\mathbf{R}_I - \mathbf{R}_J)} \tag{4.36}$$

It might appear that representing the self-energy in this way is equivalent to the MCPA (Section 4.2.2) in assuming it to be cluster diagonal, however this is not the case. Coarse-graining the self-energy in reciprocal space does not destroy the translational invariance. Unlike the MCPA, sites in different clusters are connected and hence the self-energy is *independent of the origin of the set of clusters in real space.* Σ^{IJ} depends only on the difference between the cluster sites I and J, irrespective of which site in the lattice is chosen to be site I. It may be interpreted as a *nonlocal coherent potential*, an idea which was first suggested in the 1970s [33], but at the time it was not realised how to treat the problem consistently in reciprocal space.

The next step is to determine the NLCPA effective medium, which may be achieved in a similar manner to the MCPA. We consider a cluster C with sites labelled by capital letters, and consider the cavity Green's function $\mathcal{G}_{IJ}$ defined by Eq. (4.29)

$$\overline{G}_{IJ} = \mathcal{G}_{IJ} + \sum_{K,L} \mathcal{G}_{IK} \Sigma_{KL} \overline{G}_{LJ} \tag{4.37}$$

which describes a cavity at the cluster sites. An impurity cluster embedded in the effective medium may be defined by filling up the cavity with a particular configuration of site energies $\{\epsilon_I\}$ i.e.

$$G^{imp}_{IJ} = \mathcal{G}_{IJ} + \sum_{K} \mathcal{G}_{IK} \epsilon_K G^{imp}_{KJ} \tag{4.38}$$

In the same way as the MCPA, the NLCPA self-consistency condition now follows by demanding that the average of the Green's function over all impurity cluster configurations be equal to that for the effective medium itself

$$\left\langle G^{imp}_{IJ} \right\rangle = \overline{G}_{IJ} \tag{4.39}$$

However, as has been described, the treatment of the problem by the two approximations is very different in reciprocal space. In the NLCPA, the matrix elements

$\overline{G}_{IJ}$ must also satisfy Eq. (4.36) through Eq. (4.33), and the averaging over impurity clusters is continued until Eq. (4.33) and Eq. (4.39) are satisfied simultaneously so that self-consistency is achieved. Unlike the MCPA, integrating over tiles in Eq. (4.33) and then summing over the tiles means that an integral is essentially performed over the whole Brillouin zone in analogy to the conventional single-site CPA. Furthermore, since this Brillouin zone integration does not involve matrices in cluster-site space, it is no more computationally demanding than the CPA. Finally, note that the NLCPA becomes exact for an infinite cluster and reduces to the CPA for a single-site cluster, in which case the self-energy reduces to the single-site coherent potential.

In order to illustrate some of the improvements of the NLCPA over the conventional CPA, Moradian [11] used a simple one-dimensional tight-binding model to investigate the onset of split-band behaviour. Here I use a similar model with slightly different parameters in order to compare to exact numerical results (histograms) obtained by Gonis [6]. Fig. 4.1 shows the exact density of states results for two pure one-dimensional materials described by nearest neighbour hopping $W = 1.0$ and random site energies $\epsilon_A = +2.0$ and $\epsilon_B = -2.0$. Fig. 4.2 shows exact results for an $A_{50}B_{50}$ alloy together with the CPA results. Although the CPA correctly separates the density of states into two subbands, the gap at $E = 0.0$ should be just vanishing. However the contributions near band edges are due to large clusters of like atoms which are not described by the single-site CPA. Figs. 4.3 and 4.4 show four-site and eight-site NLCPA calculations respectively for the same parameters. It is clear that the result gets closer to the exact result as the cluster size increases. The band gap at $E = 0.0$ is gradually filled in, and the increasing structure in the density of states arises from statistical fluctuations in the local environment of a site which are smoothed out by the single-site mean-field CPA.

However, in order to carry out first-principles ab-initio calculations, an approach compatible with density functional theory (Chapter 2) is required i.e. a method for solving the Kohn-Sham equations (Eq. 2.7) rather than solving a Schrödinger equa-

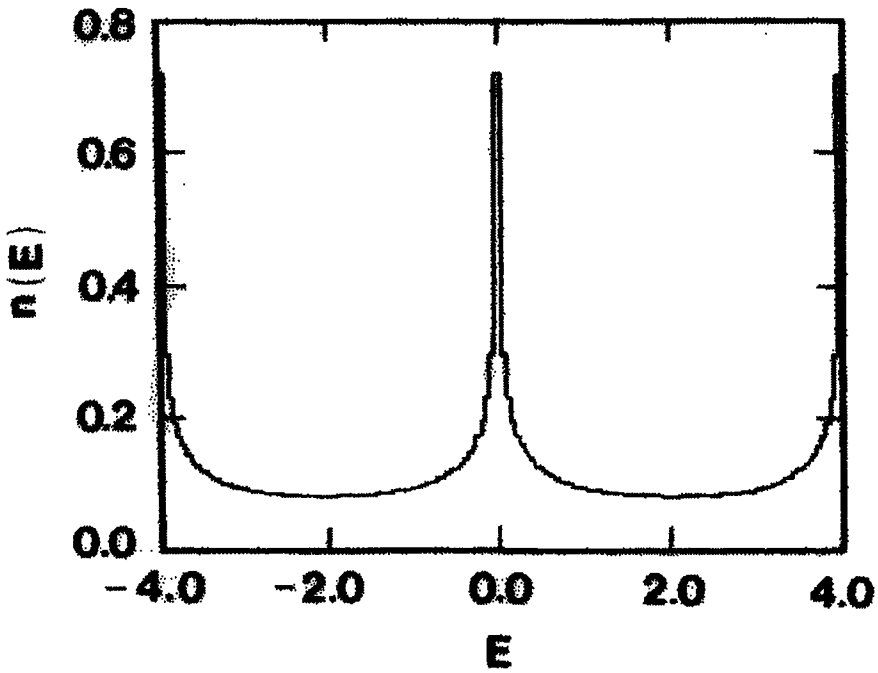

Figure 4.1: Exact density of states histogram for two pure one-dimensional materials described by a nearest neighbour tight-binding Hamiltonian with $\epsilon_A = -\epsilon_B = 2.0$ and $W = 1.0$. Figure reproduced from '*Green Functions for Ordered and Disordered Systems*' Vol. 4 of *Studies in Mathematical Physics* (North Holland, 1992) by A. Gonis

tion for the tight-binding model Hamiltonian Eq. (4.11). For disordered systems, this means an approach based on multiple-scattering theory (Chapter 2). The reformulation of the NLCPA in terms of multiple scattering theory is the subject of the next chapter.

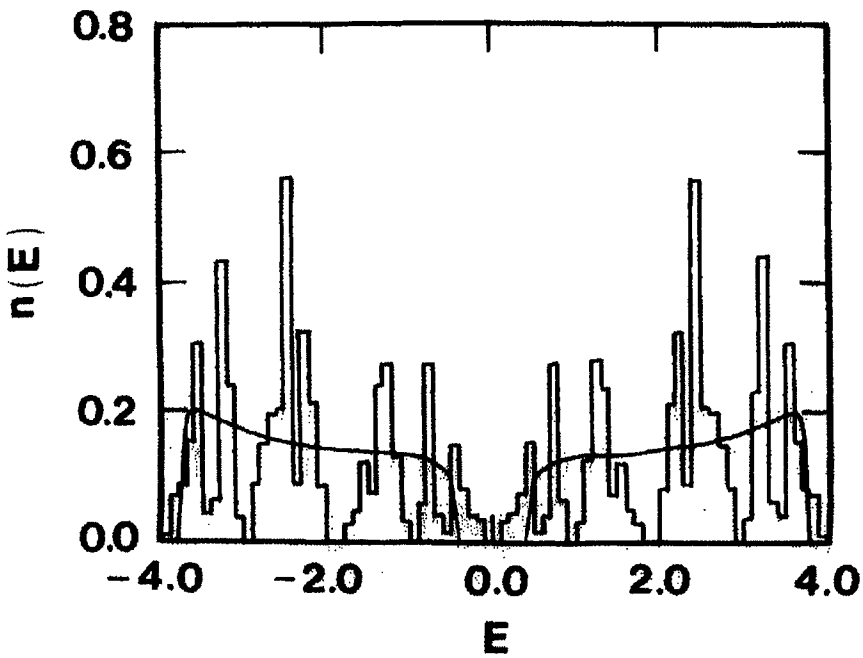

Figure 4.2: Exact density of states histogram together with the CPA results (solid line) for an $A_{50}B_{50}$ alloy of the two pure materials shown in Fig. 4.1. Figure reproduced from '*Green Functions for Ordered and Disordered Systems*' Vol. 4 of *Studies in Mathematical Physics* (North Holland, 1992) by A. Gonis

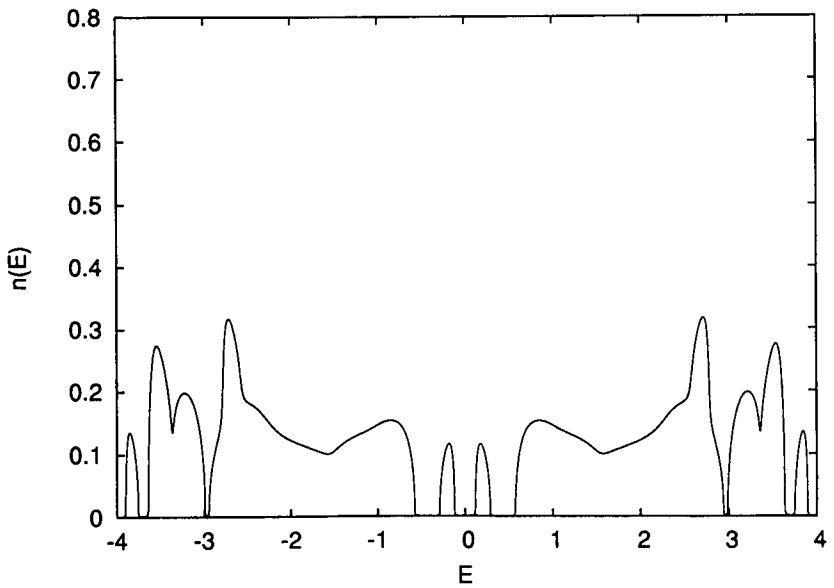

Figure 4.3: A four site NLCPA calculation for the density of states of an $A_{50}B_{50}$ alloy of the two pure materials shown in Fig. 4.1

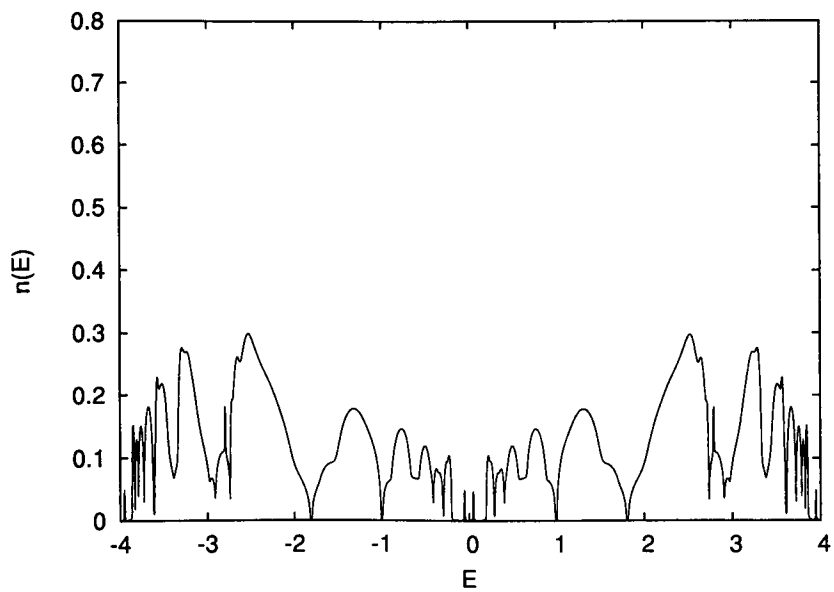

Figure 4.4: An eight site NLCPA calculation for the density of states of an $A_{50}B_{50}$ alloy of the two pure materials shown in Fig. 4.1

Chapter 5

KKR-NLCPA Formalism

The aim of this chapter is to derive the nonlocal coherent-potential approximation (NLCPA) (Section 4.2.3) within the framework of KKR multiple scattering theory [24, 25]. Much of the work in this chapter and the following two chapters has been published in Ref. [66].

Because the language of multiple scattering theory is so different from the context in which the NLCPA originates (i.e. static limit of the Dynamical Cluster Approximation), here some of the principal differences between the treatment of the problem in this chapter and that of Ref. [10] are given. First note that use is not made of a tight-binding model Hamiltonian. Instead a Schrödinger equation is solved numerically in each unit cell and the 'out-going wave' solution is matched to the incoming waves from all the other unit cells. This is known as the multiple scattering approach [24, 25] to the problem of electronic structure in solids and is the foundation of the Korringa-Kohn and Rostoker (KKR) band theory method described in Chapter 2. Consequently, the principal virtue of the formalism presented in this chapter, as opposed to those based on tight-binding model Hamiltonians, is that it prepares the ground for first-principles calculations based on density-functional theories [15]. In multiple scattering theories the object of interest is not the self-energy and the diagrammatic language of perturbation theory is not used. In this chapter it will be

shown that the quantities that play the role of the self-energy in multiple scattering theory are the effective scattering amplitudes $\underline{\hat{t}}$ and effective structure constants $\underline{\hat{G}}(\mathbf{R}^{ij})$. These formal reasons fully account for the fact that the arguments are not based on restoring momentum conservation and introducing approximate Laue functions to renormalise diagrams as in Ref. [10], but the theory is constructed in terms of real and reciprocal space clusters. Nevertheless, the final algorithm described in Sec. 5.2 is equivalent to that investigated by Jarrell and Krishnamurthy [10]. The aim in reformulating the problem is for the purpose of carrying out a first-principles calculation, in other words to develop a non-local KKR-CPA [3]. This opens up a way of treating SRO and other short-range effects on the electronic structure of realistic parameter-free models of alloys.

5.1 Derivation

5.1.1 Screening of the Structure Constants

An idea for the way to include nonlocal scattering correlations into the KKR framework is given by considering the molecular coherent potential approximation (Section 4.2.2), and in particular Eq. (4.26). The off-diagonal cluster-site matrix elements of the self-energy $\underline{\Sigma}_C$ may be interpreted as modifying the hopping terms within each cluster, but not between clusters as the self-energy is cluster diagonal. In the limit of an infinitely large cluster however, the exact self-energy defined in Eq. (4.17) relating all the sites of the lattice would be obtained, which may be interpreted as modifying the hopping terms between all the sites of the lattice. Note that unlike the hopping terms in tight-binding models, the structure constants in KKR theory are not potential dependent, and furthermore they are always determined to all orders in the lattice. In KKR theory, charge self-consistency is achieved through combination with density functional theory, and so for disordered systems concepts such as off-diagonal disorder required for tight-binding models are automatically taken into account. However, the analogue of the above idea within the

KKR framework is to screen the structure constants. We assume that the exact configurationally-averaged medium may be represented by a new effective medium with scattering path matrix

$$\underline{\widehat{\tau}}^{ij} = \underline{\widehat{t}}\,\delta_{ij} + \sum_{k \neq i} \underline{\widehat{t}}\,\underline{\widehat{G}}(\mathbf{R}^{ik})\,\underline{\widehat{\tau}}^{kj} \tag{5.1}$$

Here a circumflex symbol denotes an effective medium quantity, and in addition to effective local t-matrices $\underline{\widehat{t}}$, we have a new *effective propagator* defined by

$$\underline{\widehat{G}}(\mathbf{R}^{ij}) = \underline{G}(\mathbf{R}^{ij}) + \underline{\widehat{\delta G}}^{ij} \tag{5.2}$$

This is composed of the usual free-space KKR structure constants $\underline{G}(\mathbf{R}^{ij})$ which account for the lattice structure plus a *translationally-invariant* effective disorder term $\underline{\widehat{\delta G}}^{ij}$ $\left(\equiv \widehat{\delta G}^{ij}_{lm,l'm'}(\mathbf{R}^{ij})\right)$. The matrix $\underline{\widehat{\delta G}}^{ij}$ takes into account, in an averaged manner, the effect of all nonlocal scattering correlations on the propagation due to the disorder configurations. Note that nonlocal charge correlations may be taken into account later by combination with density functional theory (see Chapter 8).

Since the effective medium is translationally-invariant, we may solve in reciprocal space by applying a lattice Fourier transform to Eq. (5.1) and obtain

$$\underline{\widehat{\tau}}(\mathbf{k}) = \underline{\widehat{t}} + \underline{\widehat{t}}\left(\underline{G}(\mathbf{k}) + \underline{\widehat{\delta G}}(\mathbf{k})\right)\underline{\widehat{\tau}}(\mathbf{k}) \tag{5.3}$$

Therefore the real-space matrix elements are given by the Brillouin zone integral

$$\underline{\widehat{\tau}}^{ij} = \frac{1}{\Omega_{BZ}} \int_{\Omega_{BZ}} d\mathbf{k} \left(\underline{\widehat{t}}^{-1} - \underline{\widehat{\delta G}}(\mathbf{k}) - \underline{G}(\mathbf{k})\right)^{-1} e^{i\mathbf{k}(\mathbf{R}_i - \mathbf{R}_j)} \tag{5.4}$$

The aim is to develop a cluster theory which systematically determines approximations to the above exact effective medium. However unlike the MCPA, we require this site-to-site translational invariance to be retained. Clearly, the problem with developing such a theory is dealing with the effective disorder term in both real space, $\underline{\widehat{\delta G}}^{ij}$, and reciprocal space, $\underline{\widehat{\delta G}}(\mathbf{k})$.

5.1.2 Treatment in Real Space

To treat the problem in real space, the first step is to divide the lattice up into a set of periodically repeating clusters. These clusters must be chosen to preserve the point-group symmetry of the lattice, which is described in detail in Section 5.3. The next step is to generalise the KKR-CPA method [3, 5] by considering configurations of an impurity *cluster* embedded in the effective medium described by Eq. (5.1). To do this, we follow the approach of the embedded cluster method (KKR-ECM) (Section 4.2), but with the effective medium given by Eq. (5.1).

Eq. (5.1) for sites i, j belonging to a cluster C can be written in the form

$$\underline{\hat{\tau}}^{ij} = \underline{\hat{t}}\,\delta_{ij} + \sum_{k\in C} \underline{\hat{t}}\,\underline{\hat{G}}(\mathbf{R}^{ik})\underline{\hat{\tau}}^{kj} + \sum_{k\notin C} \underline{\hat{t}}\,\underline{\hat{G}}(\mathbf{R}^{ik})\underline{\hat{\tau}}^{kj} \tag{5.5}$$

where the sum over all sites k has been split into those involving sites k within the cluster and sites k outside of the cluster. It can be shown [6] (see Eq. (4.5) that

$$\sum_{k\notin C} \underline{\hat{G}}(\mathbf{R}^{ik})\underline{\hat{\tau}}^{kj} = \sum_{l\in C} \underline{\hat{\Delta}}^{il}\underline{\hat{\tau}}^{lj} \tag{5.6}$$

with the cluster renormalised interactor $\underline{\hat{\Delta}}^{ij}$ given by the expansion

$$\underline{\hat{\Delta}}^{ij} = \sum_{k\notin C} \underline{\hat{G}}(\mathbf{R}^{ik})\underline{\hat{t}}\,\underline{\hat{G}}(\mathbf{R}^{kj}) + \sum_{k\notin C, l\notin C} \underline{\hat{G}}(\mathbf{R}^{ik})\underline{\hat{t}}\,\underline{\hat{G}}(\mathbf{R}^{kl})\underline{\hat{t}}\,\underline{\hat{G}}(\mathbf{R}^{lj}) + \cdots \tag{5.7}$$

Inserting Eq. (5.6) into Eq. (5.5) and using the notation that sites belonging to the cluster are denoted by capital letters gives

$$\underline{\hat{\tau}}^{IJ} = \underline{\hat{t}}\,\delta_{IJ} + \sum_{K} \underline{\hat{t}}\left(\underline{\hat{G}}(\mathbf{R}^{IK}) + \underline{\hat{\Delta}}^{IK}\right)\underline{\hat{\tau}}^{KJ} \tag{5.8}$$

Eq. (5.8) can be re-arranged in the form

$$\underline{\hat{\tau}}^{IJ} = \underline{\hat{t}_{cl}}^{IJ} + \sum_{K,L} \underline{\hat{t}_{cl}}^{IK}\,\underline{\hat{\Delta}}^{KL}\,\underline{\hat{\tau}}^{LJ} \tag{5.9}$$

to include the effective *cluster t-matrix* defined by

$$\underline{\hat{t}_{cl}}^{IJ} = \underline{\hat{t}}\,\delta_{IJ} + \sum_{K\neq I} \underline{\hat{t}}\,\underline{\hat{G}}(\mathbf{R}^{IK})\underline{\hat{t}_{cl}}^{KJ} \tag{5.10}$$

Eq. (5.9) is simply a re-arrangement or 'renormalisation' of Eq. (5.1) so that the site matrix elements of all matrices involve the cluster sites only. The cluster t-matrix $\widehat{\underline{t}_{cl}}^{IJ}$ describes the scattering within the cluster, and all scatterings outside of the cluster are taken into account by the effective medium cluster renormalised interactor $\widehat{\underline{\underline{\Delta}}}^{IJ}$. The cluster renormalised interactor describes all paths from the cluster site I to the cluster site J which only involve intermediate sites outside of the cluster. It is independent of the contents of the cluster and can be viewed as describing the effective medium from which the cluster has been removed i.e. replaced by a *cavity*. An 'impurity cluster' embedded in the effective medium may be defined simply by filling up this cavity with a particular configuration of site potentials. Clearly, the path matrix for sites I, J belonging to such an impurity cluster is given by

$$\underline{\tau}_{imp}^{IJ} = \underline{t}_{cl,imp}^{IJ} + \sum_{K,L} \underline{t}_{cl,imp}^{IK} \, \widehat{\underline{\underline{\Delta}}}^{KL} \, \underline{\tau}_{imp}^{LJ} \tag{5.11}$$

with the impurity cluster t-matrix defined by

$$\underline{t}_{cl,imp}^{IJ} = \underline{t}^{I} \delta_{IJ} + \sum_{K \neq I} \underline{t}^{I} \, \underline{G}(\mathbf{R}^{IK}) \, \underline{t}_{cl,imp}^{KJ} \tag{5.12}$$

For a cluster containing N_c sites each scattering according to $\underline{t}^A$ or $\underline{t}^B$, there are 2^{N_c} possible impurity cluster configurations.

The usual KKR-CPA self-consistency condition may now be generalised in an analogous manner to the MCPA (Section 4.2.2), i.e. consider paths starting and ending on the impurity cluster sites and demand that the average over all configurations be equal to the path matrix for the effective medium itself:

$$\langle \, \underline{\tau}_{imp}^{IJ} \, \rangle = \widehat{\underline{\tau}}^{IJ} \tag{5.13}$$

In principle, if this process were to be carried out self-consistently, we would determine an effective cluster t-matrix $\widehat{\underline{t}_{cl}}^{IJ}$ and hence generate effective disorder terms $\widehat{\underline{\delta G}}^{IJ}$ for the cluster sites i.e.

$$\widehat{\underline{\underline{\delta G}}} = \widehat{\underline{\underline{t}}}^{-1} - \widehat{\underline{\underline{t}}}_{cl}^{-1} - \underline{\underline{G}} \tag{5.14}$$

which follows by rearranging Eq. (5.10). Here the double underscores denote matrices in *cluster site* space and angular momentum space, and $\underline{\underline{\hat{t}}}^{-1}$ is the diagonal part of $\underline{\underline{\hat{t}}}_{cl}^{-1}$.

To develop such a self-consistent algorithm however, the problem needs to be treated consistently in reciprocal space. In contrast to the MCPA, here $\underline{\underline{\hat{\tau}}}^{IJ}$, $\underline{\underline{\hat{t}}}$, and $\underline{\underline{\widehat{\delta G}}}^{IJ}$ correspond to an effective medium which we require to be invariant under translation from site to site. To preserve this periodicity, during each self-consistency cycle we must have

$$\underline{\underline{\hat{\tau}}}^{IJ} = \frac{1}{\Omega_{BZ}} \int_{\Omega_{BZ}} d\mathbf{k} \left(\underline{\underline{\hat{t}}}^{-1} - \underline{\underline{\widehat{\delta G}}}(\mathbf{k}) - \underline{\underline{G}}(\mathbf{k}) \right)^{-1} e^{i\mathbf{k}(\mathbf{R}_I - \mathbf{R}_J)} \tag{5.15}$$

This follows by applying a lattice Fourier transform to Eq. (5.1) and then considering the cluster sites I, J. Clearly, to carry out the above integration numerically, we must have a specific representation of the function $\underline{\underline{\widehat{\delta G}}}(\mathbf{k})$ which is consistent with our real space treatment of the problem.

The way forward is to use the coarse-graining idea from the nonlocal coherent potential approximation (Section 4.3.3) and apply it to the effective disorder matrix, i.e. proceed by coarse-graining $\underline{\underline{\widehat{\delta G}}}(\mathbf{k})$ over the Brillouin zone. Unlike many other attempts at the problem [6], this coarse-graining approach has been shown to yield herglotz analytic results [8].

5.1.3 Treatment in Reciprocal Space

Dividing the lattice into tiles (periodically repeating clusters) of N_c sites in real space may be interpreted as dividing or 'coarse-graining' the first Brillouin zone in reciprocal space into N_c tiles centred at the cluster momenta $\{\mathbf{K}_n\}$. The set of $\mathbf{K}_n$ values are related to a set of cluster sites $\{I, J\}$ in real space by the Fourier transformation [10, 11, 12]

$$\frac{1}{N_c} \sum_{\mathbf{K}_n} e^{i\mathbf{K}_n(\mathbf{R}_I - \mathbf{R}_J)} = \delta_{IJ} \tag{5.16}$$

The fundamental assumption we make is to approximate the effective medium disorder matrix $\underline{\widehat{\delta G}}(\mathbf{k})$ by the set of N_c values $\underline{\widehat{\delta G}}(\mathbf{K}_n)$, each of which is formally defined to be the average of $\underline{\widehat{\delta G}}(\mathbf{k})$ over the momenta $\tilde{\mathbf{k}}$ lying within the tile centred at $\mathbf{K}_n$ i.e.

$$\underline{\widehat{\delta G}}(\mathbf{K}_n) = \frac{N_c}{N} \sum_{\tilde{\mathbf{k}}} \underline{\widehat{\delta G}}(\mathbf{K}_n + \tilde{\mathbf{k}}) \tag{5.17}$$

Consistent with this approximation, the corresponding effective medium path matrix defined in Eq. (5.3) is approximated by the coarse-grained values $\{\underline{\hat{\tau}}(\mathbf{K}_n)\}$, each of which are defined as

$$\underline{\hat{\tau}}(\mathbf{K}_n) = \frac{N_c}{\Omega_{BZ}} \int_{\Omega_{\mathbf{K}_n}} d\mathbf{k} \left(\underline{\hat{t}}^{-1} - \underline{\widehat{\delta G}}(\mathbf{K}_n) - \underline{G}(\mathbf{k}) \right)^{-1} \tag{5.18}$$

Each integral is over the reciprocal space tile $\Omega_{\mathbf{K}_n}$ of volume N_c/Ω_{BZ} surrounding the point $\mathbf{K}_n$. These integrals are straightforward since each $\underline{\widehat{\delta G}}(\mathbf{K}_n)$ is constant within its coarse-graining tile.

Eq. (5.16) may be used to consider a real space representation of the coarse-grained effective disorder matrix and path matrix defined above. The real and reciprocal space effective disorder matrix elements are related by

$$\underline{\widehat{\delta G}}^{IJ} = \frac{1}{N_c} \sum_{\mathbf{K}_n} \underline{\widehat{\delta G}}(\mathbf{K}_n) e^{i\mathbf{K}_n(\mathbf{R}_I - \mathbf{R}_J)} \tag{5.19}$$

$$\underline{\widehat{\delta G}}(\mathbf{K}_n) = \sum_{J \neq I} \underline{\widehat{\delta G}}^{IJ} e^{-i\mathbf{K}_n(\mathbf{R}_I - \mathbf{R}_J)} \tag{5.20}$$

and the real and reciprocal space path matrix elements are related by

$$\underline{\hat{\tau}}^{IJ} = \frac{1}{N_c} \sum_{\mathbf{K}_n} \underline{\hat{\tau}}(\mathbf{K}_n) e^{i\mathbf{K}_n(\mathbf{R}_I - \mathbf{R}_J)} \tag{5.21}$$

$$\underline{\hat{\tau}}(\mathbf{K}_n) = \sum_{J} \underline{\hat{\tau}}^{IJ} e^{-i\mathbf{K}_n(\mathbf{R}_I - \mathbf{R}_J)} \tag{5.22}$$

Clearly, the effect of this coarse-graining is to reduce the range of the nonlocal scattering correlations that are treated exactly in real space. However, since the coarse-graining does not destroy the translational invariance, $\underline{\widehat{\delta G}}^{IJ}$ depends only on the difference between the cluster sites I and J, irrespective of which site in the lattice is chosen to be site I. In other words, the real space clusters are connected and $\underline{\widehat{\delta G}}^{IJ}$ and $\underline{\hat{\tau}}^{IJ}$ are independent of the origin of the clusters.

Inserting Eq. (5.18) into Eq. (5.21) means that the real space effective medium path matrix for sites I, J within a cluster is now given by

$$\underline{\widehat{\tau}}^{IJ} = \frac{1}{\Omega_{BZ}} \sum_{\mathbf{K}_n} \left(\int_{\Omega_{\mathbf{K}_n}} d\mathbf{k} \left(\underline{\hat{t}}^{-1} - \underline{\widehat{\delta G}}(\mathbf{K}_n) - \underline{G}(\mathbf{k}) \right)^{-1} e^{i\mathbf{K}_n(\mathbf{R}_I - \mathbf{R}_J)} \right) \tag{5.23}$$

This equation is used to replace Eq. (5.15), and we are now able to iterate to self-consistency until Eq. (5.13) and Eq. (5.23) are satisfied simultaneously. For clarity the full KKR-NLCPA algorithm is summarised in Section 5.2.

5.2 Algorithm

All real space matrices in the algorithm are super-matrices (denoted by double underscores) in cluster-site and angular momentum space. For a particular energy E,

1. Make a guess for the effective cluster t-matrix $\underline{\hat{t}}_{cl}^{\,IJ}$ (Eq. (5.10)) for the first iteration. Do this by placing an average t-matrix (ATA), $\underline{\bar{t}} = P(A)\underline{t}^A + P(B)\underline{t}^B$ (where P(A) is the probability of a site being occupied by an A atom) on each cluster site, and for the site to site propagation terms the free-space structure constants i.e. set $\underline{\widehat{\delta G}}^{IJ} = 0$.

2. Calculate $\underline{\widehat{\delta G}}^{IJ}$ using Eq. (5.10) i.e.

$$\underline{\underline{\widehat{\delta G}}} = \underline{\underline{\hat{t}}}^{-1} - \underline{\underline{\hat{t}}}_{cl}^{\,-1} - \underline{\underline{G}}$$

   where $\underline{\underline{\hat{t}}}^{-1}$ is the diagonal part of $\underline{\underline{\hat{t}}}_{cl}^{\,-1}$. For the first iteration $\underline{\widehat{\delta G}}^{IJ}$ will of course be zero.

3. Convert the matrix elements $\underline{\widehat{\delta G}}^{IJ}$ to coarse-grained reciprocal space using Eq. (5.20).

4. Calculate the coarse-grained matrix elements $\underline{\hat{\tau}}(\mathbf{K}_n)$ using Eq. (5.18) and convert them to real space using Eq. (5.21).

5. Calculate $\underline{\underline{\widehat{\Delta}}}^{IJ}$ by solving Eq. (5.9) i.e.

$$\underline{\underline{\widehat{\Delta}}} = \underline{\underline{\widehat{t}}}_{cl}{}^{-1} - \underline{\underline{\widehat{\tau}}}^{-1}$$

6. Calculate $\underline{\tau}_{imp}{}^{IJ}$ for each impurity cluster configuration using Eq. (5.11) and average over all 2^{N_c} configurations to obtain a new effective path matrix at the cluster sites $\underline{\widehat{\tau}}^{IJ}$.

7. Calculate the new cluster t-matrix $\underline{\widehat{t}}_{cl}{}^{IJ}$ by solving Eq. (5.9) using $\underline{\widehat{\tau}}^{IJ}$ above and $\underline{\underline{\widehat{\Delta}}}^{IJ}$ from step 5 i.e.

$$\underline{\underline{\widehat{t}}}_{cl} = \left(\underline{\underline{\widehat{\tau}}}^{-1} + \underline{\underline{\widehat{\Delta}}}\right)^{-1}$$

8. Compare the new cluster t-matrix elements $\underline{\widehat{t}}_{cl}{}^{IJ}$ with those in step 1. If they are not equal to within the desired accuracy, repeat as necessary steps $2 \rightarrow 8$ using the new cluster t-matrix until convergence within the desired accuracy is achieved.

Note that the integrations over the reciprocal space tiles in step 4 only involve the inversion of a matrix in angular momentum space and therefore computational time is not increased over the conventional KKR-CPA regardless of cluster size. This is in contrast to many other cluster methods such as the MCPA where the integration over the Brillouin zone requires the inversion of a super-matrix in cluster-site and angular momentum space *for each value of* $\mathbf{k}$. Furthermore, for computational purposes it is not actually necessary to include the free-space structure constants in the impurity cluster t-matrix; these may be left inside the cavity.

5.3 Cluster Momenta $\{\mathbf{K}_n\}$

The method for finding a suitable set of cluster sites $\{I, J\}$ and the corresponding set of cluster momenta $\{\mathbf{K}_n\}$ satisfying Eq. (5.16) has been described in Ref. [10] for a simple two-dimensional square lattice (see Chapter 7 for a generalisation to the case of three-dimensional cubic lattices).

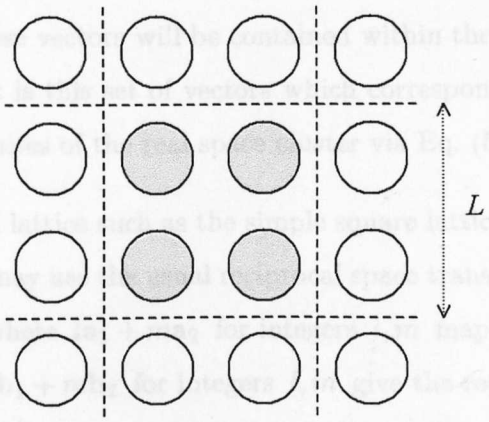

Figure 5.1: Real-space tiling (dashed lines) for a four-site cluster (filled circles) on a two-dimensional square lattice. The linear size L of the tile is $2a$ where a is the lattice constant.

Firstly, a suitable real space cluster must be chosen. As has already been described, coarse-graining reciprocal space into tiles centred at the cluster momenta $\{\mathbf{K}_n\}$ may be interpreted as coarse-graining real space into a set of periodically repeating clusters i.e a superlattice. Therefore, a real space cluster must have periodic boundary conditions. Moreover, as explained in Ref. [10], in order to obtain suitable reciprocal space tiles about the cluster momenta, the cluster must also preserve the full point-group symmetry of the lattice. A suitable real space cluster for a given lattice is therefore chosen by surrounding its sites with a 'tile' which preserves the point-group symmetry and can be periodically repeated to fill out the entire lattice. In other words, we have a consistent coarse-graining of real and reciprocal space into tiles. A simple example of a four-site cluster for a two-dimensional square lattice is shown in Fig. 5.1.

For a set of cluster sites $\{I, J\}$, the next step is to find the corresponding set of cluster momenta $\{\mathbf{K}_n\}$ satisfying Eq. (5.16). Note that if a Fourier transform is taken with respect to the differences in distance between the centres of the tiles, then a 'reduced' first Brillouin zone of a superlattice is obtained (see for example the molecular coherent potential approximation, Section 4.2.2). Higher Brillouin

zones of the superlattice are centred at its reciprocal lattice vectors, and it is clear that a set of N_c of these vectors will be contained within the first Brillouin zone of the original lattice. It is this set of vectors which correspond to the differences in distance between the sites of the real space cluster via Eq. (5.16).

For a two-dimensional lattice such as the simple square lattice shown in Fig. 5.1, to find these vectors we may use the usual reciprocal space transformations of the form $\mathbf{b}_i = 2\pi\mathbf{a}_i/|\mathbf{a}_1 \times \mathbf{a}_2|$ where $l\mathbf{a}_1 + m\mathbf{a}_2$ for integers l, m map out the centres of the real space tiles, and $l\mathbf{b}_1 + m\mathbf{b}_2$ for integers l, m give the reciprocal lattice vectors of this superlattice. N_c vectors of this form within the first Brillouin zone may be taken to be our set of cluster momenta $\{\mathbf{K}_n\}$ and these will satisfy Eq. (5.16). Note that care must be taken to ensure the chosen vectors are not equivalent i.e. do not differ by a reciprocal lattice vector of the original lattice.

The reciprocal space tiles surrounding the cluster momenta $\{\mathbf{K}_n\}$ correspond to the reciprocal space of the real space tiles. Using the example of the four-site cluster for a two-dimensional square lattice, the real space tiles are squares of size L^2 where $L = 2a$. The reciprocal space tiles are therefore squares of size $(2\pi/L)^2$ which together will fill out an area the size of the first Brillouin zone. Integrating over these tiles is equivalent to integrating over the first Brillouin zone of the lattice. This is because parts of tiles lying outside of the first Brillouin zone can be translated through reciprocal lattice vectors to lie within the first Brillouin zone. This is illustrated for the four-site cluster in Fig. 5.2.

5.4 Correlation Length

The range of nonlocal correlations that are accurately treated in real space as a result of the coarse-graining in reciprocal space has been described in Refs. [7, 8, 9, 10].

In the context of the KKR-NLCPA, first note that after self-consistency has been achieved, the path matrix for any sites i, j in the lattice may be obtained through

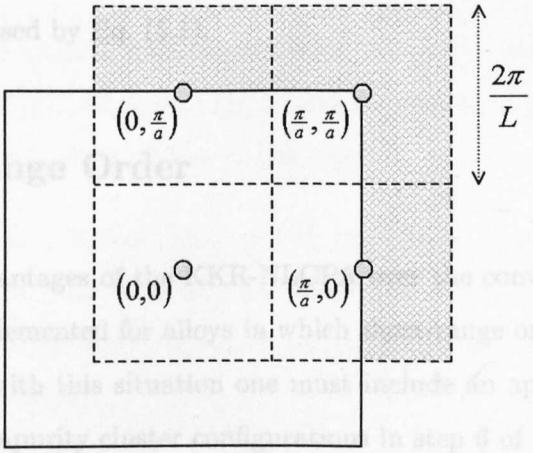

Figure 5.2: Reciprocal-space tiles (dashed lines) of linear size $2\pi/L$ where $L = 2a$ surrounding the cluster momenta (filled dots) for the four-site real-space cluster shown in Fig. 5.1. The shaded regions may be translated through reciprocal lattice vectors to lie within the first Brillouin zone (solid line).

the Brillouin zone integral

$$\underline{\widehat{\tau}}^{ij} = \frac{1}{\Omega_{BZ}} \sum_{\mathbf{K}_n} \left(\int_{\Omega_{\mathbf{K}_n}} d\mathbf{k} \left(\underline{\widehat{t}}^{-1} - \underline{\widehat{\delta G}}(\mathbf{K}_n) - \underline{G}(\mathbf{k}) \right)^{-1} e^{i\mathbf{k}(\mathbf{R}_i - \mathbf{R}_j)} \right) \tag{5.24}$$

where the function $\underline{\widehat{\delta G}}(\mathbf{K}_n)$ can be interpolated in order to obtain smooth spectral densities in analogy to Ref. [67].

The KKR-NLCPA reduces to the KKR-CPA for $N_c = 1$ since in this limit the $\underline{\widehat{\delta G}}(\mathbf{K}_n)$ vanish, and the KKR-NLCPA effective t-matrix is the same as the usual KKR-CPA effective t-matrix. Here a single site is treated exactly with all nonlocal correlations at mean-field level. As the cluster size N_c is increased, nonlocal scattering correlations are systematically included in the effective medium. To see this, consider a real space cluster of linear size L (see Section 5.3). Sampling the first Brillouin zone of the lattice at the cluster momenta $\{\mathbf{K}_n\}$ means sampling at intervals of $2\pi/L$, and according to Nyquist's sampling theorem [68], this means that correlations of a finite range $\leq L/2$ only are accurately treated in real space, which is proportional to the cluster size. Therefore the $\underline{\widehat{\delta G}}^{ij}$ which modify the propagation are cut off if the distance between i and j is outside the range of the cluster

size. The KKR-NLCPA becomes exact as $N_c \to \infty$ where $\mathbf{K}_n \to \mathbf{k}$, recovering the exact medium expressed by Eq. (5.1).

5.5 Short-Range Order

One of the main advantages of the KKR-NLCPA over the conventional KKR-CPA is that it can be implemented for alloys in which short-range ordering or clustering is present. To deal with this situation one must include an appropriate weighting for each of the 2^{N_c} impurity cluster configurations in step 6 of the algorithm. Note that such short-range order will not destroy the translational invariance because it will be restored by the configurational averaging. Clearly the amount of short-range order that can be included into the electronic structure is limited in range by the cluster size and hence correlation length. Indeed in a fully self-consistent calculation in which a measure of short-range order determined through linear-response theory is input into the electronic structure, the short-range order parameter would also need to be coarse-grained.

5.6 Calculating Observables

Observables such as the configurationally-averaged density of states may be calculated from the configurationally-averaged Green's function, and so in this section an expression for the configurationally-averaged Green's function is derived within the KKR-NLCPA.

5.6.1 Site-Diagonal Green's Function

The expression for the Green's function before averaging is given by Eq. (3.15)

$$G(E, \mathbf{r}_i, \mathbf{r}'_j) = \sum_{LL'} Z^i_L(E, \mathbf{r}_i) \tau^{ij}_{LL'} Z^j_{L'}(E, \mathbf{r}'_j)$$

$$-\sum_{L} Z_L^i(E,\mathbf{r}_i)\tilde{J}_L^i(E,\mathbf{r}_i')\delta_{ij} \tag{5.25}$$

where $L(=l,m)$ is an angular momentum index and $\mathbf{r}_i(\mathbf{r}_j')$ lies within the unit cell centred at site $i(j)$. $Z_L^i(E,\mathbf{r}_i)$ and $\tilde{J}_L^i(E,\mathbf{r}_i)$ are the regular and irregular solutions respectively of the single-site problem at site i [28].

Consider $\mathbf{r}$ and $\mathbf{r}'$ in the neighbourhood of a cluster site I. Denoting a configuration of the remaining cluster sites by γ, as a generalisation of Ref. [28] and Section 3.1.1 the first step is to average over the subset of possible lattice structures that leave the potential in site I fixed:

$$\langle G(E,\mathbf{r},\mathbf{r}')\rangle_I = \sum_{LL'} Z_L^I(E,\mathbf{r}_I)\left(\sum_{\gamma} P(\gamma|I)\langle\tau_{LL'}^{II}\rangle_{I,\gamma}\right) Z_{L'}^I(E,\mathbf{r}_I') - \sum_{L} Z_L^I(E,\mathbf{r}_I)\tilde{J}_L^I(E,\mathbf{r}_I') \tag{5.26}$$

where $\langle\tau_{LL'}^{II}\rangle_{I,\gamma}$ is the path matrix for paths starting and ending at site I conditionally averaged so that the potential on site I is known (to either be of type A or B for a binary alloy) and the configuration of the remaining sites in the cluster is known to be γ. $P(\gamma|I)$ is the probability that the configuration γ of the remaining cluster sites occurs given the type of potential at site I. The final step is to average over the possible occupants of site I itself:

$$\begin{aligned}\langle G(E,\mathbf{r},\mathbf{r}')\rangle = \sum_{LL'}\Bigg[&P(A)Z_L^A(E,\mathbf{r}_I)\left(\sum_{\gamma} P(\gamma|A)\langle\tau_{LL'}^{II}\rangle_{A,\gamma}\right) Z_{L'}^A(E,\mathbf{r}_I') \\ &+P(B)Z_L^B(E,\mathbf{r}_I)\left(\sum_{\gamma} P(\gamma|B)\langle\tau_{LL'}^{II}\rangle_{B,\gamma}\right) Z_{L'}^B(E,\mathbf{r}_I')\Bigg] \\ -\sum_{L}\Big[&P(A)Z_L^A(E,\mathbf{r}_I)\tilde{J}_L^A(E,\mathbf{r}_I') + P(B)Z_L^B(E,\mathbf{r}_I)\tilde{J}_L^B(E,\mathbf{r}_I')\Big]\end{aligned} \tag{5.27}$$

where $P(A)$ and $P(B)$ are the probabilities that site I is an A atom or B atom respectively (i.e. the concentrations of A and B atoms in the lattice). This can be rewritten as

$$\begin{aligned}\langle G(E,\mathbf{r},\mathbf{r}')\rangle = \sum_{LL'}\Bigg[&\sum_{\gamma} P(A,\gamma)Z_L^A(E,\mathbf{r}_I)\langle\tau_{LL'}^{II}\rangle_{A,\gamma} Z_{L'}^A(E,\mathbf{r}_I') \\ &+\sum_{\gamma} P(B,\gamma)Z_L^B(E,\mathbf{r}_I)\langle\tau_{LL'}^{II}\rangle_{B,\gamma} Z_{L'}^B(E,\mathbf{r}_I')\Bigg] \\ -\sum_{L}\Big[&P(A)Z_L^A(E,\mathbf{r}_I)\tilde{J}_L^A(E,\mathbf{r}_I') + P(B)Z_L^B(E,\mathbf{r}_I)\tilde{J}_L^B(E,\mathbf{r}_I')\Big]\end{aligned} \tag{5.28}$$

where (A,γ) and (B,γ) denote cluster configurations with an A atom and B atom on site I respectively.

Eq. (5.28) is still exact at this stage, but now an approximation needs to be made. In the KKR-NLCPA, the cluster-restricted-averaged quantity $\langle \tau^{II}_{LL'} \rangle_{I,\gamma}$ is constructed using an 'impurity' cluster of configuration (I,γ) embedded in the KKR-NLCPA effective medium. By using Eq. (5.9) to eliminate the cluster renormalised interactor from Eq. (5.11), this is given by

$$\langle \tau^{II}_{LL'} \rangle_{I,\gamma} = \left[\left(\underline{\underline{\widehat{\tau}}}^{-1} + \underline{\underline{t}}^{-1}_{cl,I,\gamma} - \underline{\underline{\widehat{t}}}^{-1}_{cl} \right)^{-1} \right]^{II}_{LL'} \tag{5.29}$$

where $\underline{\underline{t}}_{cl,I,\gamma}$ is an impurity cluster t-matrix $\underline{\underline{t}}_{cl,imp}$ with configuration (I,γ), and the notation implies taking the $\{II\}^{th}$ site and $\{LL'\}^{th}$ angular momentum element of the super-matrix on the right hand side.

Note that it does not matter which cluster site is chosen to be site I in all the above formulae as $\widehat{G}(E,\mathbf{r},\mathbf{r}')$, the resulting approximation to $\langle G(E,\mathbf{r},\mathbf{r}') \rangle$, is a translationally-invariant quantity. This is because site-to-site translational invariance is restored once the averaging has been performed over the impurity cluster configurations.

Site-diagonal observable quantities may now be defined as in Section 2.2.4 and Section 3.1.1. For example, the configurationally-averaged density of states per site is given by

$$\rho(E) = -\frac{1}{\pi} Im \int_{\Omega_I} \widehat{G}(E,\mathbf{r},\mathbf{r}) d\mathbf{r} \tag{5.30}$$

where the integral is over Ω_I, the volume of site I.

The new theory that has been presented in this chapter needs to be illustrated with a computationally simple test case before applying to realistic systems. For this purpose, the next chapter illustrates the KKR-NLCPA with calculations for the configurationally-averaged density of states for a simple one-dimensional model, which is formally identical to the KKR-NLCPA for realistic systems but is computationally much simpler.

Chapter 6

1D Results

KKR theory in three dimensions deals with three-dimensional potential wells of finite range surrounding the atomic nuclei, the famous muffin-tin potential shown in Fig. 2.1. A very useful caricature of this realistic situation can be constructed in one dimension. In this case the unit cell is a line segment and the potential wells are described by a function $V(x)$ of one spatial variable only. Interestingly, one may regard the sign of x as an angle and develop an analogue of the three-dimensional angular momentum expansion of the usual KKR theory. Since it was first formulated by Butler [69] it has been made good use of by a number of authors, for example see Refs. [70, 71, 72]. While it is computationally simple, as one might expect, it is formally identical to KKR in three dimensions. For example there are two 'angular momentum' values $L = 0, 1$ (and hence all real space super-matrices in the KKR-NLCPA algorithm have dimension $2N_c$) and there is an explicit expression for the structure constants. See the Appendix for details.

Results obtained for the configurationally-averaged density of states using the KKR-NLCPA for such a one-dimensional model alloy are presented in this chapter. It should be stressed that the purpose of using this model is to demonstrate that a realistic three-dimensional calculation is feasible, and to demonstrate possible improvements that could be obtained over the existing KKR-CPA approach.

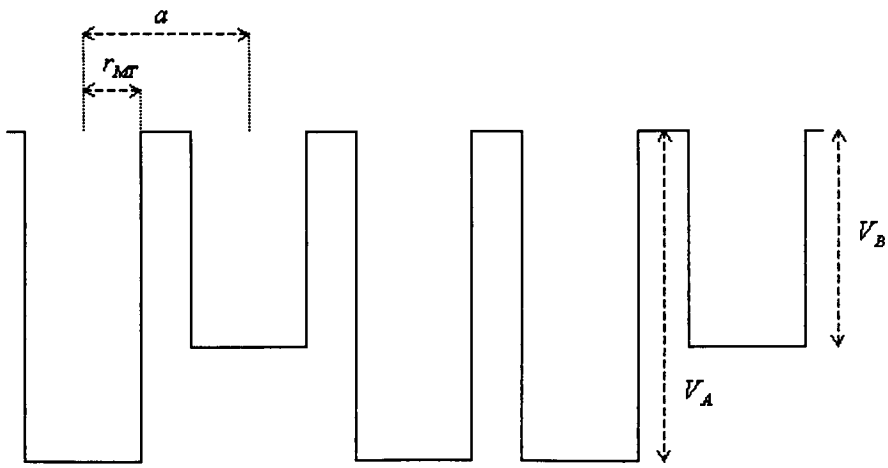

Figure 6.1: Potential wells of depth V_A and V_B for a one-dimensional KKR-NLCPA model. Also shown are the lattice constant a and the muffin-tin radius r_{MT} for a potential of type V_A.

6.1 The Model

In Section 6.2 results are given for a one-dimensional KKR-NLCPA model for a random substitutional binary alloy, comprised of A sites with concentration c and B sites with concentration $(1-c)$. The corresponding potentials are taken to be square wells of depth V_A and V_B. This is illustrated in Fig. 6.1. For details of the corresponding phase shifts see the Appendix.

In order to illustrate the coarse-graining in one dimension, Fig. 6.2(a) shows an example of a 'one-dimensional tile' for a one-dimensional four site ($N_c = 4$) cluster. Its length L is $4a$, where a is the lattice constant. The corresponding set of cluster momenta (denoted by dots) and reciprocal space tiles of length $2\pi/L$ in relation to the first Brillouin zone are shown in Fig. 6.2(b).

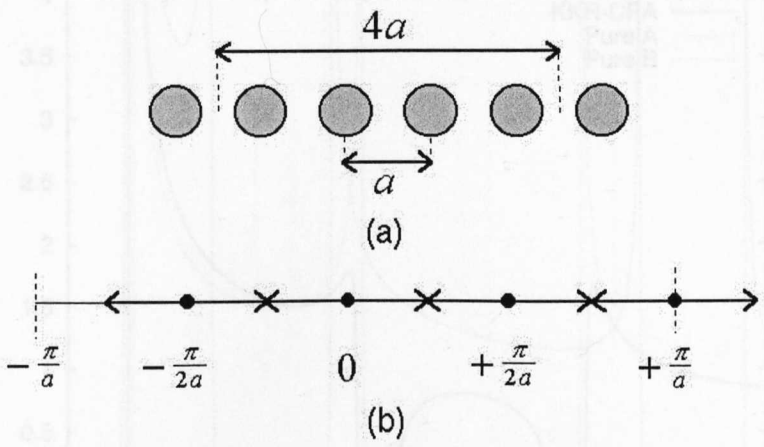

Figure 6.2: Real and reciprocal space tiling for a four site cluster in one dimension.

6.2 Results

Extensive numerical calculations of the configurationally-averaged density of states have been carried out for the one-dimensional alloy described in Section 6.1 over a wide range of parameters. In all cases it is found that the KKR-NLCPA systematically improves the density of states with increasing cluster size compared to the conventional KKR-CPA.

As a simple illustration, the following parameters are used:

$V_A = -1.2$ Ry (depth of potential well for an A site)
$V_B = -0.6$ Ry (depth of potential well for a B site)
$c = 0.8$ (concentration of A potentials)
$a = 6.00$ a.u. (lattice constant)
$r_{MT} = 2.25$ a.u. (muffin-tin radius for both V_A and V_B)

The density of states for the electrons in lattices of purely A sites and purely B sites together with the KKR-CPA result for the $A_{80}B_{20}$ alloy is shown in Fig. 6.3.

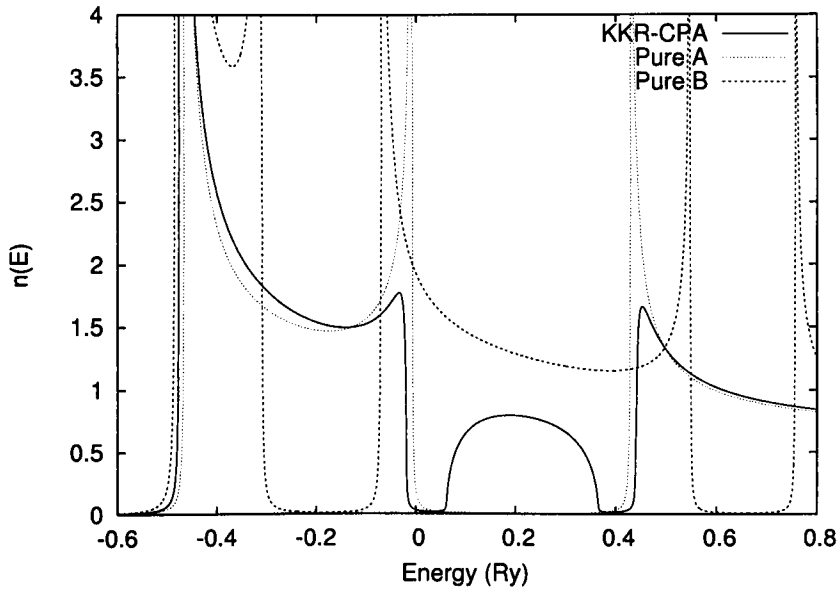

Figure 6.3: Density of states for a one-dimensional model. Results shown are for a pure A lattice, a pure B lattice and a KKR-CPA calculation for an $A_{80}B_{20}$ alloy.

The KKR-CPA result gives a very smooth density of states with an impurity band centred at ~ 0.2 Ry with band gaps either side.

For comparison, Figs. 6.4 and 6.5 show the results for four site and eight site supercell calculations. These are obtained by considering an infinite periodic supercell containing four or eight sites of a particular configuration respectively and then averaging over all 2^4 or 2^8 possible configurations respectively. The structure constants for the one-dimensional supercell in real and reciprocal space are derived in the Appendix. Although the supercell calculation converges towards the exact result as the supercell gets larger, it is not the exact result due to the finite size of the supercell, but it gives an indication of the type of structure to expect if we are to improve upon the KKR-CPA. For example, the sharp structure in the density of states and filling in of the band gaps arise from scattering from particular disorder configurations of the supercell.

A KKR-NLCPA calculation with a cluster size of four is shown in Fig. 6.6. It is

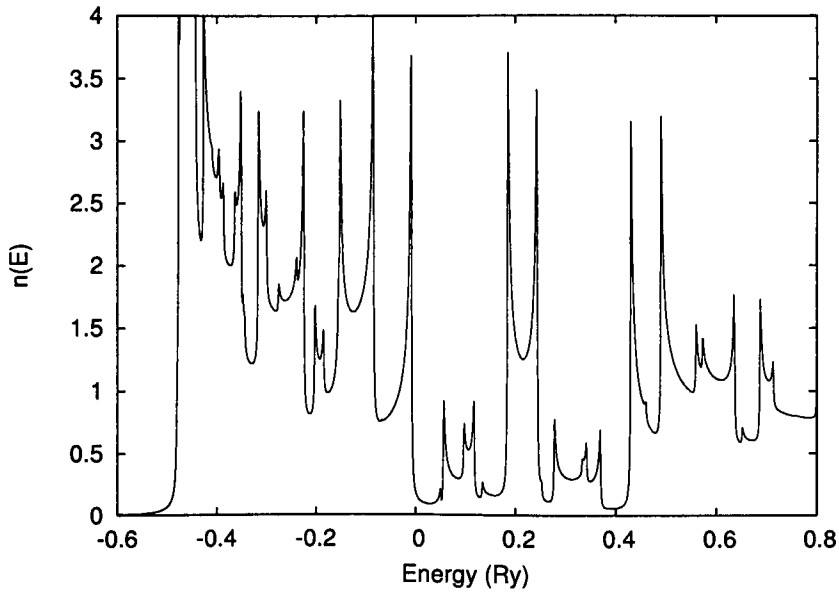

Figure 6.4: An four site ($N_c = 4$) supercell calculation for the $A_{80}B_{20}$ alloy obtained by averaging over all 2^4 possible configurations of an infinite periodic supercell containing four sites.

evident that much of the structure missing from the KKR-CPA calculation which can be associated with energy bands of particular configurations of the supercell is reproduced here. States also appear in the band gaps either side of the impurity band centered at 0.2 Ry which are absent in the KKR-CPA calculation. This is because the states near the band edges are the contributions of large clusters of like atoms and these cannot be dealt with by a single-site theory such as the KKR-CPA. To investigate this further, an eight site calculation is shown in Fig. 6.7. Clearly with increasing cluster size more and more states enter the band gaps.

6.2.1 Short-Range Order

Finally, the ability of the KKR-NLCPA to take into account the effects of short-range order is illustrated. As mentioned earlier, the KKR-NLCPA can be implemented for arbitrary ensembles including those in which the occupancy of a site by an A or

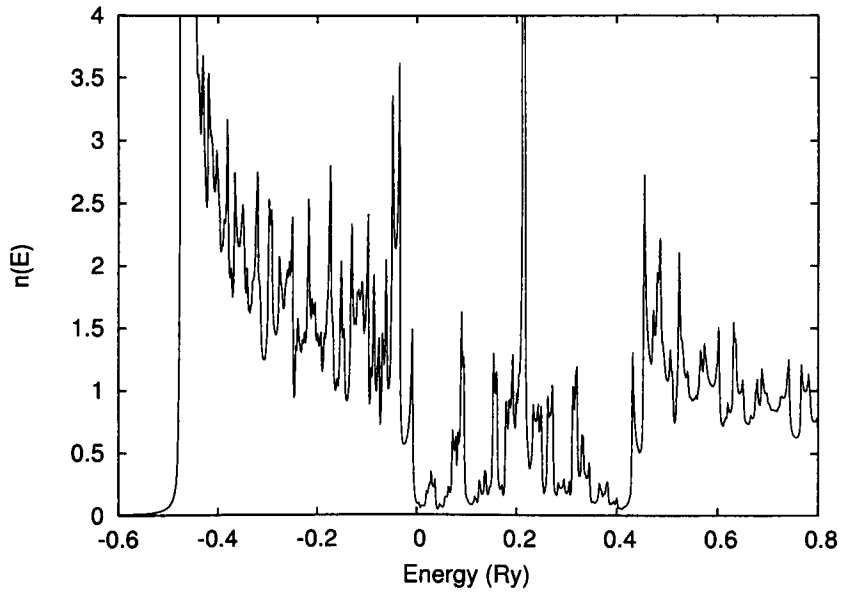

Figure 6.5: An eight site ($N_c = 8$) supercell calculation for the $A_{80}B_{20}$ alloy obtained by averaging over all 2^8 possible configurations of an infinite periodic supercell containing eight sites.

B atom is correlated to that of neighbouring sites.

In order to illustrate short-range order for this one-dimensional model, the simple example of a Markov chain is used i.e. it is assumed that the probability of finding an atom of type A or B at a site in the chain only depends on the occupancy of the previous site. The probability of an atom occupying a site is increased by a parameter α if it follows a like atom and its probability is decreased by α if it follows an unlike atom in the chain. Thus positive values of α correspond to short-range clustering and negative values of α correspond to short-range ordering. As an example, for a four site impurity cluster of configuration $ABBA$ we have $P(ABBA) = (P(A) + \alpha)(P(B) - \alpha)(P(B) + \alpha)(P(A) - \alpha)$. Note that a Markov chain satisfies the requirement that the probability distribution be periodic in order to preserve translational invariance when averaging.

In Fig. 6.8 a four site KKR-NLCPA calculation for the density of states is shown

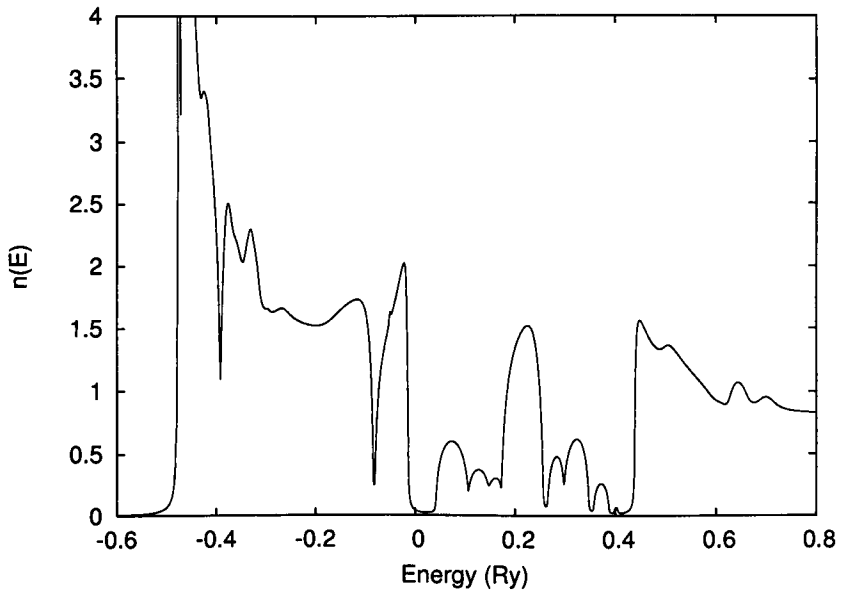

Figure 6.6: A four site ($N_c = 4$) KKR-NLCPA calculation for the $A_{80}B_{20}$ alloy. Notice the improved structure and the partial filling in of the band gaps compared with the KKR-CPA calculation in Fig. 6.3.

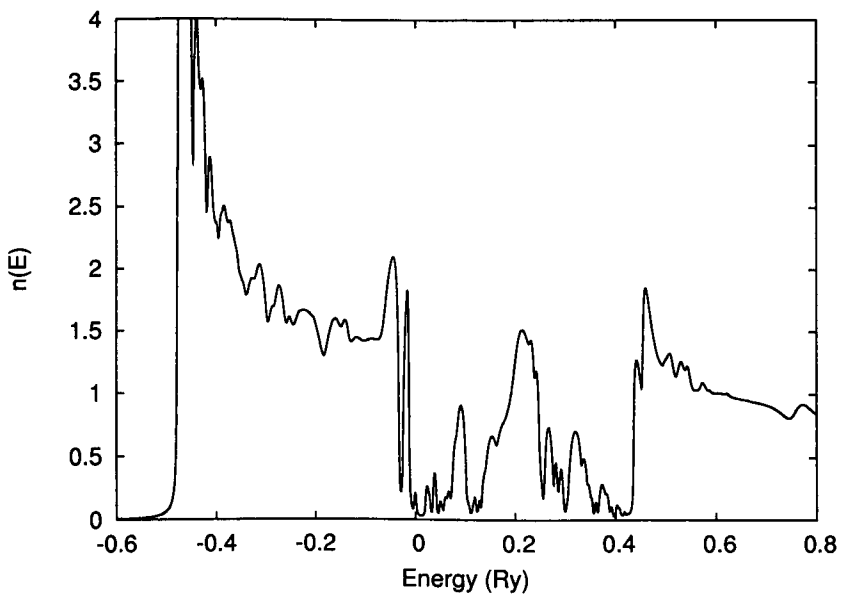

Figure 6.7: An eight site ($N_c = 8$) KKR-NLCPA calculation for the $A_{80}B_{20}$ alloy. Notice the increasing density of states inside the KKR-CPA band gaps.

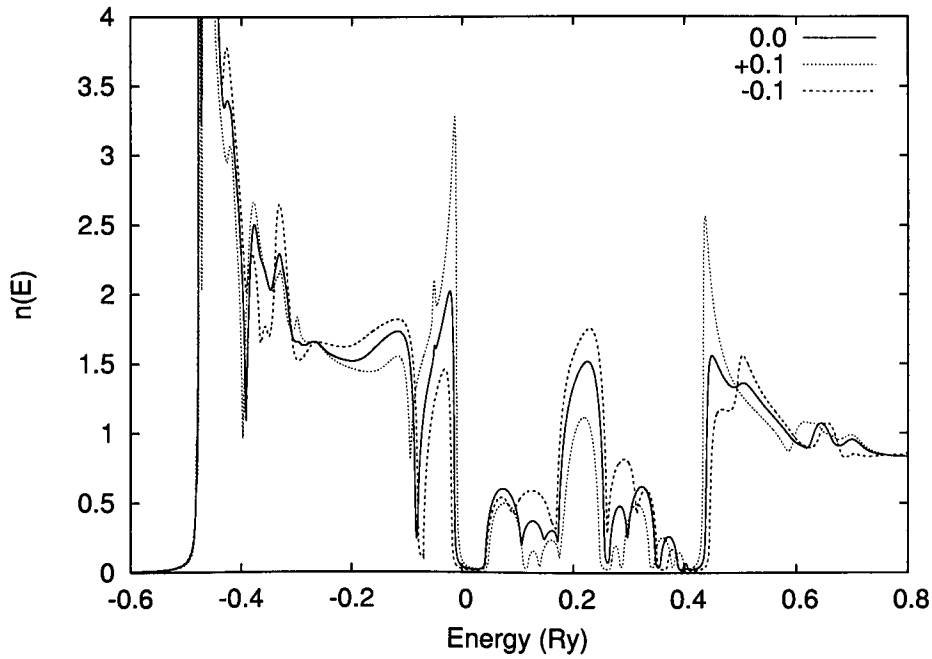

Figure 6.8: Effects of short-range ordering ($\alpha = -0.1$) and clustering ($\alpha = +0.1$) on the four site ($N_c = 4$) KKR-NLCPA calculation for the $A_{80}B_{20}$ alloy.

using the same parameters as before along with short-range order parameter values $\alpha = -0.1$, $\alpha = 0.0$ and $\alpha = +0.1$. Peaks which increase or decrease can be identified with specific cluster configurations and the increases or decreases in the amplitude of the peaks are consistent with the increased or decreased cluster probabilities.

To summarise this chapter, KKR-NLCPA results have been presented for a one-dimensional model which show filling in of KKR-CPA band gaps and increasing structure in the configurationally-averaged density of states as the cluster size increases due to nonlocal scattering correlations, and also a simple example of the ability of the KKR-NLCPA to model the effects of short-range order. The next step is to examine the feasibility of carrying out similar calculations for a realistic three-dimensional system, which is the subject of the next chapter.

Chapter 7

3D Feasibility

The aim of this chapter is to show that the KKR-NLCPA formalism is fully applicable and computationally feasible for three-dimensional simple cubic (sc), body-centered cubic (bcc), and face-centered cubic (fcc) lattices commonly found in real disordered alloys. Clearly this is an extremely important aspect of the theory, since application to realistic systems has been the problem for many other cluster theories which otherwise satisfy all the requirements for a satisfactory cluster theory (see Chapter 4).

Real-Space Tiling

Firstly, it must be shown that suitable real space clusters exist for these cubic lattices. As has already been described in Section 5.3, a real space cluster must be chosen so that its sites can be surrounded by a tile (or rather a 'block' in three dimensions) which preserves the point-group symmetry of the lattice and can be periodically repeated to fill out all space. Denoting the number of sites in a cluster by N_c, for the trivial case of $N_c = 1$, the real space tiles with the required symmetry would simply be Wigner-Seitz cells surrounding each lattice point for each of the sc, bcc and fcc lattices. For larger cluster sizes we may take the tiles to be simple

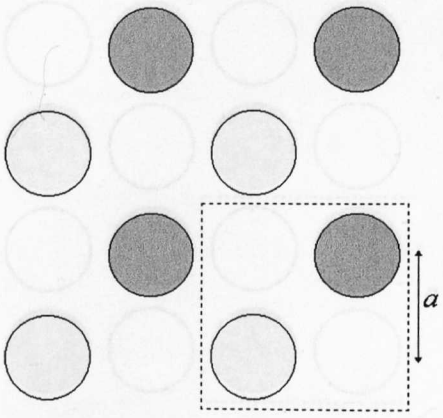

Figure 7.1: Cross-section of the real-space tiling for a two-site cluster on a bcc lattice. The shaded atoms lie out of the page and a is the lattice constant.

cubes of volume L^3 for each of these lattices. The smallest possible cluster sizes are given by considering $L = a$ (where a is the lattice constant) and this yields $N_c = 1$ for sc (trivial), $N_c = 2$ for bcc, and $N_c = 4$ for fcc lattices. The next set of allowed cluster sizes is given by considering $L = 2a$ and this yields $N_c = 8$, $N_c = 16$, and $N_c = 32$ for sc, bcc and fcc lattices respectively. Examples of this real space tiling for bcc and fcc lattices are shown in Figs. 7.1 and 7.2.

Cluster Momenta

For a set of cluster sites $\{I, J\}$, the next step is to find the corresponding set of cluster momenta $\{\mathbf{K}_n\}$ satisfying Eq. (5.16). Following Section 5.3, in this case we require three-dimensional reciprocal space transformations of the form

$$\mathbf{b}_1 = \frac{2\pi\,(\mathbf{a}_2 \times \mathbf{a}_3)}{(\mathbf{a}_1 \cdot (\mathbf{a}_2 \times \mathbf{a}_3))},\ \mathbf{b}_2 = \frac{2\pi\,(\mathbf{a}_3 \times \mathbf{a}_1)}{(\mathbf{a}_1 \cdot (\mathbf{a}_2 \times \mathbf{a}_3))},\ \mathbf{b}_3 = \frac{2\pi\,(\mathbf{a}_1 \times \mathbf{a}_2)}{(\mathbf{a}_1 \cdot (\mathbf{a}_2 \times \mathbf{a}_3))} \tag{7.1}$$

where $l\mathbf{a}_1 + m\mathbf{a}_2 + n\mathbf{a}_3$ for integers l, m, n map out the centres of the real space tiles, and $l\mathbf{b}_1 + m\mathbf{b}_2 + n\mathbf{b}_3$ for integers l, m, n give the reciprocal lattice vectors of this superlattice. Since the $\{\mathbf{a}_1, \mathbf{a}_2, \mathbf{a}_3\}$ are simple cubic, the $\{\mathbf{b}_1, \mathbf{b}_2, \mathbf{b}_3\}$ will also be simple cubic. We take N_c vectors of this form within the first Brillouin zone

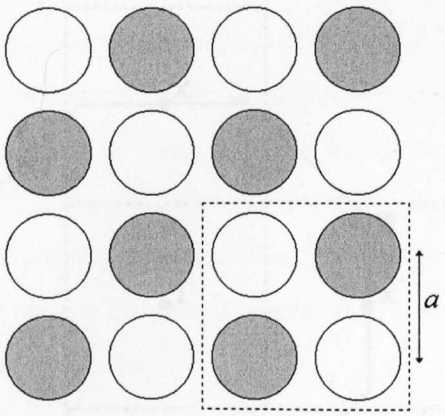

Figure 7.2: Cross-section of the real-space tiling for a four-site cluster on an fcc lattice. The shaded atoms lie out of the page and a is the lattice constant.

of the original lattice to be the set of cluster momenta $\{\mathbf{K}_n\}$ and these will satisfy Eq. (5.16). Care must be taken to ensure the chosen vectors are not equivalent i.e. do not differ by a reciprocal lattice vector of the original lattice. As an example, considering a four site cluster for an fcc lattice, the set of cluster momenta can be chosen as the Γ point and three of the X points of the first Brillouin zone. This is illustrated in Fig. 7.3. Table 7.1 gives some examples of sets of $\{\mathbf{R}_I\}$ and corresponding $\{\mathbf{K}_n\}$ values obtained using this method.

Reciprocal-Space Tiling

Since the real space clusters are cubes of volume L^3, the reciprocal space tiles surrounding these cluster momenta will be simple cubes of volume $(2\pi/L)^3$. These tiles will together fill out a volume the size of the first Brillouin zone i.e. $(2\pi/a)^3$ for sc, $2(2\pi/a)^3$ for bcc, and $4(2\pi/a)^3$ for fcc lattices respectively. An example for a four-site cluster on an fcc lattice is shown in Fig. 7.3. Integrating over these tiles is equivalent to integrating over the first Brillouin zone of the lattice. This is because parts of tiles lying outside of the first Brillouin zone can be translated through reciprocal lattice vectors (of the original sc, bcc, or fcc lattice as appropriate) to lie

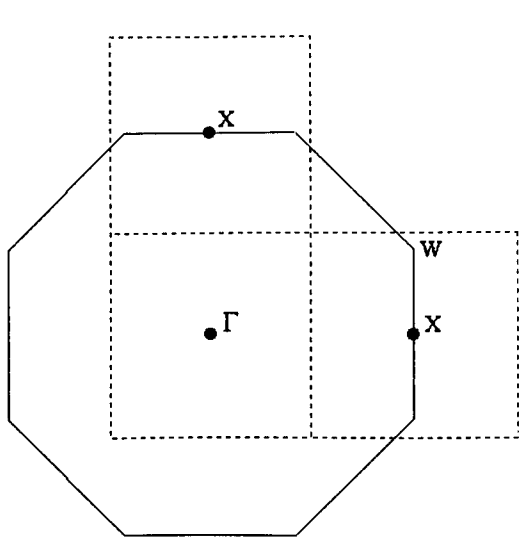

Figure 7.3: Cross-section of the reciprocal-space tiling for a four-site cluster on the fcc lattice shown in Fig. 7.2. The fourth tile is centred at the X point situated out from the page i.e. $\{\mathbf{K}_n\}$ points are $(0,0)$, $(\frac{2\pi}{a},0,0)$, $(0,\frac{2\pi}{a},0)$, $(0,0,\frac{2\pi}{a})$. Note that parts of tiles which lie outside of the first Brillouin zone may be translated through reciprocal lattice vectors to lie within the first Brillouin zone (solid line)

within the first Brillouin zone.

Computational Feasibility

In the KKR-NLCPA algorithm (Section 5.2), real space quantities such as the path matrix and cluster t-matrix are super-matrices in cluster site and angular momentum space, and increase in size as the cluster size N_c increases. For the algorithm to be computationally feasible, it is crucial that clusters of a reasonable size are possible for realistic three-dimensional lattices. Fortunately, it has been shown above that such clusters exist (see Table 7.1).

The major computational step in the algorithm is the integration over the first Brillouin zone. As mentioned in Section 5.2, the fact that this integration is simply split into integrating over "tiles" means that computational time for integrating over the Brillouin zone is not increased over the conventional KKR-CPA regardless

of cluster size. This is in contrast to many other cluster methods such as the molecular coherent potential approximation (Section. 4.2.2) where the integration over the Brillouin zone would require the inversion of a super-matrix in cluster-site and angular momentum space *for each value of* $\mathbf{k}$. However, computational time for the standard KKR-CPA can be decreased further using symmetry so that it is only necessary to integrate over the irreducible $1/48^{th}$ part of the Brillouin zone. It is likely that symmetry can also be used to decrease computational time further for the KKR-NLCPA in a similar fashion.

Table 7.1: Sets of $\mathbf{R}_I$ and $\mathbf{K}_n$ values for cubic lattices

lattice	N_c	cube edge L	$\mathbf{R}_I$ values (units of lattice constant a)	$\mathbf{K}_n$ values (units of $\frac{\pi}{a}$)
sc	1	a	$(0,0,0)$	$(0,0,0)$
	8	$2a$	$\{\mathbf{R}_I^{sc}\} = \{$ $(0,0,0)$, $(0,0,1)$, $(0,1,0)$, $(0,1,1)$, $(1,0,0)$, $(1,0,1)$, $(1,1,0)$, $(1,1,1)$ $\}$	$\{\mathbf{K}_n^{sc}\} = \{$ $(0,0,0)$, $(0,0,1)$, $(0,1,0)$, $(0,1,1)$, $(1,0,0)$, $(1,0,1)$, $(1,1,0)$, $(1,1,1)$ $\}$
bcc	2	a	$(0,0,0)$, $(\frac{1}{2},\frac{1}{2},\frac{1}{2})$	$(0,0,0)$, $(2,0,0)$
	16	$2a$	$\{\mathbf{R}_I^{sc}\}$, $\{\mathbf{R}_I^{sc} + (\frac{1}{2},\frac{1}{2},\frac{1}{2})\}$	$\{\mathbf{K}_n^{sc}\}$, $\{\mathbf{K}_n^{sc} + (2,0,0)\}$
fcc	4	a	$(0,0,0)$, $(\frac{1}{2},0,\frac{1}{2})$, $(\frac{1}{2},\frac{1}{2},0)$, $(0,\frac{1}{2},\frac{1}{2})$	$(0,0,0)$, $(2,0,0)$, $(0,2,0)$, $(0,0,2)$
	32	$2a$	$\{\mathbf{R}_I^{sc}\}$, $\{\mathbf{R}_I^{sc} + (\frac{1}{2},0,\frac{1}{2})\}$, $\{\mathbf{R}_I^{sc} + (\frac{1}{2},\frac{1}{2},0)\}$, $\{\mathbf{R}_I^{sc} + (0,\frac{1}{2},\frac{1}{2})\}$	$\{\mathbf{K}_n^{sc}\}$, $\{\mathbf{K}_n^{sc} + (2,0,0)\}$ $\{\mathbf{K}_n^{sc} + (0,2,0)\}$, $\{\mathbf{K}_n^{sc} + (0,0,2)\}$

Chapter 8

Conclusions and Future Work

In this thesis I have presented the Korringa-Kohn-Rostoker nonlocal coherent potential approximation (KKR-NLCPA), a new method for describing the electronic structure of disordered metallic systems based upon a first-principles description of the crystal potential. The theory is a reformulation in terms of multiple scattering theory of the nonlocal coherent potential approximation which has recently been developed for a simple tight-binding model. The KKR-NLCPA provides a hierarchy of improvements over the conventional mean-field KKR-CPA approach, the limitations of which I have discussed. To illustrate this I have demonstrated the KKR-NLCPA with a one-dimensional model, with the emphasis on the improved structure in the density of states with increasing cluster size due to nonlocal scattering correlations, and a simple example of its ability to model the effects of compositional short-range order. Importantly, I have shown that a realistic three-dimensional calculation is feasible by illustrating in detail the necessary coarse-graining procedure for real three-dimensional lattices. Finally, I have shown how to calculate site-diagonal observable quantities using the KKR-NLCPA, establishing the fact that once the averaging has been performed over the cluster configurations, single-site translational invariance is restored. This is crucial as it establishes a means of combining the KKR-NLCPA with density functional theory for ab-initio calculations in an analogous fashion to

the conventional KKR-CPA.

I now discuss possible future work which arises from this thesis. [73]

3D Implementation: The first step will be to implement the KKR-NLCPA for a realistic three-dimensional system. The main part of this will be to develop a routine to carry out the integration of the multiple scattering path matrix over the reciprocal space patches which coarse-grain the first Brillouin zone for fcc and bcc lattices. The code could then be straightforwardly adapted to model the effects of short-range order on the electronic structure of a realistic system by introducing a short-range order (SRO) parameter. An ideal first system to investigate would be $CuPd$. Recently, dramatic improvements in the resolving power of X-ray diffuse scattering measurements [74] have uncovered remarkable and possibly technologically important ordering processes in $Cu_{1-c}Pd_c$ which have not been observed before [75]. Occurring in the concentration range $0.21 < c < 0.28$ at a temperature $200K$ above the order-disorder transition temperature T_c, these ordering processes are likely to have a direct electronic origin. As a result, high resolution Positron Annihilation experiments [76] on the Fermi Surface are being planned in this concentration range in order to examine the connection between these novel ordering processes and the electronic structure, and the KKR-NLCPA code could be used to help interpret these experiments.

Transport Properties

A further development would be to use a KKR-NLCPA electronic structure calculation to examine the effects of SRO on transport properties, for example the electronic structure information around the Fermi energy could be used to calculate the resistivity from the Kubo-Greenwood formula [77, 78, 79, 80]. Indeed resistivity measurements are actually used in industry to control physical properties by monitoring the changes in SRO which occur in annealing processes. An example of an alloy which could be used as an illustrative case study is Ag_cZn_{1-c} [81], which follows the expected trend of decreasing resistivity with increasing SRO. However

there are a set of alloys where the opposite trend occurs, which is known as a 'komplex' state [82]. This occurs when a late transition metal is alloyed with a mid-row element. The KKR-NLCPA could be used to find a first-principles electronic explanation of this phenomenon, for example using $Ni_{80}Mo_{20}$ as a case study.

Combination with DFT: In order for first-principles ab-initio (parameter-free) calculations to be carried out for disordered materials, the KKR-NLCPA needs to be combined compatibly with density functional theory. The conventional KKR-CPA has been successfully combined with density functional theory, however the limitations of the resulting theory have been described in Chapter 3. The implementation requires the solution of the Kohn-Sham equations for electrons moving in the disordered arrays of the effective potentials associated with A and B sites which are insensitive to their environments. Therefore nonlocal charge correlations and lattice displacement effects are neglected. However, combination of the KKR-NLCPA with DFT provides a natural and systematic way of taking these effects into account accurately.

A scheme could be formulated in which the total energy becomes a functional of partially averaged cluster charge densities for the possible cluster configurations. This would probably need to be minimised with respect to these partially averaged cluster charge densities, which can be calculated by combination with the KKR-NLCPA. Thus charge correlations would be taken into account naturally in accordance with the size of the cluster. In order to deal with lattice displacements, mechanical equilibrium needs to be achieved. The theory above could be adapted so that the total energy also becomes a functional of the displaced nuclear positions in the cluster configurations, and then minimised with respect to these displaced nuclear positions. In order to combine with the KKR-NLCPA, the multiple scattering theory basis of the KKR-NLCPA needs to be adapted to deal with displaced atoms. Similar developments for lattice displacements have already been made in the context of supercell calculations which will be helpful in developing the SCF-KKR-NLCPA theory.

An example of a system that could be used as an illustrative case study is $CuAu$, which is the archetypal example of a big-atom/small-atom system. The current SCF-KKR-CPA method gives qualitatively reasonable results but is unsatisfactory quantitatively, and this is likely to be due to the neglect of lattice displacements on the magnitude of nesting pieces of the Fermi surface. Another example of an iso-electronic big-atom/small-atom system is CrW, where applying concentration-wave theory (see below) using electronic structure determined by the SCF-KKR-CPA currently leads to an incorrect prediction for the low temperature phase stability. This arises from the SCF-KKR-CPA requiring the average net charge on a single site to vanish, and at the same time being incapable of dealing with the size difference between W and Cr atoms. Charge is thus assumed to spill over from the large W to the small Cr atoms leading to the prediction that the alloy will order at a high T_c. However, experimentally the alloy is found to phase separate. An SCF-KKR-NLCPA description of the disordered phase of these systems could be used to explain the electronic reasons for the behaviour described above from first principles.

Statistical Mechanics: To go further and examine the compositional fluctuations as the temperature is lowered and to attempt to predict the low temperature behaviour, the corresponding statistical mechanics theory needs to be developed. Atomic ordering in alloys can be described in terms of 'concentration waves' [54]. As the atoms begin to arrange themselves as the alloy cools, the probability of finding a particular atomic species occupying a lattice site (the site dependent concentration c_i) varies from site to site and traces out a static concentration wave, with a wavevector characteristic of the low temperature behaviour. The main result of concentration-wave theory as shown by Györffy and Stocks [5] is that $S^{(2)}(\mathbf{q}, T)$, the lattice Fourier transform of the direct correlation function

$$S^{(2)}_{jk} = \left. \frac{\delta^2 \Omega\{c_i\}}{\delta c_j \delta c_k} \right|_{\{c_i = c\}}$$

provides direct information on the stability of the disordered alloy to concentration fluctuations at a given temperature T [5]. Here Ω is the averaged electronic Grand Potential for an inhomogeneous concentration distribution $\{c_i\}$. However the role

of the inhomogeneous concentration distribution is purely formal since the result is evaluated for a homogeneous concentration distribution c, and hence all information required may be obtained from a standard SCF-KKR-CPA electronic structure calculation for the disordered phase. From this, a measure of the short-range order in the system can be determined via the Warren-Cowley short-range-order parameter

$$\alpha(\mathbf{q}, T) = c(1-c)/(1 - \beta c(1-c)S^{(2)}(\mathbf{q}, T))$$

where c is the concentration of one of the constituents and $\beta = (k_B T)^{-1}$. This can be compared with data obtained from X-ray diffuse scattering experiments [1]. After the development of the SCF-KKR-NLCPA, the next step will be to address the generalisation of this mean-field concentration-wave theory to the nonlocal case. This means addressing the non-trivial idea of a 'nonlocal' inhomogeneous concentration distribution with the averaged electronic Grand Potential provided by an SCF-KKR-NLCPA calculation. Such a theory would have a significant impact on understanding alloy phase diagrams from first-principles.

Itinerant Magnetism: Metallic magnets at finite temperature provide other incidences of disorder. The 'disordered local moment' (DLM) [83, 84] picture of finite temperature metallic magnetism is based on the assumption that it is possible to separate fast and slow motions in the interacting electron gas. On a time scale τ, long in comparison with an electronic hopping time, but short when compared to a typical spin fluctuation time, the spin orientations of the electrons leaving a site are sufficiently correlated with those arriving such that a non-zero magnetisation exists when the appropriate quantity is averaged over τ. These are the 'local moments' which can change their orientations, $\{\hat{e}_i\}$, on the longer time scale while their magnitudes fluctuate rapidly on the time scale τ. The spin polarised version of DFT can be adapted to describe the states of the system for each orientational configuration $\{\hat{e}_i\}$. The role of a classical 'spin' (local moment) Hamiltonian, albeit a highly complicated one, is played by the electronic Grand Potential for the constrained system $\Omega\{\hat{e}_i\}$. The first-principles DLM theory of itinerant magnetism was constructed by combining a mean-field theory for the statistical mechanics of

the 'spins' and the spin-polarised SCF-KKR-CPA to describe the electronic structure. However, the DLM theory currently fails for systems such as nickel, and it is thought that this may be due to the fact that the DLM theory is currently unable to describe short-range correlations between the orientations of the local moments because of its single site mean-field nature. This problem could be investigated by using a spin polarised SCF-KKR-NLCPA as the electronic structure basis since this would be capable of describing these short-range correlations.

Appendix A

A.1 KKR Theory in One Dimension

The problem is to solve the one-dimensional Schrödinger equation

$$\left(-\left(\frac{d}{dx}\right)^2 + V(x)\right)\phi(x) = E\phi(x) \tag{A.1}$$

where V can be written as a sum of symmetric and non-overlapping contributions V_i which vanish outside a 'one-dimensional muffin-tin' radius r_{MT} about each site i. In Eq. (A.1) the units of energy are Rydbergs and the units of length are atomic units.

Writing a general point x in the form

$$x = r_i\hat{x}_i + R_i \tag{A.2}$$

where $r_i = |x - R_i|$ is the distance and $\hat{x}_i = (x - R_i)/r_i$ the direction with respect to a potential centre R_i, then 'one-dimensional spherical harmonics' may be defined as

$$Y_0(\hat{x}_i) = \frac{1}{\sqrt{2}}, \quad Y_1(\hat{x}_i) = \frac{\hat{x}_i}{\sqrt{2}} \tag{A.3}$$

along with one-dimensional Bessel and Neumann functions

$$j_0(\sqrt{E}r) = \cos(\sqrt{E}r), \quad j_1(\sqrt{E}r) = \sin(\sqrt{E}r) \tag{A.4}$$

and

$$n_0(\sqrt{E}r) = \sin(\sqrt{E}r), \quad n_1(\sqrt{E}r) = -\cos(\sqrt{E}r) \tag{A.5}$$

Using these coordinates and basis functions, KKR theory in one dimension can be derived in complete analogy to the three-dimensional case. For a detailed review of KKR theory in one dimension see Refs. [69, 70].

Note that the Green's function is given by the expression

$$G^{ij}(x,x';E) = \sum_{ll'}\{Z_l(x_i;E)\tau^{ij}_{ll'}(E)Z_{l'}(x_j;E) - \delta_{ij}\delta_{ll'}Z_l(x_<;E)J_l(x_>;E)\} \quad \text{(A.6)}$$

and the density of states per site by

$$n(E) = -\frac{1}{\pi}Im\int dx\, G^{ii}(x,x,E) \quad \text{(A.7)}$$

For a symmetric potential V_i, the t-matrix takes the form

$$t_l^{-1}(E) = \frac{-1}{i\sqrt{E}}(1 + i\cot\delta_l(E)) \quad \text{(A.8)}$$

where $\delta_l(E)$ is the phase shift.

Finally, the real space structure constants are given by the expression

$$g^{ij}(E) = \frac{e^{i\sqrt{E}|R_{ij}|}}{i\sqrt{E}}\begin{pmatrix} 1 & -i\,sgn\,R_{ij} \\ i\,sgn\,R_{ij} & 1 \end{pmatrix} \quad \text{(A.9)}$$

where a is the lattice constant and $R_{ij} = a(j-i)$. This is a 2×2 matrix because of the two values of angular momentum l. In reciprocal space this becomes

$$g(k) = \frac{1}{i\sqrt{E}}\begin{pmatrix} \left(\frac{e^{i(\phi+\theta)}}{1-e^{i(\phi+\theta)}} + \frac{e^{i(\phi-\theta)}}{1-e^{i(\phi-\theta)}}\right) & \left(\frac{e^{i(\phi+\theta)}}{1-e^{i(\phi+\theta)}} - \frac{e^{i(\phi-\theta)}}{1-e^{i(\phi-\theta)}}\right) \\ -\left(\frac{e^{i(\phi+\theta)}}{1-e^{i(\phi+\theta)}} - \frac{e^{i(\phi-\theta)}}{1-e^{i(\phi-\theta)}}\right) & \left(\frac{e^{i(\phi+\theta)}}{1-e^{i(\phi+\theta)}} + \frac{e^{i(\phi-\theta)}}{1-e^{i(\phi-\theta)}}\right) \end{pmatrix} \quad \text{(A.10)}$$

$$= \frac{1}{i\sqrt{E}}\begin{pmatrix} \left(-1 + \frac{i\sin\phi}{\cos\theta-\cos\phi}\right) & \left(\frac{\sin\theta}{\cos\theta-\cos\phi}\right) \\ -\left(\frac{\sin\theta}{\cos\theta-\cos\phi}\right) & \left(-1 + \frac{i\sin\phi}{\cos\theta-\cos\phi}\right) \end{pmatrix} \quad \text{(A.11)}$$

where $\phi = \sqrt{E}a$ and $\theta = ka$.

A.1.1 Phase Shifts

Following Section 2.2.1, the phase shifts for this model may be determined by considering the Schrödinger equation written in spherical polar coordinates for a single

potential V_i, and matching at the muffin-tin boundary r_{MT} the solutions and their derivatives for the radial part i.e.

$$A_l j_l(qr_{MT}) = B_l j_l(kr_{MT}) + C_l n_l(kr_{MT}) \tag{A.12}$$

for the solutions, and

$$A_l q j_l'(qr_{MT}) = B_l k j_l'(kr_{MT}) + C_l k n_l'(kr_{MT}) \tag{A.13}$$

for the derivatives. Here

$$k = \sqrt{\frac{2mE}{\hbar^2}} \text{ and } q = \sqrt{\frac{2m(E+V_i)}{\hbar^2}} \tag{A.14}$$

and V_i may take the form V_A or V_B. From Eqs. (A.12) and (A.13), using the normalisation $\tan\delta_l(E) = -C_l/B_l$ leads to the phase shifts

$$\delta_0(E) = \cot^{-1}\left(\frac{k + q\tan(qr_{MT})\tan(kr_{MT})}{q\tan(qr_{MT}) - k\tan(kr_{MT})}\right) \tag{A.15}$$

$$\delta_1(E) = \cot^{-1}\left(\frac{k + q\cot(qr_{MT})\cot(kr_{MT})}{k\cot(kr_{MT}) - q\cot(qr_{MT})}\right) \tag{A.16}$$

These satisfy the requirement that $\delta_0(E=0) = \frac{\pi}{2}$ and $\delta_1(E=0) = 0$ in one dimension.

A.1.2 Supercell Structure Constants

In order to aid the interpretation of the comparison between the results for the KKR-CPA and KKR-NLCPA, in Section 6.2 results are also given for a supercell calculation. This requires an expression for the structure constants for a one-dimensional supercell both in real and reciprocal space, which I derive in this section.

The expression for the usual real space structure constants in one dimension is given by Eq. (A.9)

$$g^{ij}(E) = \frac{e^{i\sqrt{E}|R_{ij}|}}{i\sqrt{E}} \begin{pmatrix} 1 & -i\,sgn\,R_{ij} \\ i\,sgn\,R_{ij} & 1 \end{pmatrix} \tag{A.17}$$

where a is the lattice constant and $R_{ij} = a(j-i)$.

For a supercell containing a particular configuration of N_c sites, a lattice Fourier transform must be performed which takes into account its periodicity. This may be defined by

$$g^{IJ}(q) = \sum_{n=-N}^{n=+N} g^{I(J+nN_c)} e^{iq(nN_c a)} \tag{A.18}$$

with n an integer and q a 'vector' in the first Brillouin zone of the superlattice. The site indices have been denoted with capital letters to avoid confusion with the complex number i.

First consider the angular momentum matrix element g_{00}^{IJ}. Applying Eq. (A.18) yields

$$\begin{aligned} g_{00}^{IJ}(q) &= \frac{1}{i\sqrt{E}} \sum_{n=-N}^{n=+N} e^{i\sqrt{E}a|J-I+nN_c|} e^{iqa(nN_c)} \\ &= \frac{1}{i\sqrt{E}} e^{i\sqrt{E}a|J-I|}(1-\delta_{IJ}) \\ &\quad + \frac{1}{i\sqrt{E}} \sum_{n=1}^{n=+N} e^{i\sqrt{E}a|J-I+nN_c|} e^{iqa(nN_c)} \\ &\quad + \frac{1}{i\sqrt{E}} \sum_{n=+N}^{n=1} e^{i\sqrt{E}a|J-I-nN_c|} e^{-iqa(nN_c)} \end{aligned} \tag{A.19}$$

where n has been relabelled $-n$ in the final term. The $(1-\delta_{IJ})$ is needed in the first term since the structure constants are defined to be zero when $I = J$.

Note that $|J-I| < |nN_c|$ for $n \geq 1$. Therefore,

$$\begin{aligned} |J-I+nN_c| &= (J-I) + |nN_c| \quad for \quad n \geq 1 \\ |J-I-nN_c| &= -(J-I) + |nN_c| \quad for \quad n \geq 1 \end{aligned} \tag{A.20}$$

Eq. (A.19) becomes

$$\begin{aligned} g_{00}^{IJ}(q) &= \frac{1}{i\sqrt{E}} \Big\{ e^{i\sqrt{E}a|J-I|}(1-\delta_{IJ}) \\ &\quad + \sum_{n=1}^{n=+N} e^{i\sqrt{E}a(J-I)} e^{i\sqrt{E}a|nN_c|} e^{iqa(nN_c)} \\ &\quad + \sum_{n=1}^{n=+N} e^{-i\sqrt{E}a(J-I)} e^{i\sqrt{E}a|nN_c|} e^{-iqa(nN_c)} \Big\} \end{aligned} \tag{A.21}$$

Letting $\phi = \sqrt{E}a$ and $\theta = qa$, Eq. (A.21) may be arranged in the form of geometric sums

$$\begin{aligned} g_{00}^{IJ}(q) &= \frac{1}{i\sqrt{E}}\Big\{e^{i\phi|J-I|}(1-\delta_{IJ}) \\ &\quad + \sum_{n=1}^{n=+N} e^{i\phi(J-I)}\left[e^{iN_c(\phi+\theta)}\right]^n \\ &\quad + \sum_{n=1}^{n=+N} e^{-i\phi(J-I)}\left[e^{iN_c(\phi-\theta)}\right]^n\Big\} \end{aligned} \tag{A.22}$$

Finally, letting $n \to \infty$ yields

$$\begin{aligned} g_{00}^{IJ}(q) &= \frac{1}{i\sqrt{E}}\Big(e^{i\phi|J-I|}(1-\delta_{IJ}) \\ &\quad + \frac{e^{i\phi(J-I)}e^{iN_c(\phi+\theta)}}{1-e^{iN_c(\phi+\theta)}} + \frac{e^{-i\phi(J-I)}e^{iN_c(\phi-\theta)}}{1-e^{iN_c(\phi-\theta)}}\Big) \end{aligned} \tag{A.23}$$

Now consider the angular momentum matrix element g_{10}^{IJ}. Applying the Fourier transform Eq. (A.18) gives

$$\begin{aligned} g_{10}^{IJ}(q) &= \frac{1}{\sqrt{E}}\sum_{n=-N}^{n=+N} sgn(J-I+nN_c)e^{i\sqrt{E}a|J-I+nN_c|}e^{iqa(nN_c)} \\ &= \frac{1}{\sqrt{E}}sgn(J-I)e^{i\sqrt{E}a|J-I|}(1-\delta_{IJ}) \\ &\quad + \frac{1}{\sqrt{E}}\sum_{n=1}^{n=+N} sgn(J-I+nN_c)e^{i\sqrt{E}a|J-I+nN_c|}e^{iqa(nN_c)} \\ &\quad + \frac{1}{\sqrt{E}}\sum_{n=+N}^{n=1} sgn(J-I-nN_c)e^{i\sqrt{E}a|J-I-nN_c|}e^{-iqa(nN_c)} \end{aligned} \tag{A.24}$$

Letting $\phi = \sqrt{E}a$ and $\theta = qa$, and using Eq. (A.20), this may be arranged in the form of geometric sums

$$\begin{aligned} g_{10}^{IJ}(q) &= \frac{1}{\sqrt{E}}\Big\{sgn(J-I)e^{i\phi|J-I|}(1-\delta_{IJ}) \\ &\quad + \sum_{n=1}^{n=+N} sgn(J-I+nN_c)e^{i\phi(J-I)}\left[e^{iN_c(\phi+\theta)}\right]^n \\ &\quad + \sum_{n=1}^{n=+N} sgn(J-I-nN_c)e^{-i\phi(J-I)}\left[e^{iN_c(\phi-\theta)}\right]^n\Big\} \end{aligned} \tag{A.25}$$

Since $|J-I| < |nN_c|$ for $n \geq 1$ then

$$\begin{aligned} sgn(J-I+nN_c) &= +1 \\ sgn(J-I-nN_c) &= -1 \end{aligned} \tag{A.26}$$

Finally, letting $n \to \infty$ yields

$$g_{10}^{IJ}(q) = \frac{1}{\sqrt{E}}\left(sgn(J-I)e^{i\phi|J-I|}(1-\delta_{IJ}) + \frac{e^{i\phi(J-I)}e^{iN_c(\phi+\theta)}}{1-e^{iN_c(\phi+\theta)}} - \frac{e^{-i\phi(J-I)}e^{iN_c(\phi-\theta)}}{1-e^{iN_c(\phi-\theta)}}\right) \tag{A.27}$$

Using the fact that $g_{00}^{IJ} = g_{11}^{IJ}$ and $g_{10}^{IJ} = -g_{01}^{IJ}$ leads to the final expression for the supercell structure constants in reciprocal space

$$\begin{aligned} g^{IJ}(q) &= \frac{1}{i\sqrt{E}}\begin{pmatrix} e^{i\phi|J-I|}(1-\delta_{IJ}) & -i\,sgn(J-I)e^{i\phi|J-I|}(1-\delta_{IJ}) \\ i\,sgn(J-I)e^{i\phi|J-I|}(1-\delta_{IJ}) & e^{i\phi|J-I|}(1-\delta_{IJ}) \end{pmatrix} \\ &+ \frac{1}{i\sqrt{E}}\left(\frac{e^{i\phi(J-I)}e^{iN_c(\phi+\theta)}}{1-e^{iN_c(\phi+\theta)}} + \frac{e^{-i\phi(J-I)}e^{iN_c(\phi-\theta)}}{1-e^{iN_c(\phi-\theta)}}\right)\begin{pmatrix} 1 & 0 \\ 0 & 0 \end{pmatrix} \\ &+ \frac{1}{i\sqrt{E}}\left(\frac{e^{i\phi(J-I)}e^{iN_c(\phi+\theta)}}{1-e^{iN_c(\phi+\theta)}} - \frac{e^{-i\phi(J-I)}e^{iN_c(\phi-\theta)}}{1-e^{iN_c(\phi-\theta)}}\right)\begin{pmatrix} 0 & 0 \\ i & 0 \end{pmatrix} \\ &+ \frac{1}{i\sqrt{E}}\left(\frac{e^{i\phi(J-I)}e^{iN_c(\phi+\theta)}}{1-e^{iN_c(\phi+\theta)}} - \frac{e^{-i\phi(J-I)}e^{iN_c(\phi-\theta)}}{1-e^{iN_c(\phi-\theta)}}\right)\begin{pmatrix} 0 & -i \\ 0 & 0 \end{pmatrix} \\ &+ \frac{1}{i\sqrt{E}}\left(\frac{e^{i\phi(J-I)}e^{iN_c(\phi+\theta)}}{1-e^{iN_c(\phi+\theta)}} + \frac{e^{-i\phi(J-I)}e^{iN_c(\phi-\theta)}}{1-e^{iN_c(\phi-\theta)}}\right)\begin{pmatrix} 0 & 0 \\ 0 & 1 \end{pmatrix} \end{aligned} \tag{A.28}$$

This expression reduces to Eq. (A.10) for a single-site supercell ($N_c = 1$ and $I = J$), and can be manipulated into various simpler forms in analogy to Eq. (A.11).

Bibliography

[1] W. Schweika, *Disordered Alloys: Diffuse Scattering and Monte Carlo Simulations* (Springer Tracts in Modern Physics, Heidelberg, 1998).

[2] F. Ducastelle, *Order and Phase Stability in Alloys*, Vol. 3 of *Cohesion and Structure* (North Holland, Amsterdam, 1991).

[3] B. L. Gyorffy, Phys. Rev. B **5**, 2382 (1972).

[4] B. L. Gyorffy and G. M. Stocks, in *Electrons in Disordered Metals and at Metallic Surfaces*, edited by P. Phariseau, B. L. Gyorffy, and L. Scheire (Plenum, New York, 1974), p. 89.

[5] B. L. Gyorffy *et al.*, in *Proceedings of the NATO Advanced Study Institute on Alloy Phase Stability*, edited by G. M. Stocks and A. Gonis (Kluwer, Dordrecht, 1987), p. 421.

[6] A. Gonis, *Green Functions for Ordered and Disordered Systems*, Vol. 4 of *Studies in Mathematical Physics* (North Holland, Amsterdam, 1992).

[7] M. H. Hettler *et al.*, Phys. Rev B. **58**, 7475 (1998).

[8] M. H. Hettler, M. Mukherjee, M. Jarrell, and H. R. Krishnamurthy, Phys. Rev. B **61**, 12739 (2000).

[9] T. Maier, M. Jarrell, T. Pruschke, and J. Keller, Eur. Phys. J. B **13**, 613 (2000).

[10] M. Jarrell and H. R. Krishnamurthy, Phys. Rev. B **63**, 125102 (2001).

[11] R. Moradian, Ph.D. Thesis, University of Bristol (2001).

[12] R. Moradian, B. L. Gyorffy, and J. F. Annett, Phys. Rev. Lett. **89**, 287002 (2002).

[13] N. W. Ashcroft and N. D. Mermin, *Solid State Physics* (Holt, Rinehart and Winston, New York, 1976).

[14] J. Callaway and N. H. March, Solid State Phys. **38**, 135 (1984).

[15] R. M. Dreizel and E. K. U. Gross, *Density Functional Theory* (Springer, New York, 1990).

[16] W. Kohn and L. J. Sham, Phys. Rev. **140**, A1133 (1965).

[17] U. V. Barth and L. Hedin, J. Phys. C: Solid State Phys. **5**, 1629 (1972).

[18] L. H. Thomas, Proc. Cambridge Philos. Soc. **23**, 542 (1927).

[19] E. Z. Fermi, Phys. **48**, 73 (1928).

[20] P. Hohenberg and W. Kohn, Phys. Rev. **136**, B864 (1964).

[21] J. Kubler, *Theory of Itinerant Electron Magnetism* (Oxford University Press, Oxford, 2000).

[22] J. Korringa, Physica **13**, 392 (1947).

[23] W. Kohn and N. Rostoker, Phys. Rev. **94**, 1111 (1954).

[24] A. Gonis and W. H. Butler, *Multiple Scattering Theory in Solids* (Springer, New York, 1999).

[25] P. Weinberger, *Electron Scattering Theory for Ordered and Disordered Matter* (Oxford University Press, Oxford, 1990).

[26] P. Strange, *Relativistic Quantum Mechanics* (Cambridge University Press, Cambridge, 1998).

[27] B. L. Gyorffy and M. J. Stott, in *Band Structure Spectroscopy of Metals and Alloys*, edited by D. J. Fabian and L. M. Watson (Academic Press, New York, 1973), p. 385.

[28] J. S. Faulkner and G. M. Stocks, Phys. Rev. B **21**, 3222 (1980).

[29] P. Lloyd and P. V. Smith, Adv. in Phys. **21**, 69 (1972).

[30] S. Gasiorowicz, *Quantum Physics* (John Wiley and Sons, New York, 1974).

[31] A. Zunger, S.-H. Wei, L. G. Ferreira, and J. E. Bernard, Phys. Rev. Lett. **65**, 353 (1990).

[32] T. C. Choy, *Effective Medium Theory - Principles and Applications* (Oxford University Press, Oxford, 1999).

[33] J. M. Ziman, *Models of Disorder* (Cambridge University Press, Cambridge, 1979).

[34] L. Nordheim, Ann. Phys. (Lipz) **9**, 607 (1931).

[35] J. Korringa, J. Phys. Chem. Solids **7**, 252 (1958).

[36] P. Soven, Phys. Rev. **156**, 809 (1967).

[37] D. W. Taylor, Phys. Rev. **156**, 1017 (1967).

[38] R. J. Elliott, J. A. Krumhansl, and P. L. Leath, Rev. Mod. Phys. **46**, 465 (1974).

[39] H. Ehrenreich and L. Schwartz, in *Solid State Physics* (Academic, New York, 1976), Vol. 31, p. 149.

[40] R. Valming and D. Vollhardt, Phys. Rev. B **45**, 4637 (1992).

[41] A. Gonis, G. M. Stocks, W. H. Butler, and H. Winter, Phys. Rev. B **29**, 555 (1984).

[42] H. Winter and G. M. Stocks, Phys. Rev. B. **27**, 882 (1983).

[43] G. M. Stocks and H. Winter, Z. Phys. B **46**, 95 (1982).

[44] D. D. Johnson *et al.*, Phys. Rev. Lett. **56**, 2088 (1986).

[45] D. D. Johnson *et al.*, Phys. Rev. B. **41**, 9701 (1990).

[46] L. D. Landau and E. M. Lifshitz, *Statistical Physics, 2nd Ed.* (Pergamon Press, Oxford, 1969).

[47] F. J. Pinski *et al.*, Phys. Rev Lett. **66**, 766 (1991).

[48] A. Zunger, in *Statics and Dynamics of Alloy Phase Transformations*, Vol. 319 of *NATO Advanced Study Institute Series B: Physics*, edited by A. Gonis and P. E. A. Turchi (Plenum, New York, 1993).

[49] L. W. Lu, S.-H. Wei, and A. Zunger, Phys. Rev. Lett. **66**, 1753 (1991).

[50] R. Magri, S.-H. Wei, and A. Zunger, Phys. Rev. B **42**, 11388 (1990).

[51] F. J. Pinski, J. B. Staunton, and D. D. Johnson, Phys. Rev B. **57**, 15177 (1998).

[52] J. B. Staunton, D. D. Johnson, and F. J. Pinski, Phys. Rev. B. **50**, 1450 (1994).

[53] B. L. Gyorffy *et al.*, Phil. Trans. R. Soc. London **334**, 515 (1991).

[54] A. G. Khachaturyan, *Theory of Structural Transformations in Solids* (Wiley, New York, 1983).

[55] C. Domb, Adv. Phys. **9**, 149 (1960).

[56] K. Binder, *Applications of the Monte Carlo Method in Statistical Physics* (Springer, Berlin, 1984).

[57] A. Gonis, W. H. Butler, and G. M. Stocks, Phys. Rev. Lett. **50**, 1482 (1983).

[58] B. G. Nickel and W. H. Butler, Phys. Rev. Lett. **30**, 373 (1973).

[59] R. Mills and P. Ratanavararaksa, Phys. Rev. B **18**, 5291 (1978).

[60] S. S. A. Razee, S. S. Rajput, R. Prasad, and A. Mookerjee, Phys. Rev. B **42**, 9391 (1990).

[61] A. Mookerjee, J. Phys. C **6**, 1340 (1973).

[62] A. Georges, G. Kotliar, W. Krauth, and M. Rozenberg, Rev. Mod. Phys. **68**, 13 (1996).

[63] J. Hubbard, Proc. Roy. Soc. A **281**, 401 (1964).

[64] Y. Kakehashi, Phys. Rev. B **45**, 7196 (1992).

[65] M. Tsukada, J. Phys. Soc. Jpn **32**, 1475 (1972).

[66] D. A. Rowlands, J. B. Staunton, and B. L. Gyorffy, Phys. Rev. B. **67**, 115109 (2003).

[67] Th. Maier, Ph.D. Thesis, University of Regensburg (2000).

[68] D. F. Elliot and K. R. Rao, *Fast Transforms: Algorithms, Analyses, Applications* (Academic, New York, 1982).

[69] W. H. Butler, Phys. Rev. B **14**, 468 (1976).

[70] J. Schwitalla and B. L. Gyorffy, J. Phys.:Condens.Matter **10**, 10955 (1998).

[71] J. Schwitalla and B. L. Gyorffy, Philosophical Magazine B **78**, 441 (1998).

[72] J. Schwitalla and B. L. Gyorffy, J. Phys.:Condens.Matter **11**, 7125 (1999).

[73] J.B. Staunton and B.L. Gyorffy; private communication.

[74] H. Reichert *et al.*, Phys. Rev. Lett. **90**, 185504 (2003).

[75] H. Reichert et. al., unpublished data (2003).

[76] I. Wilkinson *et al.*, Phys. Rev. Lett. **87**, 216401 (2001).

[77] R. Kubo, J. Phys. Soc. Jpn. **12**, 570 (1957).

[78] D. A. Greenwood, Proc. Phys. Soc. **71**, 585 (1958).

[79] R. H. Brown, P. B. Allen, D. M. Nicholson, and W. H. Butler, Phys. Rev. Lett. **62**, 661 (1989).

[80] H. Yang, J. C. Swihart, D. M. Nicholson, and R. H. Brown, Phys. Rev. B. **47**, 107 (1993).

[81] M. Migschitz, W. Garlipp, and W. Pfeiler, Acta. Mat. **44**, 2831 (1996).

[82] H. Thomas, Z. Phys. **129**, 219 (1951).

[83] B. L. Gyorffy *et al.*, J. Phys. F:Met. Phys. **15**, 1337 (1985).

[84] J. B. Staunton and B. L. Gyorffy, Phys. Rev. Lett. **69**, 371 (1992).